



(Model ID = 454913)

Ineris - 206552 - 2822195 - v1.0

22/04/2025

Methods for assessing and preventing accidental risks

Phenomenology and modelling of confined gas explosions - Ω 31

PREAMBLE

Omega reports are the property of INERIS. Users are only granted a right of use, which does not imply any transfer of ownership.

The Oméga report is based on available and objective data (scientific or technical) and the regulations in force, as well as the practices and methodologies developed by INERIS. Although INERIS endeavours to provide reliable content, it does not guarantee the absence of errors or omissions in these documents.

This report is intended for users with specific professional skills in the field of accidental risks. The information it contains has no legal or regulatory value.

This information is general and cannot, under any circumstances, meet the specific needs of each user. Users are therefore solely responsible for the use and interpretation they make of the reports. Similarly, any modification or transfer of these documents will be their sole responsibility.

Under no circumstances may INERIS be held liable in this respect. In any event, INERIS may only be held liable on the basis of the French version of these reports.

Name of department responsible for the report: FIRE DISPERSION EXPLOSION DEPARTMENT

Editor: GREGOIRE Yann

Verification: LEPRETTE EMMANUEL

Approval: Document approuvé le 22/04/2025 par BOUET REMY

Table of contents

1.	Introduction	6
1.1	OMEGA repositories	6
1.2	Scope and objectives	6
1.3	The phenomenon studied: reference case	6
1.4	Approach adopted	7
2.	Accidentology	8
2.1	Some past accidents	8
2.1.1	Explosion at the London School in New London, Texas	8
2.1.2	House explosions in Merrimack Valley	8
2.1.3	Flight TWA800 on 17 July 1996	10
2.2	Teaching	12
3.	Phenomenology of a confined explosion	13
3.1	Reference situation	13
3.1.1	What is an explosion?	13
3.1.2	The hexagon of the explosion	15
3.1.3	Types of explosive mixtures	15
3.1.4	Ignition limits	16
3.1.5	Sources of ignition	17
3.1.6	Containment	18
3.2	Cloud formation in confined space	18
3.3	Flame propagation under deflagration conditions	18
3.3.1	The expansion rate of combustion products	19
3.3.2	The velocity of combustion	20
3.3.3	Flame propagation velocity	22
3.4	Flame disturbances	23
3.4.1	Natural" flame disturbances: Combustion instabilities	23
3.4.2	Flame disturbances induced by flow turbulence	24
3.4.3	Flame distortion caused by obstacles	28
3.4.4	Effects of heterogeneities in cloud richness	29
3.4.5	Summary of flame disturbance modes	29
3.5	Pressure generation	29
3.5.1	Fully enclosed volume	29
3.5.2	Case of an enclosure fitted with a vent	31
3.5.3	Case of 2 closed enclosures connected by an opening	40
3.5.4	Explosion in a pipe	41
3.5.5	Case of an enclosure connected to a discharge pipe	44
3.5.6	Effect of a pipe between 2 enclosures	45
3.6	Special case of flame propagation under detonation conditions	46
3.6.1	Phenomenology	46
3.6.2	CJ and ZND models	46

3.6.3	Piston model.....	49
3.7	Some specific features of explosions involving dust or hybrid mixtures.....	51
3.8	Effects of the explosion on the enclosure where the explosion occurs.....	52
3.9	External effects.....	54
4.	Modelling and calculation of the pressure effects of confined explosions.....	56
4.1	The main categories of models.....	56
4.2	Reference situation.....	56
4.3	Multiphysics modelling, CFD approach.....	57
4.3.1	Foundations of the method.....	57
4.3.2	CFD for explosions.....	58
4.3.3	Example of CFD modelling of confined explosions.....	59
4.3.4	Detonations.....	62
4.3.5	Modelling the deflagration to detonation transition (DDT).....	63
4.4	Phenomenological modelling of internal effects: EFFEX.....	64
4.4.1	The EFFEX tool.....	64
4.4.2	The SECEX tool.....	71
4.5	Empirical modelling of internal effects.....	73
4.5.1	The Bartknecht model.....	73
4.5.2	The NFPA68 guide model (2017).....	75
4.5.3	Molkov models.....	76
4.5.4	Bauwens model.....	78
4.5.5	Example of the use of a neural network.....	81
4.6	Modelling external effects.....	86
4.6.1	Preamble: Thermal effects.....	86
4.6.2	External overpressure wave calculation charts.....	87
4.6.3	Prediction of pressure effects using the method of European standards EN14994 or EN1449189.....	
4.6.4	The SECEX model - external module.....	90
5.	Conclusions.....	93
6.	Bibliography.....	94
6.1	Publications.....	94
6.2	Other works.....	102

To cite this document, use the link below:

Institut national de l'environnement industriel et des risques, Methods for assessing and preventing accidental risks - Phenomenology and modelling of confined gas explosions - Ω 31, Verneuil-en-Halatte, Ineris - 206552 - 2822195 - v1.0, 22/04/2025.

1. Introduction

1.1 OMEGA repositories

The OMEGA repositories constitute a global collection formalising the expertise of INERIS in the field of accidental risks. They cover the following topics

- risk analysis;
- the physical phenomena involved in an accident situation (fire, explosion, BLEVE, ETC.);
- risk reduction, accident prevention and;
- methodological aspects of regulatory services (hazard studies, critical analysis, etc.).

The purpose of these reports is to present information and data considered at the time of this writing the standard body of knowledge. These reports are made available to those involved in major accident risk management, and who have the expertise for the implementation of information therein. Some of these reports have been translated into English to facilitate their distribution. The concepts set out in these reports are not intended to replace regulatory provisions.

1.2 Scope and objectives

This report, **Ω 31-Confined Gas Explosions**, summarises the current state of knowledge on confined gas and vapour explosions, one of the subjects included in the "physical phenomena" theme mentioned above.

This report on confined explosions has as its complement the **Ω -UVCE** report on unconfined explosions, the former of which focuses on gas and vapour explosions. The specific features of confined explosions of dust and hybrid mixtures are dealt with only marginally.

This document does not treat the case of uncontained explosion phenomenon, which is the subject of the **Ω -UVCE** report.

The objectives of this document are to present:

- some accidents that have led to considerable damage, and to learn from them about how a confined explosion unfolds;
- all the conditions necessary for the occurrence of a confined explosion and the main parameters influencing flame propagation;
- a summary of the main methods available for estimating the overpressure effects generated by a confined explosion and their limitations;
- other 'innovative' approaches to estimating explosive effects.

1.3 The phenomenon studied: reference case

A typical situation is that of a flammable gas leak in a confined or semi-confined space, which results in the formation of a combustible reactive-air mixture in the enclosure. When a suitable ignition source is present within the flammable zone of the cloud, it ignites, and a flame spreads from the ignition point.

Figure 1 illustrates the development of the flame in the containment.

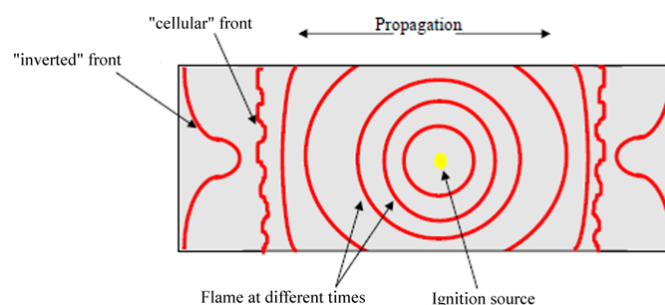


Figure 1. Flame spread as a function of time

The flame develops spherically around the ignition source. As it passes, it almost instantaneously transforms the cold reactants into hot combustion products (typically between 1000 and 2000°C), resulting in a strong expansion of the burnt gases. This volume expansion is responsible for pressure effects in general in the case of gas explosions and, more specifically, confined explosions of any kind. The flame speeds observed generally vary from a few m/s to several hundred m/s, even thousands in the specific case of detonations for confinement scales of metres or tens of metres. Heat exchange with the walls is always present but is often considered marginal in industrial safety applications. Therefore, the assumption of adiabatic compression of confined gases according to Laplace's Law is regularly considered in this field (this aspect is developed in paragraph 3.5 of this report).

The increase in pressure in the completely or partially confined enclosure between two successive instants is proportional to the quantity of gas volume produced by combustion, reduced by the amount of gas released to the outside through openings if present.

In the case of total, insulated, explosion-proof containment, the only visible external effect may be a rise in the enclosure's temperature, which is a priori very limited because of the significant difference in thermal inertia between the enclosure and its gaseous contents.

In the context of industrial safety, the question of studying confined explosions only arises when the enclosure in which the explosion occurs:

- is connected to other equipment;
- or has partial containment;
- or has total but temporary containment because it is not resistant to overpressure effects, as in the case of explosion vents.

The confined explosion is, therefore, also characterised by its associated effects.

These effects can be of several kinds:

- in the case of interconnected enclosures, the interest lies in the propagation of an explosion from one piece of equipment to its neighbours,
- in the case of an enclosure open to the outside, either permanently or when a vent is opened, the following can be observed:
 - flames and, therefore, thermal effects outside containment,
 - pressure waves, often with a strong directional effect, in the axis of the openings,
 - external explosions with the emission of isotropic overpressure waves.

1.4 Approach adopted

This report summarises the work carried out by Ineris on the phenomenology of confined explosions, methods for estimating their consequences based on experimental work carried out as part of the ministerial support programme and research results.

Chapter 2 analyses several well-documented accidents, highlighting key aspects of Chapter 3's section on the phenomenology of confined explosions. Chapter 4 focuses on modelling these effects.

2. Accidentology

2.1 Some past accidents

2.1.1 Explosion at the London School in New London, Texas

The London School explosion occurred on 18 March 1937. It was a natural gas explosion that killed 295 students and teachers.

The London School was a large steel and concrete structure built in 1932 in an area where an oil field had just been discovered (in 1930). At that time, natural gas was extracted along with oil, but it was considered a waste product because its quality varied daily, so it was burnt as waste. The school was equipped with 72 gas heaters throughout the building, fed by a tap installed to save money on a waste gas recovery pipe belonging to the Parade Gasoline Company. Although not explicitly authorised by the local oil companies, this practice was widespread in the region. Since natural gas had no relevant value, the oil companies disregarded the practice.

Untreated natural gas is both odourless and colourless, so leaks are challenging to detect and can go unnoticed. In this case study, gas leaked from the waste pipe valve and accumulated inside an enclosed crawl space that ran the length of the building's façade. The students complained of headaches for some time, but little attention had been paid to the matter.

The explosion occurred at 3.17 p.m. on March 18, 1937. It is thought to have been caused by a spark from an electric sander used during a lesson. The explosion was heard up to six kilometres from the school.

Of the more than 600 people at the school, only 130 escaped without serious injury. Estimates of the number of deaths range from 296 to 319. However, the number could be much higher as many New London residents at the time were temporary oilfield workers, and there is no way of determining how many of them collected the bodies of their loved ones in the days following the disaster.

Survivors' accounts indicate that the school's walls bulged, the roof lifted off the building and then collapsed onto the main wing of the structure provoking total failure of the building's integrity. However, there was no fire after the explosion, and some of the buildings on the 4.0-hectare campus withstood the blast. Survivors said that the blast had thrown out lockers embedded in the wall, the force of the explosion had crushed others, and the plaster had become a white mist. The force of the blast was such that a two-tonne concrete block was thrown out of the building and crushed a car parked 60 m away.

The school's gymnasium, which was only slightly damaged by the explosion, was quickly converted into several classrooms and lessons resumed ten days later. A new school was built on the site in the 2 years following the disaster. A lawsuit was filed against the school district and the Parade Gasoline Company, but the court ruled that neither could be held responsible. Experts from the US Bureau of Mines concluded that the connection to the waste gas line was defective. It had allowed gas to seep into the school, and because natural gas is invisible and odourless, the leak went undetected.

Texas legislation began requiring thiols (mercaptans) to be added to natural gas a few weeks after the explosion to reduce the damage caused by future leaks. The pungent odour of many thiols makes leaks quickly detectable, and the practice quickly spread around the world.

2.1.2 House explosions in Merrimack Valley

On 13 September 2018, a rise in pressure in natural gas lines owned by Columbia Gas caused a series of explosions with more than 80 individual fires affecting around 40 homes, in towns across the Merrimack Valley in Massachusetts. One person was killed, and 30,000 were forced to evacuate their homes temporarily.



Figure 2. Image of a house destroyed during the events in Merrimack Valley

According to the NTSB's preliminary report, customers in the accident area received gas from a low-pressure (35 mbar) distribution network, which, in turn, was supplied by a high-pressure (5 bar) main pipeline via sensor-controlled regulators. At the time of the accident, workers were replacing part of the low-pressure cast-iron pipework with newer plastic pipework. When the operators connected the high-pressure section to this new pipe, they disconnected the old one, which drained. As a result, when the old pipe was depressurised, the regulator, still connected to this sensor on the old pipe, detected zero pressure on the low-pressure side and opened completely, feeding the local distribution network at full pressure. The procedure put in place by Columbia Gas to carry out this work did not include transferring the pressure sensor from the old pipe to the new one. This faulty procedure caused a build-up of natural gas in the homes within minutes.

A few minutes before the fires and explosions, the Columbia Gas monitoring centre in Columbus, Ohio, received two high-pressure alarms for the South Lawrence system: one at 4.04 pm and the other at 4.05 pm. However, this centre had no capacity to control the network, for example, to close or open the valves. Its only function was to monitor the pressures on the distribution network and advise the field technicians accordingly. Following company protocol, at 4.06 pm, the Columbia Gas controller reported the high-pressure event to the Metering and Regulation group in Lawrence. Yet, it was a local resident who made the first call to the emergency services at 4.11 pm.

Multiple explosions and fires were reported over a very short period of time in the towns of Merrimack Valley. Over the course of the evening, emergency crews responded to between 40 and 80 fires. At one point, up to 18 fires were burning simultaneously, while emergency teams were scheduled to respond to a maximum of 10 simultaneous alarms.

The fire chief of Andover, one of the affected towns, described the affected area as a war zone, with billowing smoke in Andover and the nearby town of Lawrence. A Lawrence resident described finding his boiler on fire after his smoke alarm went off, then hearing a noise from a neighbour's house followed by a ground tremor. An explosion in a neighbouring house caused its foundations to shift, which in turn caused an attached chimney to fall on a car occupied by a fleeing resident, killing him. In addition to this death, twenty-five people were injured in Merrimack Valley during the series of explosions and fires.

Once the cause of this series of accidents had been identified, all the residents supplied by Columbia Gas in the region, some 8,600 people, were asked to evacuate their homes. Columbia Gas closed the regulator at around 4.30 pm, and all the fires were extinguished by 6.45 pm. Electricity was also cut off in the area to limit the risk of igniting any lingering gas pockets. Later, other critical valves on the natural gas distribution system concerned were closed. Around midnight, Columbia Gas technical teams escorted by emergency response personnel began shutting off the meters in each house to isolate them from the natural gas distribution network. The operation lasted all night.

On 14 September 2018, the Governor of Massachusetts declared a state of emergency. He appointed an expert third party to assess and oversee the management of the gas distribution system in the affected area. Residents gradually returned to their homes and businesses, but others remained in emergency shelters, hotels, or with friends and family. Inspections were completed, and electricity in all affected areas was restored on 16 September 2018. Nevertheless, some gas-dependent businesses, such as laundromats and restaurants, remained unable to open. Restoring gas service to the 8,600 customers affected required the replacement of around 77 km of pipeline. On 22 September 2018, National Guard troops began delivering around 7,000 hotplates to customers to replace gas cookers temporarily. Around 24,000 space heaters were supplied ahead of the winter chill, for which Columbia Gas had to pay. The company had to forego a \$33 million future rate increase effective November 2018. In early May 2019, NiSource, the parent company of Columbia Gas of Massachusetts, said that third-party claims related to the Merrimack Valley gas disaster could cost more than \$1 billion. This amount included property damage, personal injury, infrastructure damage, and mutual aid payments to other utilities that contributed to recovery and restoration efforts. Several class actions were filed for negligence and destruction of property, all of which were ultimately settled by Columbia Gas for \$143 million in July 2019. In February 2020, Columbia Gas pleaded guilty to violating federal pipeline safety laws, agreed to sell its gas distribution business in the state and pay a \$53 million fine.

2.1.3 Flight TWA800 on 17 July 1996

On 17 July 1996, TWA Flight 800 to Paris, a Boeing 747-131, exploded at 8.31 pm over the Atlantic Ocean at an altitude of 13,700 feet. This occurred 12 minutes after take-off at 20:19 from John F. Kennedy (JFK) airport in New York.

All 18 crew members and 212 passengers were killed.

The aircraft, TWA Flight 881, had just completed a transatlantic flight from Athens and arrived at the JFK terminal at 4:38 p.m. The crew did not detect any anomalies, and, as planned, a crew change was made. A check of the aircraft at around 6 p.m. also revealed no problems, apart from damage to a paraffin gauge, which the mechanics judged to be of no consequence. The wing tanks were filled, sufficient for the planned flight, and the centre tank was left empty.

During the investigation to determine the cause of the explosion, the fuselage of the aircraft was reconstructed:



Figure 3. Reconstruction of the aircraft fuselage after the accident

According to the NTSB's (National Transport Safety Board) analysis of the damaged fuselage, several indicators pointed to an explosion at the bottom of the 747's center fuel tank shortly before the plane broke up.

US investigators eventually found that the ignition source of the explosion in the central fuel tank was frayed electrical wiring, which would have created a spark. Carbon deposits were found around the electrical connections that had caused the problem.

It was concluded that a kerosene vapour explosion had occurred in the nearly empty center tank, tearing the aircraft's structure and causing it to disintegrate.

A flammable vapour-air mixture was all that was needed for the fuel tank to explode. The key factor to understand the TWA 800 explosion is why a flammable mixture occurred in the fuel tank.

The aircraft's central tank volume is around 60 m³, with a floor area of around 40 m². On the ground and empty of fuel, it contains 72 kg of air. The stoichiometric air/fuel mass ratio for aviation kerosene is typically 14.6. With these dimensions, a mass of 4.93 kg of fuel vapour is sufficient to produce a stoichiometric flammable vapour/air mixture. The limit drops to 2.5 kg for a lean but flammable mixture (about half the stoichiometric concentration).

This corresponds to the evaporation of around 3 litres of fuel distributed over the 40 m² tank floor, giving a puddle thickness of less than 1 mm.

However, to evaporate and form a lean mixture with air at atmospheric pressure, paraffin a component of the gauge in the tank needs a temperature of around 45°C (Figure 4). At the time of the explosion of flight TWA 800, the ambient temperature was only 22°C.

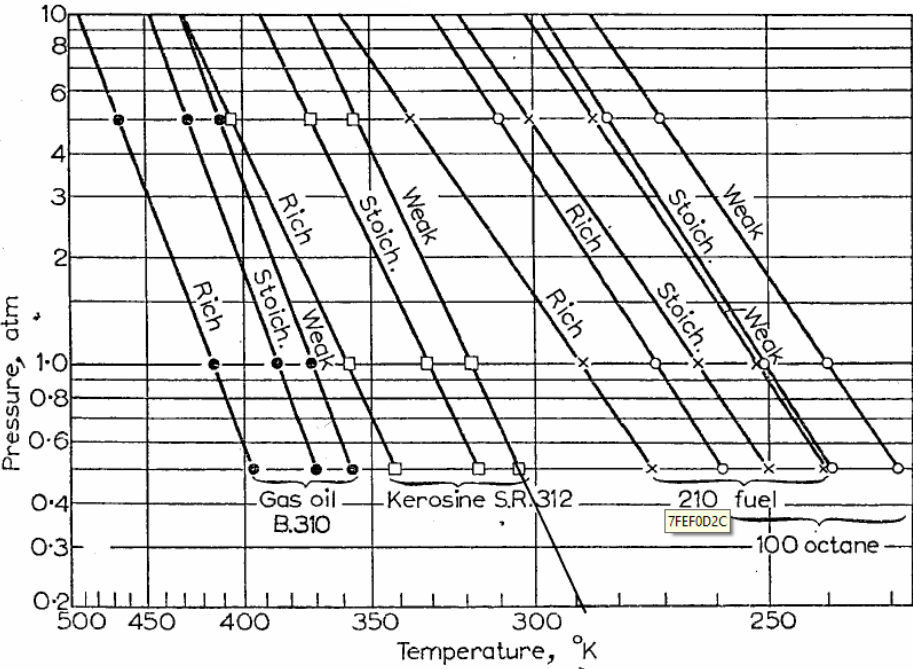


Figure 4. Calculated flammability limits for paraffin, diesel and petrol (Mullins and Penner, 1959)¹

¹ These limits are orders of magnitude, as the values may vary moderately with the variable composition of commercial fuels.

As the aircraft rises, the ambient pressure decreases, reducing the pressure in the fuel tank. This reduces the mass of air in the tank but has no influence on the mass of fuel present in liquid and vapour form. As the partial pressure of air decreases, the percentage of vapour increases. The net effect is that the overall mixture in the tank becomes richer as the aircraft climbs, gradually entering the flammable range from the lean side.

However, even at the altitude at which the aircraft exploded, the decrease in pressure is insufficient to lead to the formation of a flammable mixture, as the temperature, already low on the ground, decreases with altitude.

A heat source was missing, which would have heated the fuel sufficiently to produce a flammable vapour. The investigation showed (through tests) that this heat source was the air conditioning unit under the tank, which heated the paraffin to a temperature between 37 and 50°C, sufficient to form the ATEX.

In May 1997, Boeing recommended that airlines worldwide inspect the wiring and piping in the centre fuel tanks of all wide-body 747 aircraft.

2.2 Teaching

Unlike materials naturally in a condensed phase, the combustible gases used in industry are light elements with a density of the same order of magnitude as that of air, around 1 kg/m³. Therefore, there is a particular interest in storing them in a state where they occupy less space. By compressing them or cooling them (in the case of cryogenic mixtures) in special tanks or pipes, these gases are isolated in volumes that can be used on an industrial scale. Still, their conditions are very different from those they would have in the air. As a result, the slightest opening or loss of tightness leads to a thermodynamic rebalancing between the tank and the air, resulting in a leak of varying intensity. It is clear from accident reports that transport tanks and pipelines are regularly the source of accident situations.

In the event of a leak, combustible gases are released into the air, where they can mix and form an explosive mixture with the oxygen in the air. The accidents at Merrimack Valley show that the possible ignition sources are numerous and often unknown, making it difficult to protect against them.

Explosive events are all the more dangerous because they are brief and difficult to anticipate. Gases that are often colourless and odourless, and therefore undetected by people unaware of their presence, can be ignited by sources as weak as static electricity. The characteristic duration of the phenomenon is on the order of a second at most, a relatively short period that leaves few options for protection.

In the event of an accident, this explosion phenomenon almost invariably gives rise to other dangerous effects of varying scope and duration, such as collapses, projections and fires. These indirect consequences are often the cause of fatalities.

When no mitigation system is in place, the damage caused is severe, both to people and property, often resulting in many deaths, high costs for local authorities and business failures.

3. Phenomenology of a confined explosion

3.1 Reference situation

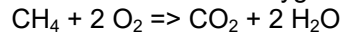
3.1.1 What is an explosion?

In the general sense, an explosion is any sudden release of energy of chemical (combustion) or mechanical (bursting) origin that generates mechanical (pressure, projections) and thermal (flames and hot gases) effects in the associated environment. Beyond this general description, this report concerns confined explosions, mainly of gases but also of various fuels (suspensions of reactive dust or fuel oil droplets). The aim is to study the consequences of an explosion, a rapid chemical reaction, on an enclosure and its environment.

Let us take the example of the combustion of CH₄ - methane gas.

According to the dictionary of the Groupement Français de Combustion (GFC), combustion is a "chemical reaction that is generally highly exothermic, autonomous, capable of sudden acceleration and accompanied by the emission of radiation. Combustion can be slow (before any sudden acceleration of the reaction) or rapid (beginning with the sudden acceleration and characterised by a high reaction rate). Depending on the containment conditions, the heat release from the combustion reaction can lead to rapid expansion of the reaction medium or a sharp increase in pressure. Radiation is generally emitted, at least in part, in the visible, near UV and IR ranges. The sudden acceleration characteristic of rapid combustion can lead to the formation of a flame. Smoke can also be observed, with or without incandescence. Combustion can release charged species: electrons and positive or negative ions. It converts potential chemical energy into thermal, mechanical, radiant and electrical energy. French standards define combustion as the exo-energetic chemical reaction between a reducing agent and oxygen or another electronegative body. In the usual sense, combustion is the reaction between a fuel and pure oxygen, diluted oxygen (air) or an oxygen-rich chemical species (ozone, hydrogen peroxide, nitric acid). This report considers only pure oxygen or oxygen in the air.

The chemical reaction equation for methane combustion in oxygen is generally written as follows:



This chemical reaction is only possible under certain conditions, and contact is necessary between the reactants:

- oxygen, the oxidiser;
- methane, the fuel.

Like any chemical reaction, combustion is only initiated if the mixture receives sufficient activation energy to trigger the reaction. The reaction then transforms the reactants (methane and oxygen) into combustion products with a lower enthalpy of formation. The difference in energy between the two states is released into the associated medium through heat (and mechanical energy, particularly for faster reactions such as detonations).

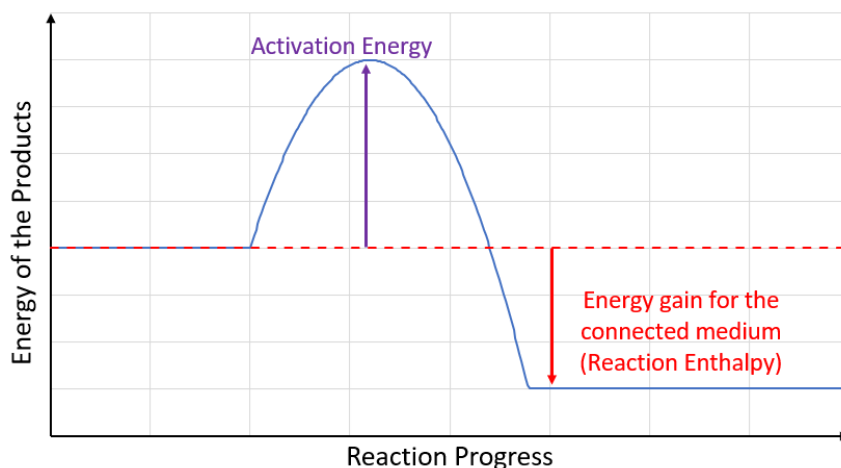


Figure 5. Schematic diagram of energy release during a chemical reaction

The ignition source provides the activation energy. This brings us back to the fire triangle: fuel, oxidiser, and ignition source.

To obtain an explosion, more conditions must be met. Explosion is associated with the idea of a sudden release of energy in a very short space of time. This time can be limited either by chemical kinetics, the speed of the reaction, or by mechanics, the mixing of species. In a burner, the speed at which the fuel and oxidant are brought into contact is controlled, and the propagation of the flame is limited by the diffusion of the species, referred to as a diffusion flame. For an explosion, the two reagents must be mixed, and flame propagation is limited by chemical kinetics, known as a premixed flame. One of the conditions necessary for a combustible gas to explode is, therefore, its mixing with the oxidant.

There are two independent combustion propagation regimes:

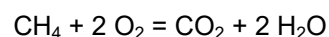
- Deflagration: the flame front moves at subsonic velocity in relation to the fresh mixture. It is sustained by the release of energy from chemical reactions, the propagation of which is controlled by the diffusion of heat and species from the chemical reaction zone towards the fresh mixture. The flow of the fresh mixture in front of the flame is disturbed by the flame because it is subsonic.
- Detonation: the flame front is characterised by a strong coupling between an incident shock wave and a chemical reaction zone. Supersonic in relation to the fresh (undisturbed) mixture, the shock wave initiates chemical reactions through the heating generated by the compression of the medium. The ensuing release of chemical energy maintains the leading shockwave. In front of the shock, the mixture is not disturbed by the reaction.

The instability of deflagration can generate disturbances in the fresh mixture that can accelerate the flame by various mechanisms. It is then possible to switch from deflagration to detonation, a phenomenon known as Deflagration Detonation Transition (DDT).

At this stage, however, it is essential to remember that in the industry:

- deflagration is the situation most often encountered,
- detonation is only observed with the most reactive species, such as hydrogen, and often under specific conditions of initiation, turbulence or confinement (for example, in the case of initiation by an intense explosion rather than a spark, in a turbulent jet from a pressurised tank, or in a long pipe following the gradual acceleration of the flame).

Let us go back to the equation for methane combustion in oxygen:



It can be seen that one mole (or volume) of CH_4 reacts with 2 volumes of O_2 . For a complete reaction, we can deduce that twice as much oxygen as methane is needed, i.e. 33% methane for 67% oxygen. Assuming that air contains 20% oxygen, one volume of methane will react with $2 / (20\%) = 10$ volumes of air. The methane explosion should, therefore, proceed optimally in the air if this proportion, known as stoichiometric, is respected. Intuitively, we understand that if we deviate from this, the reaction, if it remains possible, will be incomplete, either because of a lack of fuel (we then speak of a "lean" mixture) or because of a lack of oxidant (and therefore an excess of fuel, we then talk of a "rich" mixture). This limits the mixing of species and, thus, limits the formation of the explosion. Not only must the combustible and oxidising species be mixed, but they must also be mixed in adequate proportions. In practice, for gases, the highest combustion speeds are obtained for rich mixtures in CNTPs, containing an excess of fuel of the order of 5 to 10%.

Containment is not strictly necessary for an explosion, especially for the reactions that quickly enflame. Nevertheless, it is often an aggravating factor in an explosion, which is why it is included in the hexagon. The reason is that the flame temperature for the same mixture under the same conditions will be higher in a confined space than outside. Roughly speaking, the mass heat release Q_m is a function of the heat capacity of the gas and the temperature delta of the reaction:

$$Q_m = C * (T_{\text{après}} - T)_{\text{avant}} \quad \text{Equation 1}$$

Q_m is determined by thermodynamics. In an enclosure, the heat capacity of the gas at constant volume C_v is used for C . Outside, the heat capacity of the gas at constant pressure C_p must be used, which is higher than that at constant volume (e.g. for air $C_p/C_v = 1.4$). Consequently, the temperature reached in a confined environment is higher for the same reaction. The equations of state for gases establish a proportionality between temperature and pressure: a higher temperature also means greater pressure effects. This confirms the aggravating impact of confinement on the effects of an explosion. Beyond the purely thermodynamic aspect, in a confined space, practically all the internal energy of the reaction is converted into pressure via the expansion of the hot gases. In contrast, with no or partial confinement, the distribution of the combustion energy is no longer the same. It is achieved via phenomena of variable characteristic durations. In addition to producing hot gases, pressure waves are emitted, and gases are set in motion so that less than 10% of the reaction energy is converted into pressure energy.

3.1.2 The hexagon of the explosion

To summarise the previous paragraph, to observe a confined explosion of a fuel, whether gas, dust, aerosol or a hybrid mixture, the following six conditions must be present:

- 1) containment,
- 2) a fuel,
- 3) suspension of combustible material in this containment,
- 4) an oxidiser, usually oxygen from the air,
- 5) a mixture of fuel and combustibles in such proportions that an explosion is possible; this is known as the explosive range,
- 6) a source of ignition strong enough to trigger the explosion.

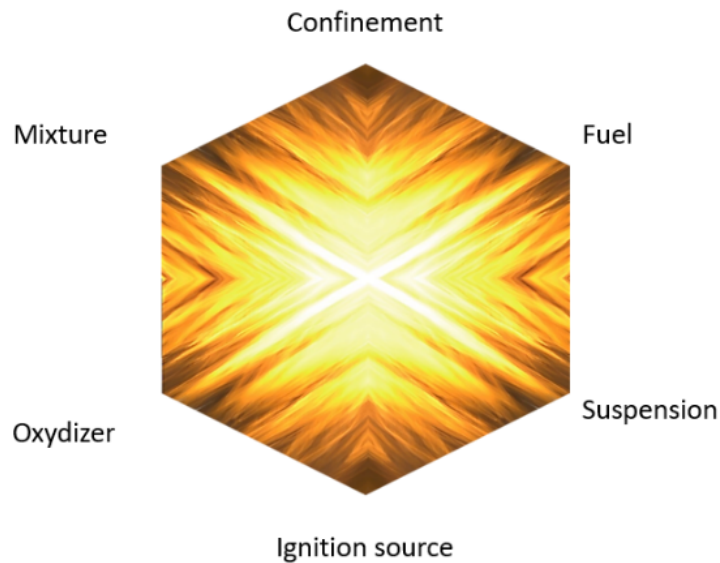


Figure 6. Hexagon of the explosion

3.1.3 Types of explosive mixtures

There are several different types of explosive mixtures: air may be mixed with a combustible gas (methane, hydrogen, etc.) or dust (coal, flour, wood, etc.). In this case, we are talking about ATEX Gas or ATEX Dust. These two main types are the best known, but there are others, such as the suspension of droplets of a combustible liquid (acetone, for example) or a mixture of gas and dust, as in mines, where a hybrid mixture of coal and methane can be observed.

In this case, we are mainly concerned with confined gas explosions. The specific features of other explosive atmospheres are not the main focus of this report and are only touched on marginally.

3.1.4 Ignition limits

Not only is the mixing of fuel and oxidant a necessary condition, but it must also be carried out in proportions that are adequate for the propagation of the explosion.

Thermodynamics indicates a reaction is possible when a fuel and an oxidiser are mixed, provided they receive adequate activation energy to initiate the reaction. In practice, a thermodynamically possible reaction is always limited by chemical kinetics. Experimental measurements show that flame speeds are largely influenced by the concentration of combustible species in their oxidant. Outside certain concentration limits, flame propagation is impossible. In air, under normal conditions of temperature and pressure (NTP), this is referred to as the lower explosive limit (LEL) or upper explosive limit (UEL). These limits can be measured experimentally or estimated using models of varying complexity (see, for example, the work of Albahri (2003) or Addai (2016)). The stoichiometry of a reaction of a compound whose formula is known can be calculated by balancing the reaction equation, as was done for methane in paragraph 3.1.1. Andrews and Phylaktou (2010) provide simple methods for estimating the concentration value at stoichiometry for more general cases of gases, hydrocarbons or dusts.

Table 1 shows some of these explosive limits and the stoichiometric concentrations for gases commonly encountered in industry.

Gas	LEL	UEL	Stoichiometry
Methane	5	15	9,5
Ethane	3	15,5	5,6
Propane	2,1	9,5	4,0
Butane	1,3	8,5	3,1
Hydrogen	4	75,6	29,5
Cyclohexane	1,2	8,3	2,3
Ammonia	16	25	22
Acetylene	2	80	7,5

Table 1. LEL, UEL and stoichiometry of common combustible gases in air (NTP)

Some gases, such as methane, have a relatively small explosive range, while others, such as acetylene, have a very wide range. Generally speaking, however, the LEL for hydrocarbons is around half the stoichiometric value.

The INRS produces and distributes a database devoted to gases and vapours. It contains information, including LEL and UEL values for over 1,000 gaseous substances: <http://www.inrs.fr/publications/bdd/caratex.html>.

These limits depend on temperature and pressure conditions. The following graph shows the LEL of hydrogen in air under different conditions:

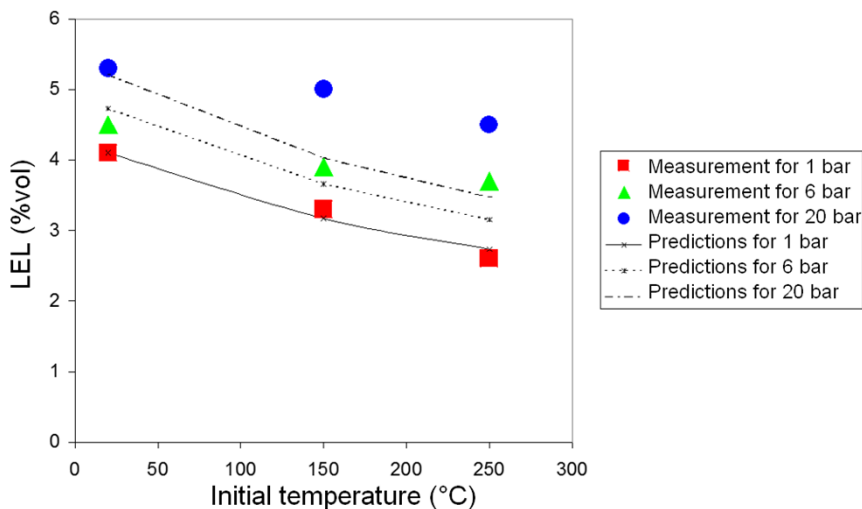


Figure 7. LEL for hydrogen in the air as a function of temperature and pressure

By definition, the LEL or UEL corresponds to a measurement in air. In an industrial process, the fraction of oxygen in the atmosphere surrounding the fuel can vary and alter these limits. If there is less oxygen, the explosive range decreases. If, on the other hand, there is an excess of oxygen (compared with air), a wider explosive range is expected. However, there is also a dependence on temperature and pressure, which can also shift the explosive range in both directions.

3.1.5 Sources of ignition

The role of the ignition source is to initiate the explosion. A variety of phenomena can cause ignition, but two main categories of ignition source are recurrently mentioned in accident analyses:

- Electrical sources:
 - sparks and Joule effect heating induced by electrical equipment,
 - sparks generated by static electricity.
- Areas where temperatures are rising:
 - Mechanical sources include intense friction (e.g. a jammed roller on a large conveyor belt, which is sometimes heated by the friction of the belt) and violent impacts of rigid bodies against the internal walls of a process.
 - Welding and grinding work carried out without taking account of the presence of an explosive atmosphere.
 - Hot zones can cover several phenomena that significantly increase a material surface's temperature (a few hundred degrees).

To characterise the ignition potential of these sources, two independent parameters are used to characterise the sensitivity of explosive atmospheres to ignition by a spark (concept of minimum ignition energy: MIE) and in a heated environment (concept of self-ignition temperature: SIT). These parameters (Table 2) depend almost exclusively on the nature of the explosive atmosphere.

Gases and vapours	Auto-ignition temperature in air (°C)	Minimum ignition energies (μJ)
Acetylene	305	17
Acetone	535	1150
Butane	285	250
Ethane	510	250
Ethylene	485	70
Hydrogen	545	17
Hexane	225	288
Methane	535	300
Methanol	460	140
Carbon monoxide	600	30
Ethyl oxide	180	200
Propane	480	240
Petrol 100/130	435	230

Table 2. Minimum ignition energies and self-ignition temperatures of certain gases (after Les Mélanges Explosifs, INRS)

The effect of the ignition source's energy on the power of the explosion is often questioned. On the other hand, if a flame arrives from another containment, a jet of combustion products can enter the enclosure and initiate the explosive cloud very violently. Cases of transition to detonation have been observed in the laboratory (Moen, 1989) for outdoor clouds initiated under similar conditions.

Experience shows that the occurrence of a "critical event", such as the leakage of a flammable fluid, does not systematically mean that the resulting flammable cloud will ignite. In the oil and gas industry, it is accepted that ignition will occur in one situation out of ten (Flauw, 2012).

3.1.6 Containment

In the context of this study, we are particularly interested in gas explosions confined within industrial equipment. We will distinguish between 2 types of equipment: enclosures with a cubic appearance and those with an elongated appearance. The enclosure in which the explosion is studied is compared to a cylinder of diameter D and length L , comparable to the actual dimensions of the equipment. To distinguish between cubic and elongated enclosures, the ratio L / D is used: less than 5 for "cubic" enclosures and more than 20 for pipes. The reason for this separation is the very different behaviour of the flames in these two situations. For the intermediate zone of L / D between 5 and 20, the choice of behaviour model is debatable and will often depend on any equipment connected to the enclosure studied.

For this study, we will use the situation of the cubic enclosure fitted with a frangible wall as a reference.

Special cases will be discussed in parallel:

- the case of two directly connected volumes,
- that of a pipeline with a high L/D ratio where a gas explosion is propagating,
- the case of the cubic enclosure connected to a discharge pipe,
- and the case of 2 cubic enclosures connected by a pipe.

3.2 Cloud formation in confined space

If necessary, the Omega 12 report will provide more details on the mechanics of gas cloud formation. In simplified terms, we consider that explosive gas in an enclosure can result from a liquid or gas leak. A puddle of flammable liquid forms a cloud by evaporation, while a gas leak forms a jet that dilutes and diffuses in the confined space. Several parameters will influence the state of the cloud, some of which are intrinsic to the chemical under consideration, such as its density or its state in relation to the pressure and temperature conditions of the enclosure. For example, in an NTP room, since hydrogen is lighter than air, it could form concentrated strata at the ceiling and poorer mixtures near the floor, whereas a dense or cold hydrocarbon vapours could form a concentrated cloud and puddle near the floor. However, these events are strongly conditioned by parameters extrinsic to the mixture, such as a flow already present in the enclosure (like forced ventilation) or strong turbulence (for example, due to a high-pressure gas leak in a non-pressurised environment).

In particular, the presence of a wall in the path of a gas jet leads to an increase in the level of turbulence. Confined jets generate more disturbed flows in their vicinity than free jets. This generally implies better diffusion of combustible species in the oxidiser and faster flames.

To go further, we can look at the work of Mecklenburgh (1986) on the evaporation of fuel puddles or that of Marshall (1983) on gas leaks in enclosures. More recently, Duclos (2019) has studied the formation of hydrogen clouds due to a leak in an enclosed space.

It is important to remember that to model the phenomena, it is necessary to know at least the size of the cloud in the containment, the reactivity of the fuel in the air (linked to the product but also to its concentration) and the level of agitation of this cloud, linked mainly to the source term (puddle, leak), the process (oxidising fluid at rest or moving) and the geometry of the containment (characteristic dimensions, presence or absence of obstacles, associated volumes, etc.).

3.3 Flame propagation under deflagration conditions

As indicated in paragraph 1.3, the typical situation is a flammable gas leak in a confined or semi-confined space, which forms a combustible reactive-air mixture in the enclosure. A suitable ignition source ignites the cloud, and a flame spreads from the ignition point.

According to the phenomenology described in paragraph 1.3, the greater the rate of thermal expansion of the combustion products and the greater the rate of transformation of the reactants into combustion products, the greater the effects of the explosion.

When an explosion occurs, flames can spread in two different ways: detonation and deflagration.

In the deflagration regime, the combusting species heat the fresh reactants, providing them with the activation energy required for combustion. This is the most common situation of interest here. Synthetically, the flame is an interface that transforms cold reactants into hot, burnt products. The reaction is not instantaneous, as the reactants are heated by diffusion processes before being converted into burnt products, at speeds that depend on the flow and chemical kinetics, among other factors. We can, therefore, define the characteristic lengths of the flame: a thermal thickness δ_L in which we go from the temperature of the reactants to that of the burnt products or a reaction thickness δ_R , shorter in which the reactants are transformed into burnt products.

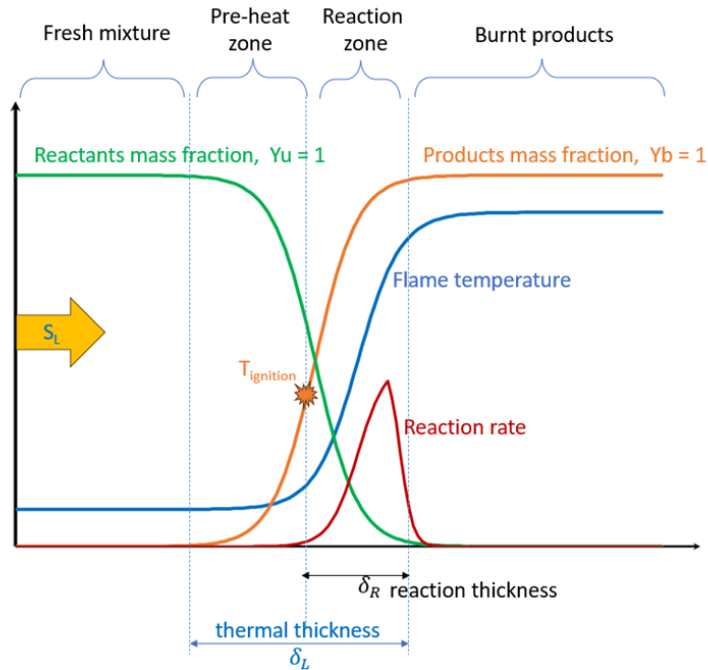


Figure 8. Diagram of flame propagation in deflagration mode

The detonation regime is a special case, described in paragraph 3.6. The major difference is that, in this case, the reactants are preheated by a shock wave, which is immediately followed by a reaction front. The models used in this case regularly consider a reaction thickness of zero, a simplifying assumption that is well suited to this case but often unsuitable for modelling deflagrations.

3.3.1 The expansion rate of combustion products

In principle, the rate of expansion by volume, α of the fluid particle through the flame is a thermodynamic parameter that depends only on the amount of heat released by combustion expressed, for example, through the application of the first principle of thermodynamics:

$$\alpha = \frac{\rho_0}{\rho_b} \approx \frac{T_b}{T_0} = \frac{\Delta H_{comb}}{c_p \cdot T_0} + 1 \quad \text{Equation 2}$$

where:

- ΔH_{comb} is the enthalpy of reaction (combustion) at T_0 expressed per unit mass of mixture;
- T_0 and T_b are the temperatures of the reactants and combustion products, respectively, assuming an adiabatic reaction;
- ρ_0 and ρ_b the densities of the reactants and combustion products respectively;
- c_p the average mass-specific heat of the combustion products.

In this sense, it is a fundamentally "intrinsic" parameter which depends only on the composition of the mixture and little on how the flame propagates. It is typically between 5 and 8 for common hydrocarbons mixed with air. Figure 9 illustrates the evolution of the expansion rate of burnt gases as a function of the composition of the mixture.

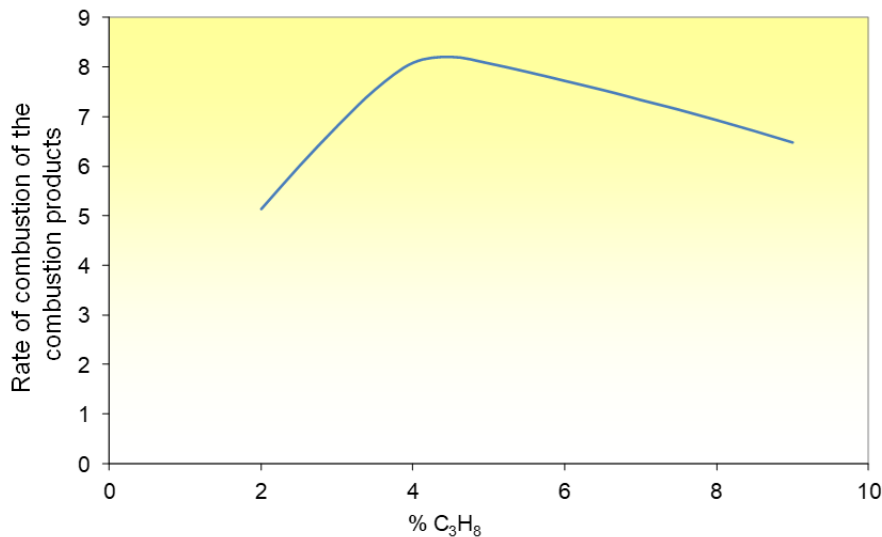


Figure 9. Example of the expansion rate of flue gases as a function of propane concentration

3.3.2 The velocity of combustion

By definition, the combustion rate is the velocity at which the flame advances relative to the reactants. It is convenient to consider it as the rate of consumption of the reagents expressed in m³ of mixture consumed per m² of flame surface per unit of time.

In the context of confined explosions, the flame can have different geometries, depending in particular on the shape of the confinement, the flow already present if the mixture is not at rest, and the ignition source (nature and location). There are more straightforward cases in which we consider a sphere expanding from the centre of the enclosure or a half-sphere propagating from an edge².

In a gaseous premix that is perfectly quiescent (undisturbed), the combustion products transfer heat to the reactants by thermal conduction (Lewis & von Elbe, 1987). Combustion obeys the classical laws of thermo-kinetics (thermodynamic equilibrium, Arrhenius laws). As all these parameters are intrinsic properties of the mixture, the combustion velocity must also be an intrinsic property of the mix. This laminar combustion velocity, or "fundamental flame velocity", S_{lad} , plays a central role in combustion processes. In a reference frame attached to the flame, this is the speed at which the reactants penetrate the flame front. A physical equation establishing the link between chemical kinetics and the thermomechanical properties of the fluid at the flame front was proposed by Zeldovitch (1980):

$$S_{lad} = \sqrt{\frac{2 \cdot \lambda \cdot Le \cdot Z \cdot R \cdot T_u^2 \cdot \exp\left(\frac{-E_a}{R \cdot T_b}\right)}{\rho_u \cdot E_a \cdot c_p \cdot (T_b - T_u)}} \quad \text{Equation 3}$$

With λ the thermal conductivity, the Lewis number (ratio of the thermal and mass diffusivities at the flame front), Z the pre-exponential factor of the Arrhenius reaction, R the gas constant, ρ the density, T the temperature, and E_a the activation energy of the reaction. Subscripts u and b refer to fresh (unburnt) and burnt gas. There are no external parameters, such as the geometry of the containment; S_{lad} is indeed an intrinsic property of the combustible mixture.

Table 3 gives some values of S_{lad} for some gases commonly encountered in industry (NFPA 68 version 2002). For methane, S_{lad} is of the order of 0.4 m/s. It is 0.46 m/s for propane and 3.3 m/s for hydrogen in quasi-stoichiometric combustion in air.

² Depending on the nature and location of the ignition source, there may be a hot surface on a wall or an isolated spark in the volume. On the other hand, if there is a particular flow in the enclosure, or if the flame arrives from connected equipment, it may be necessary to consider a flame surface with more complex shapes, such as a jet.

Combustible gas mixed with air in stoichiometric proportion	Laminar combustion velocity S_{lad} (m/s)
Hydrogen	3,3
Methane	0,4
Ethane	0,47
Propane	0,46
Butane	0,45
Pentane	0,46
Hexane	0,46
Heptane	0,46
Acetylene	1,66
Ethylene	0,8
Propylene	0,66
Butylene	0,51
Benzene	0,48
Cyclohexane	0,46
Ammonia	0,07

Table 3. Laminar combustion velocity³ of some gases in stoichiometric proportions with air (NFPA 68, 2002) NTP

It should also be noted that laminar flame speeds strongly depend on the concentration of the flammable cloud, as shown in Figure 10. The burning velocity is highest for concentrations close to stoichiometry ($\phi=1$) and decreases significantly as the concentration approaches the flammability limits.

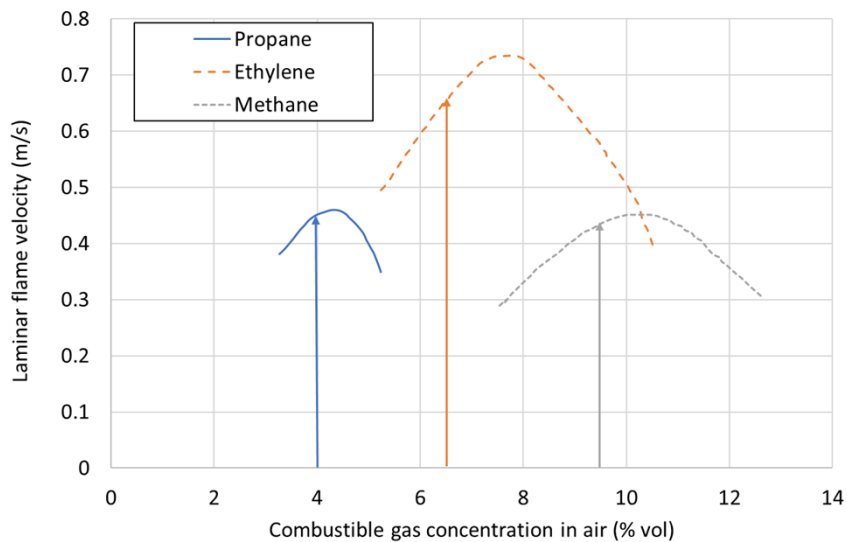


Figure 10. Evolution, of the fundamental flame velocity of some flammable mixtures as a function of the volumetric concentration C of combustible gas (Harris, 1983) CNTP

³ The values of the fundamental flame velocities (Table 3) are orders of magnitude, they may vary depending on the author.

A second characteristic parameter of the laminar flame is the thickness of the flame front, traditionally defined as the ratio between the thermal diffusivity α_{th} of the fresh gases and the laminar combustion velocity S_{lad}

$$\eta_0 = \alpha_{th} / S_{lad} \quad \text{Equation 4}$$

It should be noted that the laminar combustion velocity, S_{lad} , depends not only on the fuel richness but also on the pressure and temperature conditions, according to an empirical law (Andrews & Bradley, 1972):

$$S_{lad1} = S_{lad0} \times \left(\frac{P_1}{P_0}\right)^a \times \left(\frac{T_1}{T_0}\right)^b \quad \text{Equation 5}$$

Where:

- the indices 0 and 1 are used to identify two pairs of pressure-temperature conditions,
- P_0 and P_1 are pressures in Pa,
- T_0 and T_1 temperatures in K,
- S_{lad1} is the laminar burning velocity in m/s under pressure-temperature conditions $P_1 - T_1$
- S_{lad0} is the laminar burning velocity in m/s under pressure-temperature conditions $P_0 - T_0$
- a and b are exponents such that $-0.5 < a < 0.5$ and $1 < b < 3$ in the case of hydrocarbon-air mixtures.

In practice, the surface of the flame front is most often highly convoluted, covered with transient structures that increase the average surface area of the reaction compared with an undisturbed situation where the flame would be a smooth interface. To take account of this specificity, the flame is said to be turbulent. Statistical relationships link the "turbulent combustion velocity" to the laminar combustion velocity corresponding to the undisturbed situation (Proust, 2004).

3.3.3 Flame propagation velocity

The undisturbed flame space velocity is the product of the expansion rate α of the combustion products and the laminar flame velocity (Harris, 1983):

$$V_f = \alpha \times S_{lad} \quad \text{Equation 6}$$

The undisturbed flame is an ideal situation encountered mainly in laboratory conditions. During an industrial explosion, the flame is disturbed. It wrinkles and deforms, increasing its surface area and propagation velocity. Equation 4 then becomes:

$$V_f = \alpha \times \frac{A_t}{A} \times S_{lad} \quad \text{Equation 7}$$

Where:

- A_t is the actual flame surface,
- A is the undisturbed flame surface.

The challenge, therefore, lies in assessing the deformation of the flame and its surface variations. However, this is often very tricky. To overcome this difficulty, the evolution of flame surfaces is masked by calculating a so-called "turbulent" flame velocity. Thus, Equation 7 becomes:

$$V_f = \alpha \times \frac{A_t}{A} \times S_{lad} = \alpha \times S_t \quad \text{Equation 8}$$

As indicated in paragraph 1.3, the increase in pressure in the completely or partially confined enclosure between two successive instants is proportional to the volume of gas produced by combustion reduced by the volume of gas released to the outside through any openings. To convert the turbulent flame propagation velocity into the burnt gas production rate, this velocity is multiplied by the estimated surface area A of the flame front (which, in many models, is considered a sphere or half-sphere, as mentioned in paragraph 3.3.2).

Determining the flame area A and its turbulent velocity S_t is a critical problem, as knowledge of these parameters is often necessary to estimate the effects of the explosion.

3.4 Flame disturbances

Flame disturbances have a strong influence on the turbulent velocity St and can be linked to:

- combustion instabilities,
- to flow-induced disturbances such as turbulence,
- obstacles in its path,
- concentration gradients in flammable clouds.

3.4.1 Natural" flame disturbances: Combustion instabilities

In practice, the smooth laminar flame is difficult to observe in industrial situations. Experimental observations show (Lewis & von Elbe, 1987) that the propagation of a gaseous premixed flame is generally accompanied by vibratory or unsteady phenomena commonly referred to as "combustion instabilities".

One of the effects of these disturbances is to modify the shape of the flame, which rapidly takes on a pleated, cellular structure, which has the effect of significantly increasing the surface area of the flame compared with that of the laminar, perfectly spherical front, and thus increasing the rate of combustion (Figure 11).

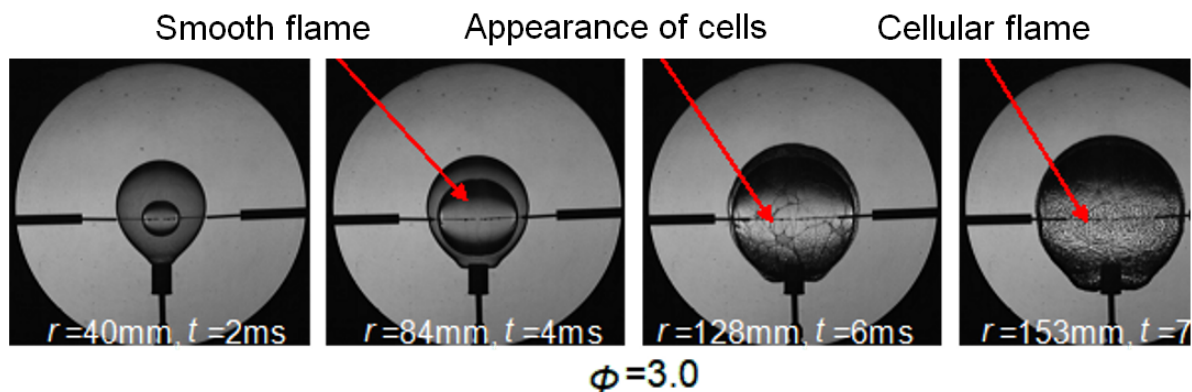


Figure 11. Illustration of the cellular structure of a flame (hydrogen/air mixture - richness equal to 3 - from Mogi, 2010)

On an industrial scale, the predominant instability mechanism is probably the hydrodynamic instability highlighted by Darrieus and Landau (Darrieus, 1938; Landau, 1944). Under this mechanism, a bulge in the flame front that penetrates the reactants increases in amplitude under the combined effect of thermal expansion of the combustion products and flame propagation (Figure 11).

The model proposed by the two authors describes a premixed flame as a surface separating fresh and burnt gases. The non-reactive flow equations govern the flow on either side of the surface. The flame propagates in a direction normal to its surface at a constant velocity. Jump conditions link the variables on both sides of the flame. Conservation of mass and momentum is ensured. According to this model, the flame is unconditionally unstable, and the perturbations grow indefinitely as the wavelengths decrease, which is inconsistent with experimental observations. Markstein (1964) improved the flame propagation model and introduced interactions with the flow. The flame speed is no longer constant but varies as a function of the radius of curvature of the flame. In particular, he demonstrated the cellular structure of flames.

More recent experiments (Bradley, 2001; Gotsintev, 1989; Daubech, 2006) strongly suggest that these unconditional instabilities could be responsible for the self-acceleration of the flame even when the initial mixture is at rest and far from any wall that could interact with the combustion front. They also confirm the rate of acceleration of combustion obtained from earlier experiments (Lannoy, 1989), which show that the rate of increase in combustion speed under the effect of hydrodynamic instabilities alone is of the order of 3 but varies as a function of the size of the explosive cloud (Figure 12).

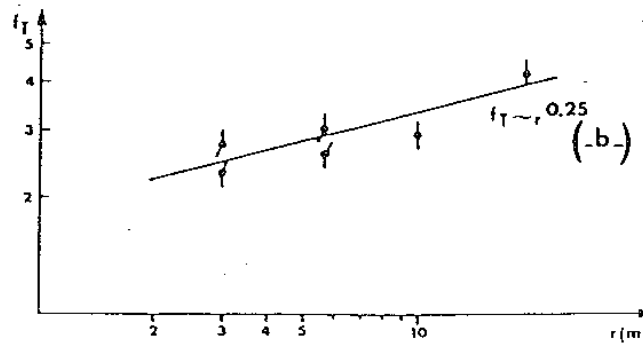


Figure 12. Flame speed as a function of distance, spherical explosion of stoichiometric air-hydrogen mixtures according to (Drenckhahn & Koch, 1985)

The complete analytical resolution of this phenomenon remains difficult. However, Joulin or Bychkov and Libermann (Joulin, 1991; Bychkov & Libermann, 2000) propose, for an axisymmetric flame in 3 dimensions and for disturbance diameters much larger than the flame thickness, to express the flame propagation velocity U_{LD} in relation to the reactants as follows:

$$U_{LD} = \left(1 + 4 \cdot \alpha \cdot \frac{(\alpha - 1)^2}{(\alpha^3 + \alpha^2 + 3 \cdot \alpha - 1)} \right) \cdot S_{lad} \quad \text{Equation 9}$$

For an expansion ratio α of the order of 8 as for a stoichiometric propane/air mixture, we obtain:

$$U_{LD} = 3.8 \cdot S_{lad} \quad \text{Equation 10}$$

The factor of 3.8 is consistent with the graph shown in Figure 12.

There are other types of instability (Rayleigh-Taylor instability, (Rayleigh, 1883 and Taylor, 1950) thermodiffusive instability) which can be superimposed on the hydrodynamic instability (Proust, 2004). Later work by Markstein (1964), such as that by Sivashinsky (Sivashinsky, 1977), Matalon and Matkowsky (Matalon & Matkowsky, 1980), and more recently, Glas (Glas, 2001), was the subject of a new analysis in 2008 (Daubech, 2008). They led to the proposal of non-linear flame behaviour equations that capture the various flame instabilities (Rayleigh-Taylor, thermo-diffusive, etc.) and propose stability criteria, including those in highly non-linear regimes (Dold & Joulin, 1995). This work showed that the degree of coupling between the flame and its environment was particularly strong. It is possible to predict this increase in U_{RT} using a generalised Taylor stability model (based on the behaviour of a reactive interface subjected to acceleration):

$$U_{RT} = \left(0.51 \cdot \sqrt{\frac{\alpha - 1}{\alpha} \cdot \eta \cdot r} \right) \cdot S_{lad} \quad \text{Equation 11}$$

Where α is the expansion rate of the combustion products, S_{lad} is the laminar flame velocity, η the flow acceleration, and r is the characteristic radius of curvature of the flame.

3.4.2 Flame disturbances induced by flow turbulence

3.4.2.1 Turbulent flow

Two flow regimes are commonly distinguished in fluid mechanics: laminar flow and turbulent flow. The boundary between the two states is characterised by the Reynolds number, defined as follows:

$$Re = \frac{U \cdot L}{\nu} \quad \text{Equation 12}$$

With U , the characteristic velocity of the flow; L , the characteristic dimension (e.g. the diameter of a pipe or an obstacle in the flow); and ν , the kinematic viscosity of the fluid.

This number reflects the ratio between the inertial forces and the viscous forces: in a low Reynolds flow (< 2000), the flow is laminar, and we observe few disturbed streamlines around obstacles (Figure 13 left). In very high Reynolds flows ($> 10^5$), vortices are observed, and the flow is highly disturbed (Figure 13 right).

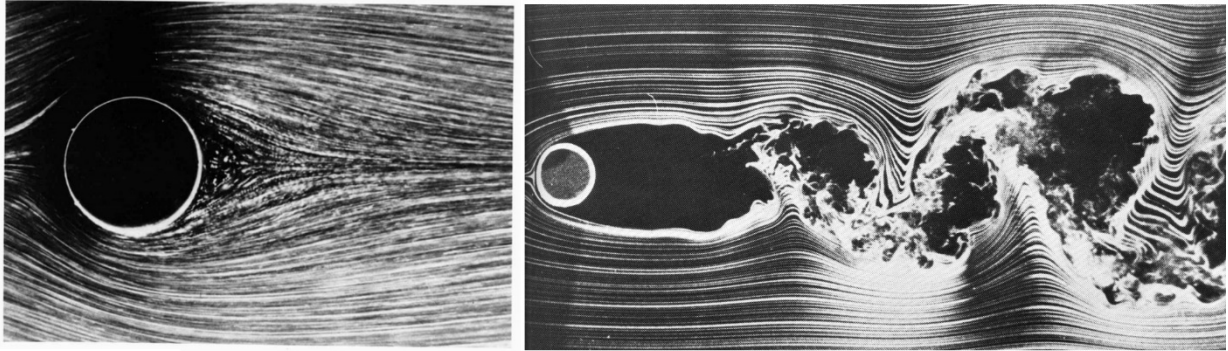


Figure 13 Trailing edge behind a cylinder in a viscous fluid. Left: laminar flow at $Re = 9.6$, photo by Sadatoshi Taneda; right: turbulent flow at $Re = 10000$, photo by Thomas Corke and Hassan Nagib.

Turbulent flow is characterised by the appearance and disappearance of vortices within the velocity field, often described as the sum of an average component and a fluctuation, usually noted u' . Vortices result from the sliding of fluid layers between them, which if the velocity gradient is large enough, leads to the appearance of "waves" and then "rollers". These large flow structures, which themselves generate velocity gradients, break up into smaller and smaller vortices until, in the end, molecular viscosity dissipates this vorticity into heat: this is the turbulent cascade. This cascade is usually considered to be in equilibrium, so it is sufficient to characterise the largest turbulence structures to define the turbulence field (Hinze, 1975). The integral scale of turbulence, L_t , is the characteristic dimension of large eddies, while u' , the intensity of velocity fluctuations, characterises the speed of rotation of these structures.

The fact remains that these two quantities are of considerable importance in the field of combustion: the flame is an interface of zero mass subject to the movements of the fluid. If the agitation is greater, then the velocity of the flame also becomes greater. There are various models for predicting these two macroscopic quantities. The most widely used is the "k - ϵ " model: the variable k corresponds to the turbulent kinetic energy, and the variable ϵ to the dissipation of this energy. An approach of this type has been proposed by Proust (2009). However, this model can only describe this phenomenon for homogeneous fluid flows. It assumes isotropic energy dissipation, which is not the case in certain complex flows involving, for example, major changes in the direction of the velocity vector.

3.4.2.2 Turbulent combustion

No general theory describes the relationship of combustion with turbulence (Williams, 1985). Failing that, correlations based on dimensionless groupings are used. Their form corresponds more or less to theoretical considerations. The option generally adopted is that the fluctuations in velocity (intensity of the turbulence u') and the size (L_t) of the turbulent movements are much smaller than that of the combustion. It is accepted that the effect of "eddies" is to crease and roll up a combustion front locally characterised by its fundamental combustion velocity (S_{lad}) and its thickness (η_0 / S_{lad}).

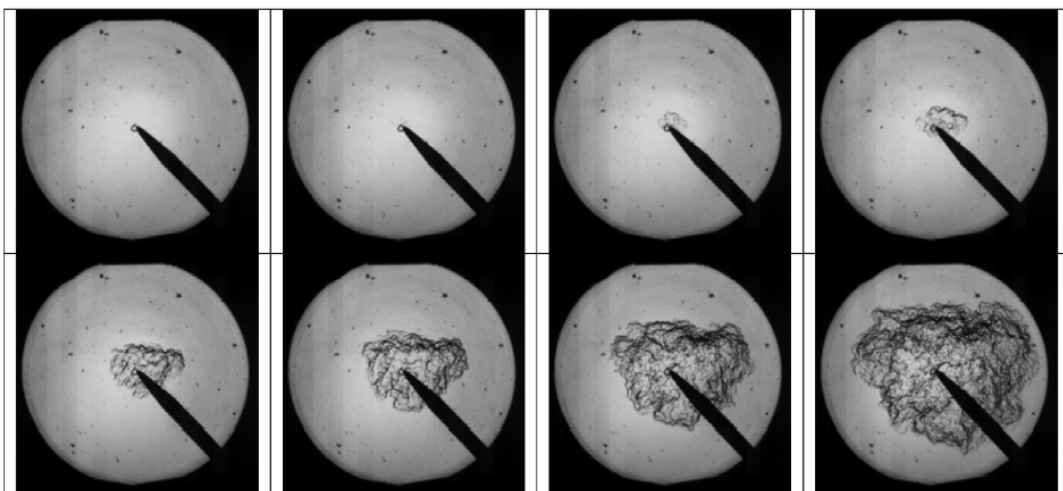


Figure 14. Example of a turbulent flame (50% H_2 - 50% CH_4) - $u' = 6$ m/s, Fairweather, 2009

A graphical representation of the different combustion regimes usually cited is shown in Figure 15.

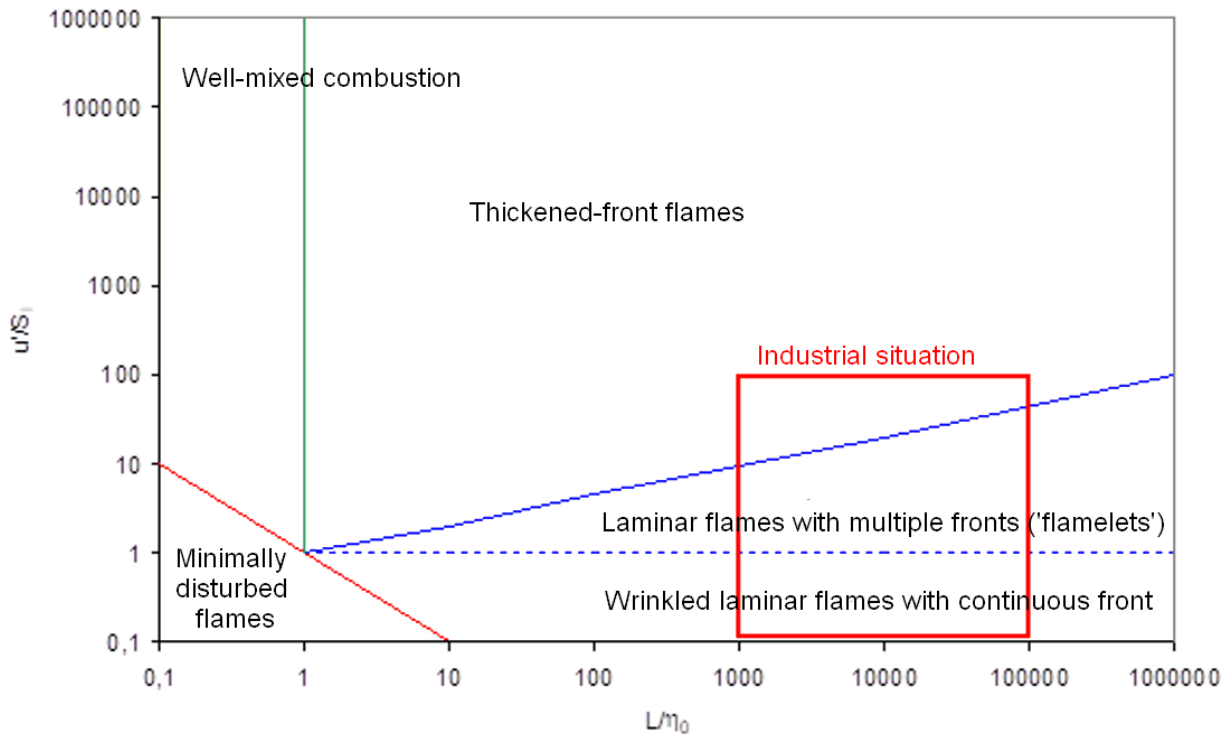


Figure 15. The different combustion regimes (Borghini, 1995 modified by Proust, 2004)

In most industrial situations, the size of the turbulent structures is much larger than that of the flame ($10^3 < L_t / \eta_0 < 10^5$) and the relative intensity of the turbulence u'/S_{lad} is smaller than 100. Under these conditions, the structure of the turbulent flame can be considered to be that of a laminar front that rolls up into the eddies (Proust, 2004), which increases the flame surface area and the combustion rate. Numerous authors (Abdel-Gayed, 1987; Bray, 1990; Gülder, 1990) have sought to link the resulting combustion rate, S_t , to the turbulence parameters (L_t, u') and the laminar flame (S_{lad}, η_0). For the most part, they arrive at a relationship of the form:

$$\frac{S_t}{S_{lad}} = K \left(\frac{u'}{S_{lad}} \right)^a \cdot \left(\frac{L_t}{\eta_0} \right)^b \quad \text{Equation 13}$$

Where K, a and b are coefficients that are relatively independent of the mixture.

Examples include:

The Bray correlation (1990):

$$S_t = 1,8 \cdot S_{lad}^{0,784} \cdot u'^{0,412} \cdot L_t^{0,196} \cdot \eta_0^{-0,196} \quad \text{Equation 14}$$

The Gülder correlation (1995):

$$\frac{S_t}{S_{lad}} = 0.62 \cdot \left(\frac{u'}{S_{lad}} \right)^{0.75} \cdot \left(\frac{L_t}{\eta} \right)^{0.25} \quad \text{Equation 15}$$

Gülder's correlation seems quite adequate for test results obtained on a small scale ($1 < L_t < 50$ mm).

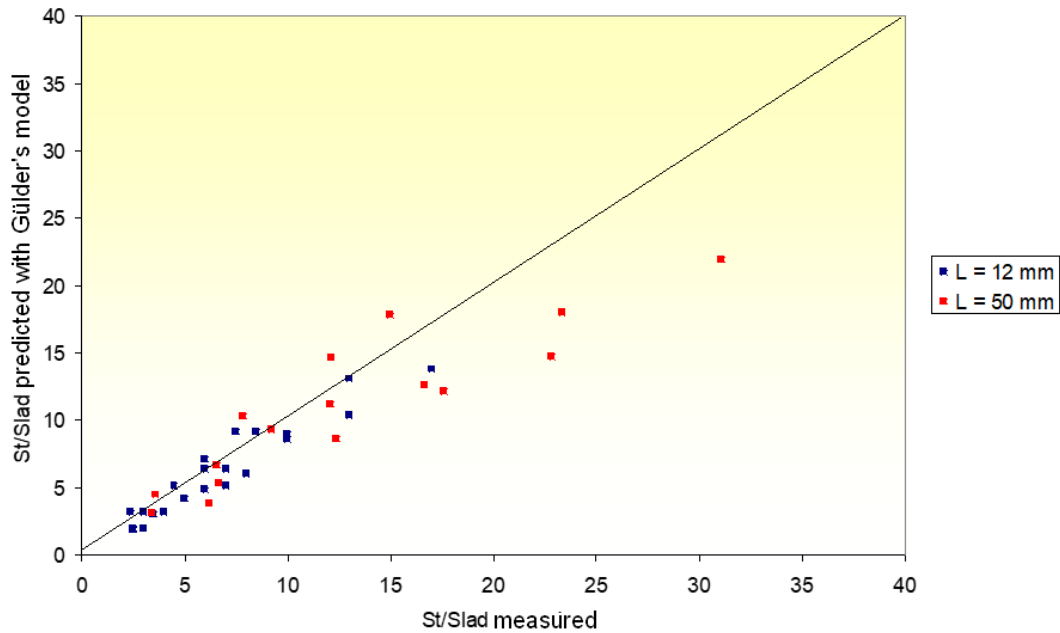


Figure 16. Comparison of combustion rates measured and calculated by the Gülder model for air-methane mixtures - $L_t = 12$ mm and 50 mm

While Gülder's correlation seems reasonably well suited to the cases presented here, it should nevertheless be borne in mind that it is only one example among dozens of other models. In 2013, Dahoe published an evaluation of 40 different models for calculating the turbulent flame velocity, S_t , from the fundamental flame velocity, S_l , measured in a sphere of 20 l for hydrogen-air and methane-air mixtures.

As part of its research into the physics of flames, INERIS is studying the link between the turbulence parameters u' and L_t and the turbulent flame velocity S_t , based on the available knowledge of flame instability, mentioned in paragraph 3.4.1. In particular, this work has led to the development of a model based on the composition of 2 velocities (Daubech, 2008):

- The burning velocity affected by the natural instabilities of the flames due to the expansion of the burnt products (Landau-Darrieus hydrodynamic instability), which is given by (Joulin, 1991 and Bychkov, 2000):

$$U_{LD} = \left[1 + 4E * \frac{(E - 1)^2}{(E^3 + E^2 + 3E - 1)} \right] * S_{lad} \quad \text{Equation 16}$$

- The combustion velocity increased by the folding of the flame due to the lower density of the burnt products which penetrate the fresh gases (Rayleigh-Taylor instability) which is given by (Bychkov, 2000):

$$U_{RT} = 0.51 * \sqrt{\left(\frac{E - 1}{E} * \eta_{acc} * r \right)} \quad \text{Equation 17}$$

Where:

- η_{acc} is the acceleration of the flow,
- r is the radius of curvature of the flame.

In the case of turbulent flow, the acceleration is typically $\eta_{acc} = u'^2 / L_t$ and the radius of curvature of the flame r is of the order of half the height of the enclosure (assuming ignition at half-height at the bottom or centre of a cubic or cylindrical containment with an L/D ratio of the order of 1 - 2).

Then, it is possible to determine the burning velocity U_{Comp} as the composition of the two previously calculated speeds U_{LD} and U_{RT} .

$$U_{COMP} = \sqrt{U_{LD}^2 + U_{RT}^2} \quad \text{Equation 18}$$

Duclos (2019) compared the flame space velocity (the velocity seen by an outside observer, typically of the order of the product $S_t \cdot E$, with the effects of mixture compressibility taken into account) with the value of U_{COMP} obtained with this model on tests carried out at INERIS:

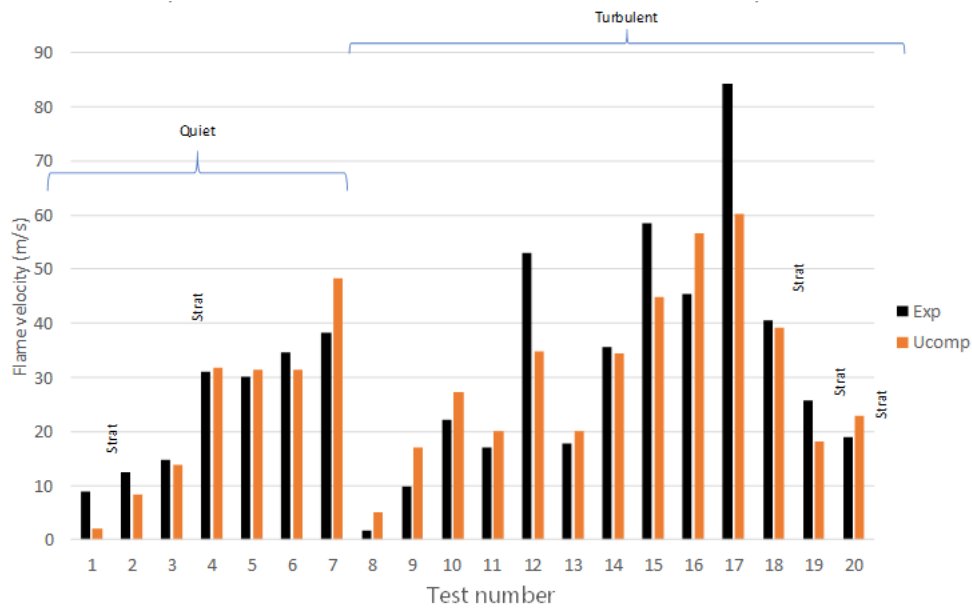


Figure 17. Comparison of U_{COMP} with experimental measurements

The agreement with experiments is satisfactory. By dividing U_{COMP} by E , we obtain an estimate of St .

3.4.3 Flame distortion caused by obstacles

On an industrial site, a flammable cloud formed by the accidental release of a combustible product develops and disperses inside an enclosure as it does outside in an environment where there may be many obstacles. When the flame bypasses an obstacle, if the flow velocity is sufficient, a turbulent wake develops downstream of the obstacle, likely to increase the combustion rate.

According to Zeuwen (1983), as soon as the Reynolds number exceeds 100 to 200, a "wake" zone forms downstream of the obstacles. This critical Reynolds number is exceeded for industrial obstacle sizes as soon as the flame propagates at a few m/s, i.e., systematically.

In the wake of obstacles, a specific velocity field appears with a zone where the flow stops at the vanishing point. As the wake moves along the axis, the velocity deficit with the peripheral flow decreases. The resulting velocity gradients are responsible for the appearance of wake turbulence.

According to Hinze (1975), the turbulence field resembles that of a jet, where u' is maximum on the axis and is about 20% of the velocity deficit on the axis. Furthermore, L_t varies in $(D \cdot x)^{1/2}$ (D is the diameter of the obstacle and x the distance along the axis in the wake). When this data is entered into the turbulent flame velocity formula (Equation 19), we obtain a turbulent combustion velocity, which can be compared with the flame velocity by multiplying S_t by the expansion rate. The result is an expression like:

$$\frac{V_{fwake}}{V_{f0}} \approx 2.\alpha. \frac{D^{1/2}}{V_{f0}^{1/4}} \quad \text{Equation 19}$$

The accelerator effect is pronounced at low-velocity levels, typically of the order of 5 for a flame velocity of 10 m/s and seems to decrease as the flame velocity increases (3 for $V_{f0} = 100$ m/s). Does this mean that this effect is dominant? Another factor needs to be taken into account. At low flame velocities, the extent of the wake is minimal because the smallest scale of the vortices (the Kolmogorov scale) is quite large. The question is how to understand the circumstances whereby the flame stretching mechanism caused by the obstacle is the dominant accelerating factor rather than that induced by turbulence alone.

Numerous works exist in the scientific literature on the effects of obstacles on the development of gas deflagrations. We refer in particular to the work of Zeuwen (1983), Hjertager (1988), Phylaktou (1991, 1994), Rzal (1992); Bjerketvedt (1983), Proust (2004), Duclos (2013)... This list of recommendations is not exhaustive, as many other researchers have worked on this subject, which remains a major theme in explosion physics research today.

3.4.4 Effects of heterogeneities in cloud richness

This subject has been examined experimentally at INERIS by Daubech (2004, 2008) on two scales. The smallest was a transparent tube with a square cross-section (3 cm x 3 cm), 2 m long, capable of withstanding a transition to detonation (over 100 bar). The second is a tunnel at the INERIS experimental site, 140 m long with a cross-section of around 9 m².

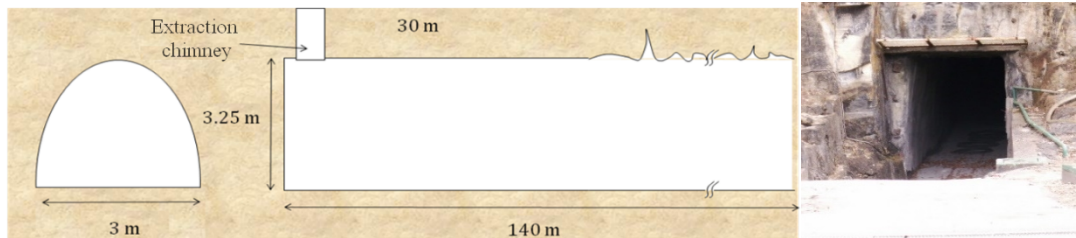


Figure 18. Diagram and photo of the entrance to gallery G1 at INERIS

Explosions of homogeneous and heterogeneous gas mixtures containing on average the same quantities of gas and, therefore, the same combustion energy were compared on these two installations. Further details on the experimental configurations used are available in the publications associated with this work or in the Ω -UVCE report on unconfined explosions.

In these heterogeneous mixtures, we systematically observe (Daubech, 2009) an increase in flame velocity in the concentration gradient. In small-scale tests, the vertical concentration gradient increased flame propagation velocity by a factor of 1.6 compared with the flame entry velocity in the gradient zone.

On a large scale, at the end of propagation, we obtained a flame 3.6 times faster and pressure effects 4 times greater with the heterogeneous mixture despite having the same average gas concentration in the 2 cases. In both cases, the generalised Taylor model (Equation 11) can be used to find the order of magnitude of the flame acceleration factor.

It is important to note that the tests also revealed an amplification of the effects of the explosion, linked to an acoustic coupling between the flame and the tube in which it propagates. More information on the behaviour of flames in tubes is presented in sections 3.5.4 to 3.5.6.

3.4.5 Summary of flame disturbance modes

It is important to remember from the four previous paragraphs that the flame, during its development, undergoes various disturbances which are inevitable and can have various origins, linked in particular to:

- the geometry of the containment and its possible congestion,
- the flow before the explosion,
- the flow generated by the explosion,
- and the state of agitation and concentration of the fuel mixture.

Estimating the effects of an explosion, therefore, requires knowledge not only of the reactivity of the explosive mixture but also of numerous extrinsic parameters, such as the state of the cloud, the level of turbulence, and the geometry of the containment, all of which are likely to change during the explosion.

3.5 Pressure generation

3.5.1 Fully enclosed volume

This is based on the reference situation of a completely closed containment, filled with a quiescent explosible gas cloud, in the absence of obstacles and ignited by a source of ignition sufficiently strong to trigger the explosion without reaching the detonation regime. (limit case briefly described in paragraph 3.6).

If we look at the overpressure measured in the enclosure as a function of time, we obtain a S-shaped curve like that shown in Figure 19:

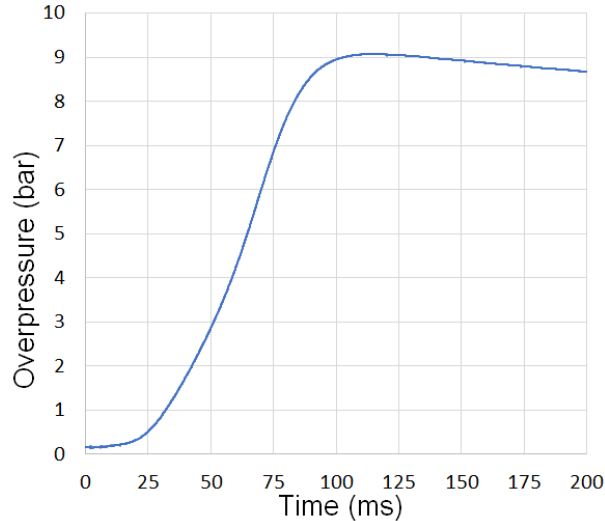


Figure 19. Pressure curve recorded during an explosion in a closed volume of 1 m³

One of the essential parameters for characterising this curve is the turbulent flame velocity, which is difficult to determine directly (Proust, 1988, 1993). The explosion is usually associated with adiabatic compression of the gases in the closed vessel. The equation of Lewis and Von Elbe (1987) describes this phenomenon; in practice, it is a modified version of Laplace's law of perfect gases:

$$\frac{1}{P} \frac{dP}{dt} = \gamma \cdot \frac{Q_+}{V} \quad \text{Equation 20}$$

where P, V and γ are the pressure in the enclosure, its volume and the ratio of the specific heats of the gas mixture and Q_+ is the volume flow of gas produced by combustion. This volume flow of gas produced is a function of the surface area of the flame A_f , the combustion rate St and the expansion rate of the combustion products E :

$$Q_+ = St \cdot A_f \cdot (E - 1) \quad \text{Equation 21}$$

The turbulent velocity term St has already been described in the previous paragraphs. The flame surface A_f is linked in the first moments of the explosion to the reactivity (for example, in the presence of concentration gradients) and agitation conditions of the cloud; then, as it approaches the walls of the enclosure, it becomes more strongly influenced by containment. It is often assumed that a sphere or half-sphere (depending on whether the point of ignition is at the centre or against a wall) extends into the enclosure until the walls constrain it, reaching a maximum value proportional to the enclosure's cross-section.

When the flame surface is at its maximum and the pressure in the enclosure approaches its maximum P_{max} , a maximum rate of pressure rise is reached:

$$\left(\frac{dP}{dt}\right)_{max} \approx \gamma \cdot \frac{P_{max}}{V} \cdot St \cdot A_{f_{max}} \cdot (E - 1) \quad \text{Equation 22}$$

Noting that the maximum flame area is a proportion of the cross-sectional area of the volume, which can also be written as $A_{f_{max}} \approx k \cdot V^{2/3}$ with k a constant, we can define a term K_{ex} independent of the enclosure and proportional to the combustion rates:

$$K_{ex} = \left(\frac{dP}{dt}\right)_{max} \cdot V^{1/3} \quad \text{Equation 23}$$

In this respect, " K_{ex} " depends on the nature of the fuel but is also largely a function of the other characteristics of the cloud, specifically the level of turbulence and the concentration. To measure " K_{ex} ", standard equipment is used, mainly a 20-litre or a 1 m³ chamber. The measurement of K_{ex} is accomplished in this standard 1 m³ chamber (ISO6184) following a specific procedure, one that addresses particularly the device used to mix the fuel and oxidizer and to position the ignition point. K_{ex} is then referred as K_g for gases (and K_{St} for dust explosions).

Using these scaling parameters in vent sizing, such as for vessels that are not fully closed, is legitimate if the physics represented in Equation 22 corresponds to the development of the explosion in these chambers. This scaling law is often referred to as the "cubic law".

The cubic law with experimental values of the constant K_g has often been used to predict the explosion overpressure in enclosures protected by explosion vents (Bartknecht, 1981). However, the method does not take geometric factors into account. It applies to mostly cubic enclosures ($L_{max} / L_{min} \sim 1$) but will fail for enclosures differing from the cubic shape ($L_{max} / L_{min} > 1$) because the flame front reaches the walls earlier than in spherical geometry. The cubic law will also fail for non-central ignition (Harris, 1983). A more serious flaw in using the cubic root law with an experimental value of K_g is that it includes turbulence conditions specific to the test chamber that sometimes differ significantly from real conditions. The developers of the method were probably very aware of these theoretical limitations, but the industrial situation calls for a pragmatic approach. The aim is to establish a reasonable maximum representation of the explosion risk to ensure the installations' safety. An experiment in a small test vessel gives little information about the turbulence that can develop in large enclosures due to instabilities and obstacles. Consequently, for gases, models based on laminar flame velocity are preferable to those based on K_g .

The cubic law is more widely used to measure the explosive properties of flammable dusts because a flammable dust-air mixture can only be maintained in a turbulent flow, making it particularly difficult to measure the laminar velocity of dust flames.

3.5.2 Case of an enclosure fitted with a vent

3.5.2.1 Idealized situation

We now consider the reference situation of a closed vessel, equipped with an explosion vent, filled with a quiescent explosive gas cloud, in the absence of obstacles and ignited by a source of ignition strong enough to trigger the explosion without reaching the detonation regime (a limit case briefly described in paragraph 3.6).

In the end, the maximum pressure P_{max} generated in closed explosion vessels is of little importance for explosions in vented enclosures since, generally speaking, windows, doors and walls will hold up to pressures of a hundred mbar at best, well below the P_{max} value of around 10 bar. An explosion vent can be used to prevent the destruction of the enclosures subjected to the explosion.

The role of an explosion vent is to allow gases to escape from the enclosure to limit the pressure rise due to the explosion to a reduced value, P_{red} , below the pressure P_{des} at which the enclosure is destroyed, which is itself below the maximum pressure P_{max} .

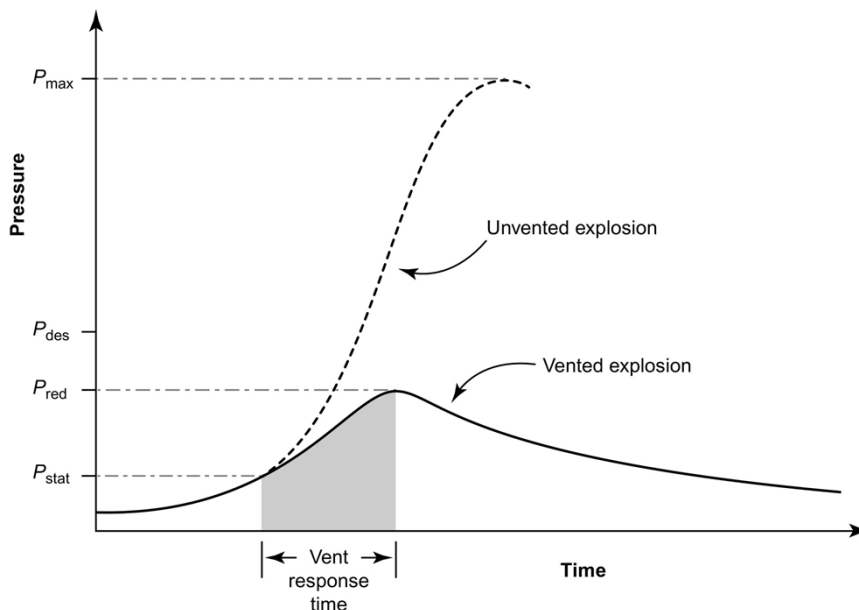


Figure 20. Illustration of the role of explosion vents, Pekalski (2005)

The increase in pressure between two successive instants is proportional to the volume of gas produced by combustion, reduced by the quantity of gas released to the outside through the openings. There is competition between what leaves the enclosure and what enters, and the pressure increase is proportional to the volume of gas produced by combustion, reduced by the quantity of gas released to the outside through the openings. Equation 20 can be rewritten:

$$\frac{1}{P} \frac{dP}{dt} = \gamma \cdot \frac{Q_+ - Q_-}{V} \quad \text{Equation 24}$$

Where Q_- is the volume flow rate of gases lost through the opening(s).

The volume flow rate of gas lost through any opening can be expressed as:

$$Q_- = C_d \cdot S \cdot V_e \quad \text{Equation 25}$$

With C_d a discharge coefficient which depends on the type of orifice, S the open area and V_e a flow velocity which depends on the state of the gases. The velocity parameter V_e , between the enclosure in state 1 and the outside in state 2, varies as a function of the ratio of the specific heats γ , the pressures P_1 and P_2 on either side of the opening (P_2 being the pressure on the outside), and the density of the mixture where the pressure is the greatest, ρ_1 .

Two flow regimes are distinguished, subsonic and shocked, depending on the number γ and the ratio of pressures P_1 and P_2 . It is assumed that mixture 1 is at a higher pressure than mixture 2 : $P_1 > P_2$.

If we have:

$$\frac{P_1}{P_2} < \left(\frac{\gamma + 1}{2} \right)^{\frac{\gamma}{\gamma - 1}} \quad \text{Equation 26}$$

Then:

$$V_e = \left(\frac{P_2}{P_1} \right)^{1/\gamma} \cdot \sqrt{\frac{2 \cdot \gamma}{\gamma - 1} \cdot \frac{P_1}{\rho_1} \cdot \left(1 - \left(\frac{P_2}{P_1} \right)^{\frac{\gamma - 1}{\gamma}} \right)} \quad \text{Equation 27}$$

Otherwise:

$$V_e = \sqrt{\gamma \cdot \frac{P_1}{\rho_1} \cdot \left(\frac{2}{\gamma + 1} \right)^{\frac{\gamma + 1}{\gamma - 1}}} \quad \text{Equation 28}$$

These equations assume that the species behave according to a ideal gas model. The model appears relatively simple when written like this. In practice, the notion of competition between gas production and its ejection through an opening implies transient, oscillatory behaviour of the gas flow. The pressure curve inside the enclosure takes a more complex form than that described in Figure 20. Harris (1983) schematised this phenomenon by presenting a diagram of the possible evolution of pressure in a vented enclosure:

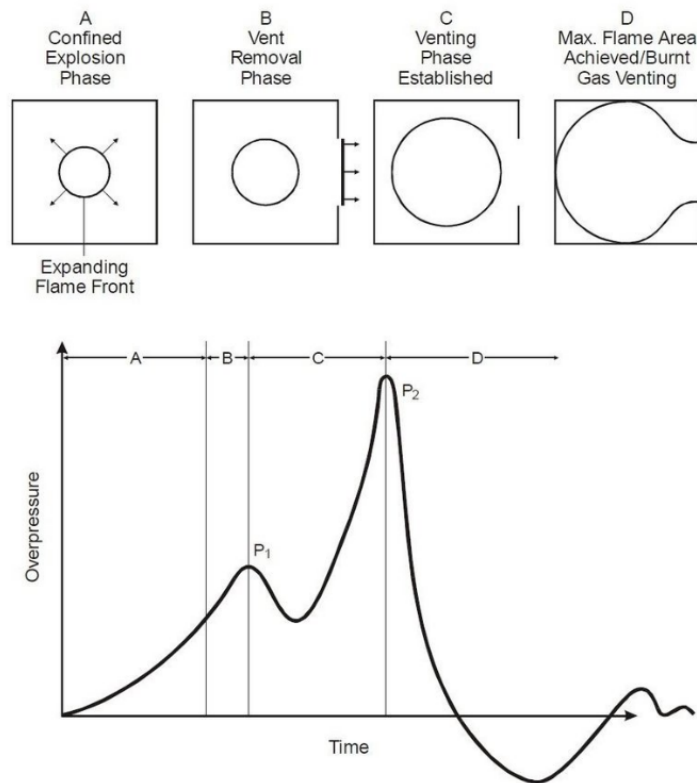


Figure 21. Illustration of the role of explosion vents, Harris (1983)

The diagram in Figure 21 shows an initial phase A, during which the flame develops in a completely confined space.

During phase B, the vent opens gradually, and the first pressure peak, P_1 , is reached. This corresponds to the vent's opening (and therefore depends on the rupture pressure of the vent and its inertia).

In this example, during phase C, this is followed by a slight decrease of pressure and then by a new pressure rise up to P_2 . The pressure decrease is due to the ejection of the fresh mixture, which occurs when the ejection rate is greater than the gas production rate due to combustion. There is competition between what is generated and what leaves the structure: the Q^- term is momentarily greater than the Q^+ term. When the vent is small or the flame grows faster, this peak P_1 may become difficult to detect or even invisible. During phase C, the flame also undergoes major deformations. Due to the pressure difference between the enclosure and the outside and the asymmetry of the problem, a non-isotropic flow directed towards the vent is created. The flame follows this flow, stretches, at its surface A_f ; whereby the combustion rate is likely increased significantly.

The second peak, P_2 , is reached when the difference between the combustion rate and the gas losses is at its maximum. It is here at the vent, where the flame has presumably reached a maximum surface area as the burnt gases escape. Since the density of the escaped gases is lower than that of the fresh mix, the ejection velocity increases. That is, the mass flow rate being equivalent, a greater volume of gas is lost. As their density is much lower than that of the fresh mixture, the ejection velocity increases; for the same mass flow rate, a greater volume of gas is lost.

At the end of phase D, the enclosure is at vacuum compared to its initial pressure. This is due to two phenomena: the directed flow, which produces suction in the enclosure, and the cooling of the hot gases. It is, therefore, common to observe some secondary pressure oscillations, but these are strongly damped.

3.5.2.2 Real situation

This phenomenological description summarises the main events observed during the explosion's expansion towards the outside. However, it omits several parts of the problem, such as the effect of the ignition point's initial position or the possible evolution of the reactants outside the enclosure towards a secondary explosion.

As shown in Figure 22, in this central ignition configuration, or close to the vent, a cloud of hot, low-density gases extends into the partially open volume in a preferred direction: that of the vent. In the opposite direction, a hot, low-density mixture moves slowly through a cold gas that has been compressed (by the explosion). The result is the formation of Taylor instabilities and a local increase in the flame surface area and, therefore, the combustion rate despite the reduced flame speed. With ignition at the bottom of the enclosure, because of the high velocity of gas ejection through the vent, these Taylor perturbations are limited, inducing a shear instability, the Kelvin-Helmholtz instability the latter of which predominates. There are, therefore, two antagonistic effects: the rate of gas evacuation with respect to the distance from the ignition source which serves to reduce the maximum overpressure; and the increase in the rate of combustion due to the isolation effects of the reactants. Soldberg (1981) highlighted situations where ignition at or near the centre of the vent led to higher overpressure effects than ignition at the opposite end of the vent, a case generally recognised as a major factor in the effects of confined explosions.

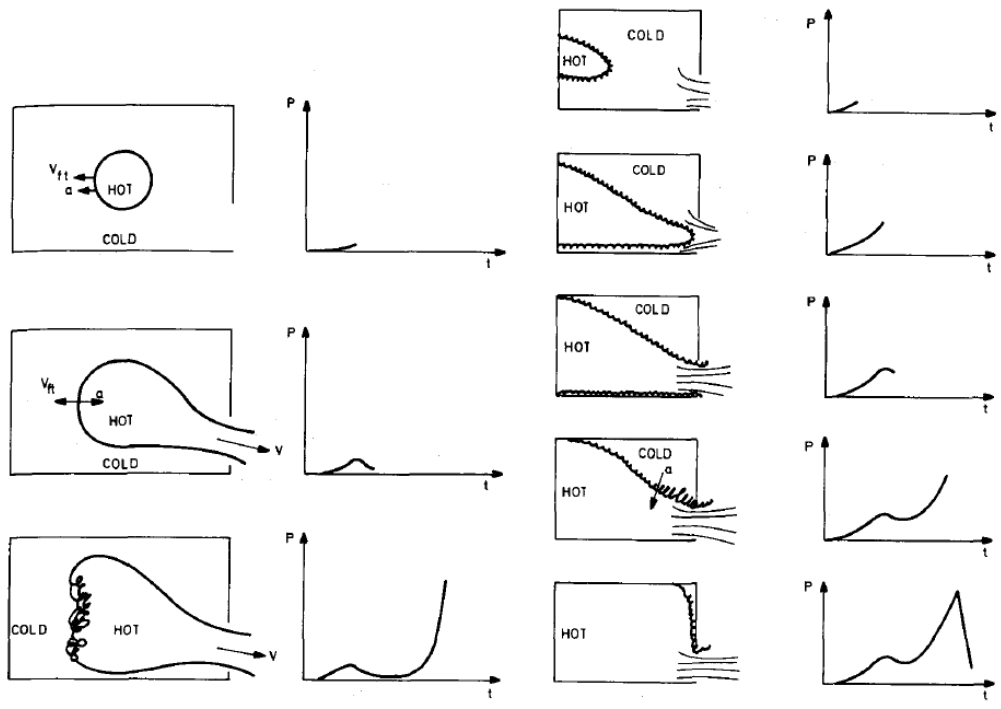


Figure 22. Illustration of the effect of the position of the ignition point (Soldberg, 1981)

Cooper (1986) attempted to clarify the overall relational mechanism of pressure generation to that of an enclosure's geometry and the location of the ignition point during the development of an explosion in a vented enclosure. An analysis has been proposed based on the following pressure signal:

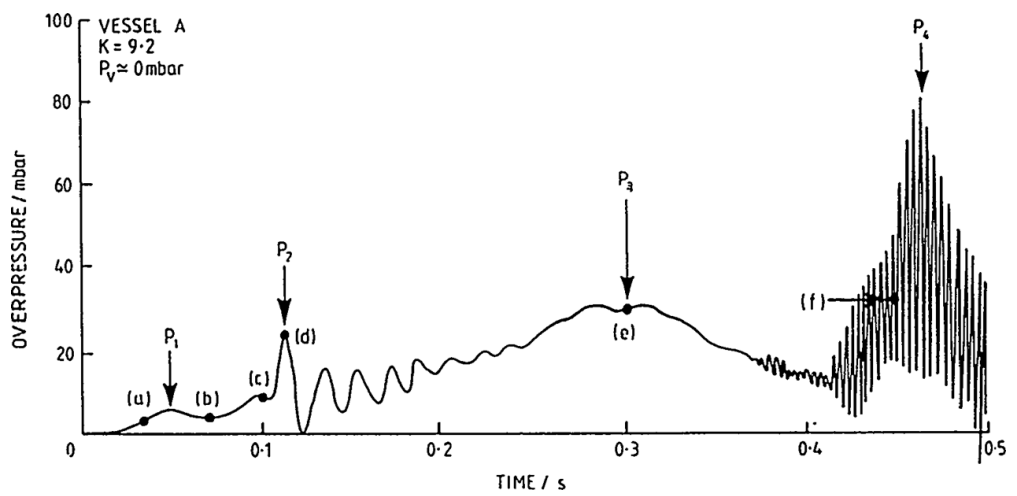


Figure 23. Experimental signal and analysis by Cooper, 1986

It is important to note that the 4 peaks numbered P_1 to P_4 in Figure 23 are not the same as those shown in Figure 21, except for P_1 . Up to point (c), the events are identical to those described by Harris in Figure 21. At (a), the vent begins to open; at P_1 , a local maximum is reached as the gas flow through the vent becomes greater than the flame production rate; at (b), a local minimum is reached, and then the rate of production of the burnt gases becomes dominant again. Point (c), therefore, corresponds to point P_2 in the Harris diagram, with the flame exiting through the vent. At this moment, the internal overpressure reaches a local maximum, not a global maximum, in accordance with the Harris model, and the flame exits the enclosure.

Then, the cloud of reactants pushed by the explosion in front of the vent ignites, creating a secondary explosion with three notable consequences arising from the acoustic-like generation of pressure due to the explosion taking place in a moving cloud .

The first consequence is an overpressure denoted by the peak, P_2 , caused by the waning discharge of gases through the vent as in the case of unshocked flow (cf. Equation 27).

The second phenomenon, the displacement of the cloud, creates a Doppler shift in the pressure signals of the external and internal gas pockets resulting in an oscillatory response and signal. These Helmholtz resonator-type oscillations appear to destabilise the flame and increase its surface area and, therefore, the rate of combustion. This leads to a rate change of the pressure which appears as a new pressure peak, P_3 leading to the appearance of a new pressure peak in the enclosure: P_3 . In practice, P_3 rarely corresponds to the maximum pressure, which is rather represented by P_2 . This effect at P_3 only becomes significant when the vent is small compared with the enclosure, when the enclosure is elongated ($L/D > 6$), or when turbulence is high (Lautkaski, 1998).

Thirdly, the flame surface decreases, allowing the internal pressure to drop as the combustion rate is then lower than the ejection rate. According to the enclosure's fundamental acoustic mode, high-frequency oscillations can be obtained. A fourth overpressure peak, P_4 , appears, corresponding to the combustion of fresh gas bubbles in the corners of the enclosure.

The effect is stronger in larger enclosures: the longer the pressure wave, the more it approaches the enclosure's fundamental periods of vibration, and the more the system can enter resonance. However, this acoustic effect seems to be relatively easy to cancel with acoustic absorbers such as barriers. Unlike the P_1 , P_2 , and P_3 peaks, it is also less pronounced as turbulence increases.

Unfortunately, modellers have encountered major difficulties when extrapolating beyond empirical = such system's complexity. That is to date, only empirical models can be used to simulate the complete phenomenon.

3.5.2.3 Secondary explosion phenomenology

Proust and Leprette (2010) published experimental data on explosions in large vented chambers in an attempt to quantify these secondary peaks and identify the dominant parameters. A key parameter is the opening ratio (vent area to enclosure cross-section ratio).

External explosion effects dominate when this ratio is large enough (typically greater than 0.4). When this ratio is sufficiently small (less than 0.2), internal explosion effects dominate, and the maximum explosion overpressure is reached when the flame surface is at its maximum. Between these limits (i.e. for a vent ratio of between 0.2 and 0.4), the external explosion triggers flame instabilities and can lead to a sharp increase in overpressure in the enclosure. The opening ratio varies according to the industrial application under consideration. For a building or a structure with large, relatively fragile walls, it is greater than 0.2, so the dynamics of the external explosion are likely to have an influence. However, in the case of a reactor, which is smaller and more resistant, it can be 10 times smaller.

Experiments have been developed to study this aspect at INERIS, particularly for hydrogen-air mixtures (Daubech, 2011). Quiescent homogeneous mixtures were ignited at the centre of the face opposing the vent. A sequence of images from one of these tests is shown in Figure 24:



Figure 24. Example of a secondary explosion (15% hydrogen/air mixture, 4 m³ tank and 0.5 m² vent, 10 ms between 2 images)

Figure 25 shows the evolution of the internal and external overpressure signal and the images extracted from the high-speed camera video.

The recordings show that, initially, the overpressure in the vessel increases steadily until the vent begins to open (at around $t = 75$ ms after ignition). When the sheet forming the vent opens, the flame accelerates in the vessel, and the overpressure increases more rapidly. In this case, when the vent opens (from about 75 to 120 ms), there is no decrease in the rate of pressure rise in the vessel: the rate of combustion increases faster than the rate of gas evacuation.

The maximum overpressure is reached when the flame leaves the tank, at around $t = 140$ ms, which is consistent with the analyses in paragraph 3.5.2.2.

Around $t = 150$ ms, the flame has consumed most of the outer cloud. At 1 m from the tank, a sudden depression is observed, which lasts until $t = 200$ ms, due to the significant acceleration of the flow in the burnt products. Around $t = 175$ -250 ms, oscillations are observed in the tank, probably of acoustic origin, while the centre of the cloud is about 2 m from the tank. These oscillations correspond to peak P₄ in Figure 23.

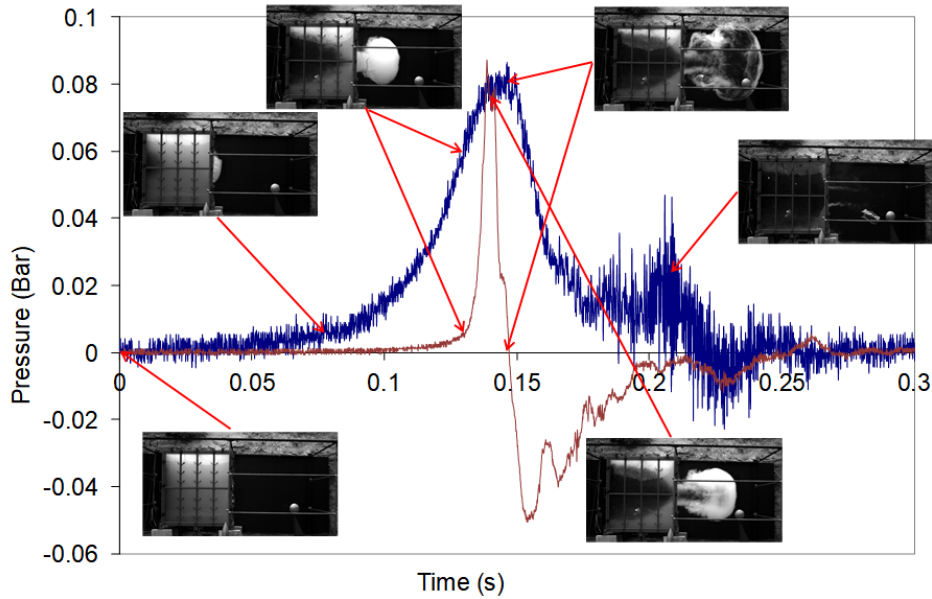


Figure 25. Comparison of high-speed camera images with pressure measurements in the enclosure (blue) and 1 m from the vent (red) for the test shown in Figure 24 (mixture at 15% H₂)

Recordings made outside the enclosure with the high-speed camera show that the external cloud accelerates from an initial velocity of around ten m/s to nearly 80 m/s over the first 2 m in front of the vent.

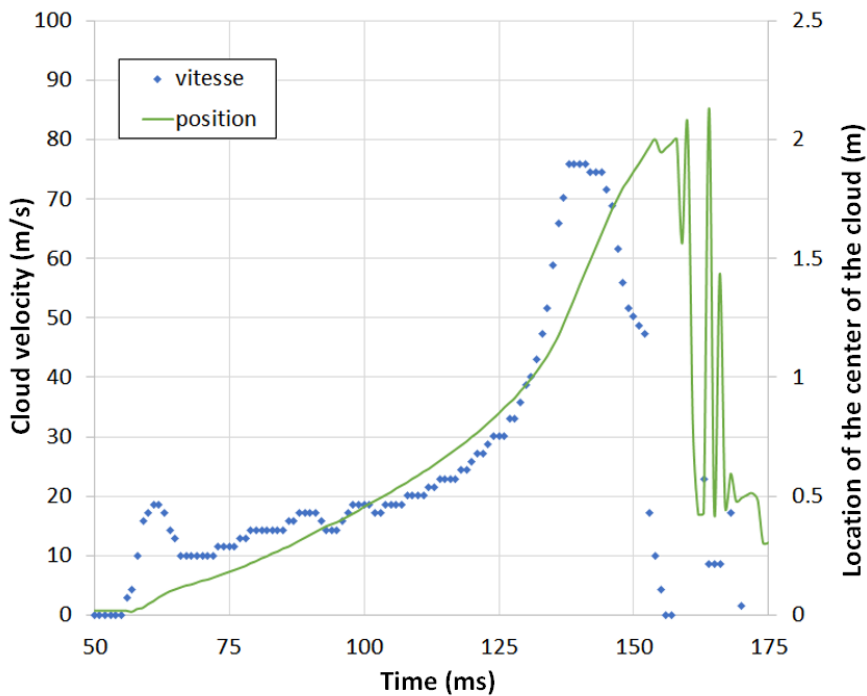


Figure 26. Position and velocity of the centre of the outer cloud during the test shown in Figure 24

Similar tests were carried out in 2019 at INERIS in a smaller volume of 1 m³, with methane (12%) and in an oxygen-enriched atmosphere (25%) to get a better view of the flame. These tests revealed a greater number of local overpressure maxima, which are compared (Figure 26) with the advance of the flame captured by a high-speed camera:

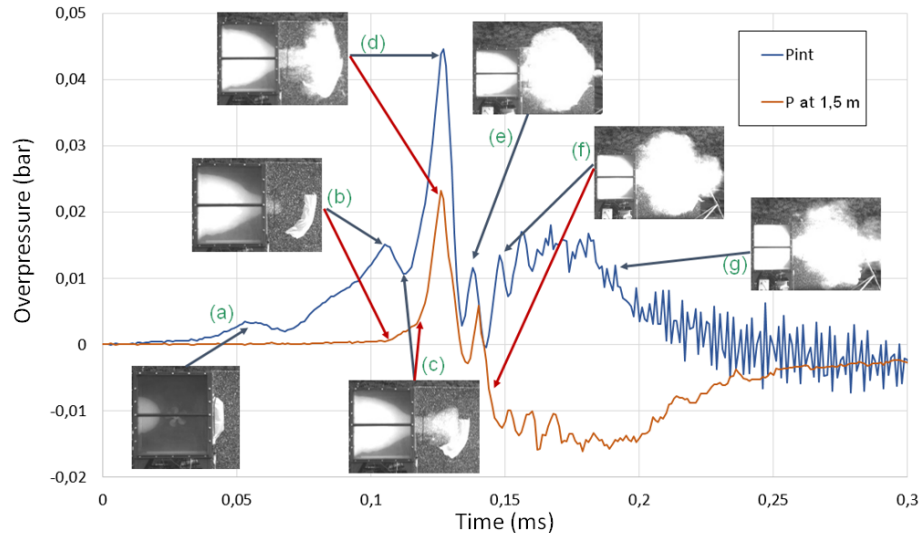


Figure 27. Comparison of images from the high-speed camera with pressure measurements in the enclosure (blue) and at 1.5 m from the vent (orange) for an ATEX explosion of methane-oxygen-nitrogen in proportions of 12, 25 and 63% by volume, respectively, in a 1 m³ enclosure

The events shown in Figure 27 can be described as follows:

- when the vent opens, fresh gas is released into the atmosphere. An initial local maximum can be seen at around $t = 58$ ms;
- the flame developing inside the enclosure is stretched toward the vent. Therefore, it reaches the vent even before it reaches the other walls. The release of burnt gases (of lower density) allows a new equilibrium between production and evacuation, visible in the second peak at $t = 105$ ms. The external overpressure at 1.5 m from the enclosure also starts to increase;
- the flame front reaches the tip of the outer cloud and begins to expand radially outside the enclosure. The rapid increase in the flame surface is correlated with a further rise in the internal pressure at $t = 113$ ms and a clear change in the slope of the external effects;
- the flame coils in the vortex ring. This is a second phase of combustion. The internal pressure increases until the flame reaches its maximum size at around $t = 121$ ms;
- the "fireball" is formed, and Helmholtz oscillations (peak P_3 in Cooper's description) are visible on the internal pressure signal. ($t=137$ ms);
- the flow of burnt gas from the enclosure pierces the fireball pocket. Outside, with the sensor inside the fireball, a strong and relatively long vacuum is measured (about 100 ms here). Oscillations of the internal pressure signal are also visible. The flame continues to develop inside the enclosure. ($t=153$ ms);
- from $t = 175$ ms, the external fireball cooled. Inside the vessel, the flame has reached the walls. The combustion of the remaining gas pockets forms the P_4 peak shown in the Cooper diagram.

In this second case, the analysis of the pressure signals using video is more consistent with Cooper's observations on the mechanisms by which these maximums are formed.

Depending on the conditions of the explosion, several types of behaviours are possible. Daubech (2016) found that a "bubble" of combustible gas almost always forms in front of the vent and explodes as soon as the flame escapes from the chamber:

- for a large vent (Figure 28.a.), the "bubble" is distinctly a vortex structure (vortex ring and surrounding "bubble") which mixing minimally with the outside atmosphere, as evidenced by the very sharp edge. The bubble's diameter is twice that of the vent, and its vortex velocity is half that of the vent flow. This closely resembles the dynamics of laminar vortices (Proust & Leprette, 2010).
- for a small vent (Figure 28.b.), a vortex bubble also forms but quickly degenerates into a transient jet. In this case, a significant quantity of the outside atmosphere is sucked into the jet.

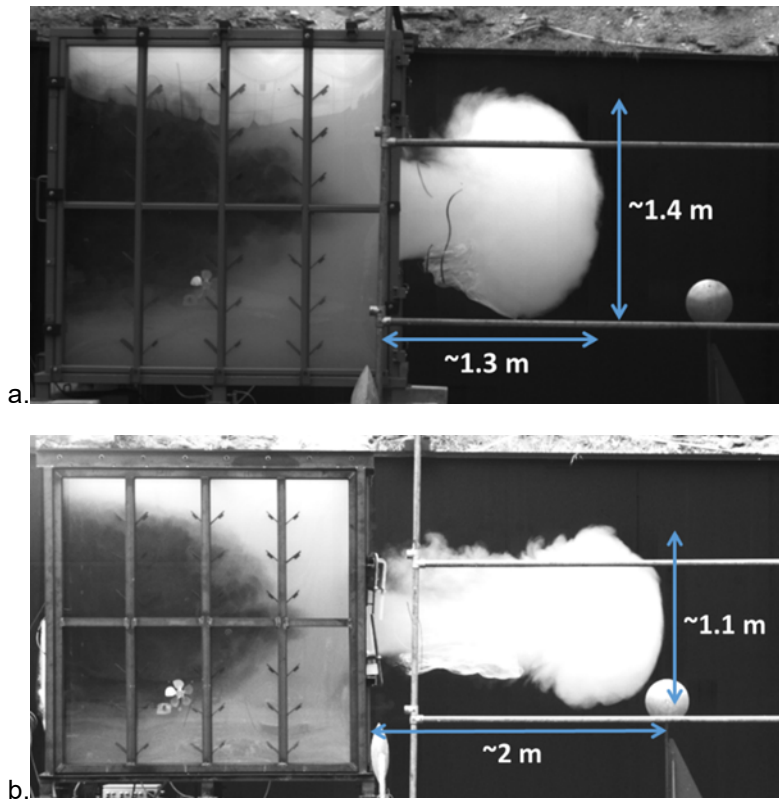


Figure 28. Comparison of high-speed camera images with pressure measurements in the enclosure

The maximum external overpressure is reached as soon as the flame reaches the vortex ring at the bubble's centre. When the flame reaches the bubble's outer edge, the external overpressure returns to zero. After the combustion of the cloud, the diameter is between 1.5 and 2 times greater than the bubble's diameter before combustion.

Beyond this qualitative description of the phenomena, it is possible to use analytical models to estimate the maximum effects of these secondary explosions. When one considers it as a sphere the equations of conservation of mass and momentum can be used to determine the volume and speed of movement of the cloud:

$$\frac{dV_b}{dt} = A_v \cdot (U - U_b) \quad \text{Equation 29}$$

$$\rho_u \cdot \frac{dV_b}{dt} \cdot (U - U_b) = \frac{1}{2} \cdot \rho_a \cdot C_x \cdot U_b^2 \cdot \frac{\pi \cdot D_b^2}{4} \quad \text{Equation 30}$$

Where:

- V_b is the volume of the cloud;
- A_v is the cross-section of the opening;
- U is the velocity at which gases are ejected from the vent;
- U_b is the speed at which the cloud is moving;
- C_x is the cloud's drag coefficient;
- ρ_u is the density of fresh gas;
- ρ_a is the density of the ambient air;
- D_b is the diameter of the cloud.

These parameters can only be expressed as a function of vent size and flow velocity. The tests suggest that the cloud moves at half the vent velocity, which is well represented by the model.

Ignition of the outer cloud occurs at its center. An acoustic source model can be used to estimate a pressure generation rate. In the open air, any pressure effects appear when the flame develops in such a way as to induce a so-called "flushing" flow in the atmosphere. This movement is accompanied by a pressure wave that can be compared (when the induced overpressure is slight enough) to that of a monopole acoustic source, whose fundamental equation takes the form:

$$\Delta P = \rho_0 \cdot \frac{1 - \frac{1}{E}}{4\pi r} \cdot \frac{d^2V}{dt^2} \quad \text{Equation 31}$$

With:

- ΔP the excess pressure generated,
- r the distance to the centre of the spherical source,
- E the expansion coefficient,
- V the volume of gas displaced.

The Multi-Energy model (see section 4.6.2.2) can also be used to determine the pressure effects due to the combustion of the outer cloud. In both cases, however, there is no estimate of the combustion rate, which will be done empirically, as the physics of combustion of the outer cloud is still unclear.

This model considers a downstream shift in the cloud due to its momentum. It is the combustion shifted in space due to the cloud momentum which consequently generates a Doppler effect. The latter of which impacts the external overpressure since the absolute velocity of the flame front downstream, in the direction of flow, is much higher than upstream, in the direction of the chamber. The result is a directional effect that manifests as a higher level of overpressure on sensors located downstream of the cloud and an attenuated overpressure at the vent. However, this model does not consider the cloud's displacement during the explosion.

External combustion ends when all the reactants have been consumed. Overall, the model tends to overestimate the external pressure peak for two reasons:

- the negative pressure phase, which corresponds to the change in acoustic regime on leaving the chamber, is poorly represented;
- the flame velocity is variable.

Of the three interaction mechanisms highlighted (§ 3.5.2.2), two can be considered with this model:

- the propagation of the external pressure wave in the chamber;
- the aerodynamic blocking of the flow at the vent by the external explosion. In the expression for the ejection flow rate Q_{ovv} , the pressure differential between the interior and exterior is calculated not in relation to atmospheric pressure but in relation to a higher external pressure during the explosion.

Due to the difficulty to account for Taylor instabilities hitherto highlighted in the intermediate situations, they have not been modelled for this discussion.

3.5.3 Case of 2 closed enclosures connected by an opening

When the enclosure subjected to the explosion is open towards another enclosure, whether the opening is permanent or a frangible wall such as a door or vent, gases will be exchanged between the two enclosures. If this is the case, the gases transmitted to the neighbouring chamber will be deducted from the material balance in the chamber under study. If, on the other hand, gases arrive in the enclosure under study during the explosion (for example, if combustion also occurs in a neighbouring enclosure), the gases received will be added to the total balance of gases produced. They will contribute to the increase in pressure.

However, the exchange of matter is not the only element that has a significant effect on pressure variations; three other aspects are important:

- 1) In practice, as demonstrated by the secondary explosion phenomenon discussed in the previous paragraph, deflagrations are expansion waves from burnt products, which push large quantities of fresh reagents ahead of them. During the expansion of the burnt products, the reagents undergo adiabatic compression, which pushes the flame to the walls of the enclosure. At the same time, only about 10-15% of the fresh material is consumed, yielding an expansion rate of 8 as given in the example of a spherical flame starting at the center of a spherical enclosure. These values vary with the shape of the flames, the enclosures, and the expansion rate. The important physical concept here is that the flames push large quantities of unburnt material ahead of them, which in the case of a vent generates a secondary explosion that is not confined to the outside. Confined explosions in the case of communicating enclosures, can also occur as a result of the movement of unburnt material even in areas where there was initially no fuel.
- 2) In interconnected enclosures, the passage of gases from one element to another generates vortices and turbulence in the receiving enclosure, which can significantly increase flame velocity and accelerate flame growth. Turbulence is created by jets within the equipment itself, known as confined jets (*Figure 29*).

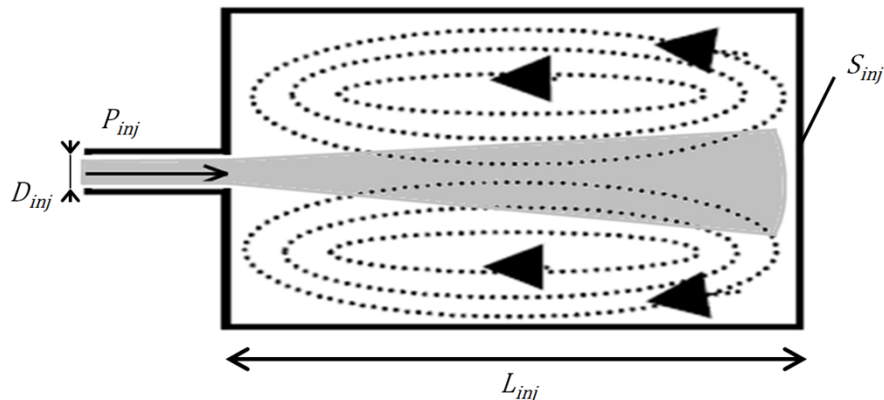


Figure 29. Vortex flow around a confined jet

When a jet forms, it induces through momentum transfer a sustained swirling motion in the surrounding atmosphere (*Figure 29*). When the flame enters this turbulent cloud, it rolls up in these large eddies, and the combustion rate increases significantly. These vortices are characterised in particular by the integral scale of the turbulence L_t , linked to the size of the vortices, and the turbulent fluctuation velocity u' , linked to their velocity. L_t and u' depend mainly on the geometry of the confinement and the orifice, as well as the pressure upstream of the jet. It is shown empirically that the flame velocity in these eddies can be described by the Gülder model (Equation 15, page 26) when the turbulence parameters u' and L_t are known.

- 3) Now we have two explosions of different violence in two enclosures of potentially different volumes connected by an opening. Depending on the respective violence of the two explosions and the geometric characteristics of the opening and the two confinements, we can obtain an oscillating system, with each enclosure influencing the evolution of the explosion in its neighbour. Numerical simulation of this type of phenomenon can be extremely complex. It should be remembered that an acoustic resonance can be established between the two enclosures in the manner of the P4 peak in the Cooper diagram (see paragraph 3.5.2.2).

3.5.4 Explosion in a pipe

The previous results assume a single, homogeneous pressure in the enclosure. This approximation is acceptable in a cuboid volume whose dimensions are equivalent in the 3 Cartesian directions. A ratio of the length L to the diameter D of the enclosure is generally used to determine the elongation of the enclosure. When the ratio L/D is less than 5, the assumption of homogeneous pressure allows events to be described with satisfactory accuracy. Beyond that point, the validity of the assumption must be questioned, particularly in the case of pipes where L/D ratios of 20 to 100 are not uncommon.

In a tube, a flame, even a laminar one, is first accelerated by the fluid set in motion by the expansion of the combustion products. Several superimposed phenomena lead to significant self-acceleration of the flame. The flame front and, therefore, the flame surface, which directly affects the burnt gas production rate, can be significantly modified as the flame advances through the pipe, particularly if obstacles are present. In all cases, the speed of the flame typically increases from 1 m/s to several hundred m/s, or even more than 1000 m/s in the event of a transition to detonation, depending on the nature of the explosive mixture and the geometry of the installation, over relatively short distances. (Ginsburg and Buckley, 1963).

3.5.4.1 Academic case of the closed-bottom tube

Proust (2015) examined the 'academic' case of a flame propagating in an explosive mixture confined in a duct closed at the ignition end and open at the other end. In this work, he outlined different flame acceleration mechanisms.

The most widely accepted mechanism is the continuous increase in turbulence of the reactive mixture, induced by the expansion of the burnt products, which pushes the reagents in front of the flame (Borghini, 1988; Clarke, 1989). Turbulence is generated by friction on the pipe walls in proportion to the average flow velocity. The burning velocity is then increased, which increases the production rate thereby expanding the burnt gases. The cycle repeats itself, and the flame self-accelerates. The Reynolds number must play a key role in this process, encompassing both the effect of turbulence generation (Hinze, 1975) and turbulent combustion (Bray, 1990). This may also explain why the empirical formulae in NFPA68-69 present pipe diameter as a dominant parameter for flame acceleration and pressure rise within a pipe. More recently, Ciccarelli and Dorofeev (2008) published a review of the state of the art on this subject.

The analysis proposed by Ciccarelli supports the idea that flow turbulence due to wall friction would be the main mechanism for flame acceleration throughout a process leading to the transition to detonation. Some relevant mathematical developments have been found (Veser, 2002; Dorofeev, 2007; Kuznetsov, 2005; Silvestrini, 2008). For example, Silvestrini proposes the following correlation:

$$V_f = 6.5 \cdot E \cdot S_l \cdot \exp \left[0.0061 \cdot (E - 1) \cdot \frac{X}{D} \cdot \left(\frac{D}{0.015} \right)^{0.4} \right] \quad \text{Equation 32}$$

Where S_l is the laminar combustion velocity, E is the expansion rate of the burnt products, X is the abscissa of the flame in the pipe, D is the diameter of the pipe, and V_f is the flame velocity at X . This correlation establishes a link between flame velocity and X/D . However, this type of correlation does not work for all the experimental data, notably experiments performed after its publication (Thomas, 2010; Blanchard, 2010). These models are more the result of a fit with existing experimental data than a formal theoretical development, which may explain these differences. More fundamentally, some (unfortunately very limited) measurements of the turbulence generated in the flow in front of the flame (Jones & Thomas, 1991) do not show a correlation between flame velocity and turbulence intensity, suggesting that other mechanisms for flame acceleration are at work.

It has been demonstrated theoretically (Deshaies & Joulin, 1989) that other mechanisms can also explain the acceleration of the flame in the tubes. In particular, a series of compression waves would produce the progressive acceleration of the flow in front of the flame due to the expansion of the burnt products. The temperature of the reactants in front of the flame increases accordingly, as does the combustion rate and the flame, itself, accelerates.

There are also flame instabilities generated by these same pressure waves (Markstein, 1954), but their exact role in the flame acceleration process in a tube is still under debate. These instabilities are thought to be triggered by the pressure wave emitted when the flame is partially extinguished at the wall just after ignition. About twenty-five years ago, Kerampran (2000) conducted an experimental analysis of pre-mixed gaseous flames propagating in a straight tube. A two-stage propagation was demonstrated, the first corresponding to the development of the flame around the ignition point, producing an elongated parabolic flame. The flame slows down as the sides of this parabola are extinguished at the wall. Shortly afterwards, the flame front becomes strongly undulating at the centre and accelerates more or less regularly. However, this observation contradicts the supposed acceleration of the flame by the flow turbulence, which must be much greater at the wall. Small vortices appear in the flame's wake but remain very limited. In this case, the driving parameter for the appearance and development of instabilities (Markstein, 1964; Bychkov, 2000) should mainly be the flame expansion velocity ($E \cdot S_{lad}$).

More recently, Daubech and Lecocq (2018) following the work of Proust (2015) on the understanding the mechanisms of flame acceleration in pipes, carried out gas explosion tests in straight pipes with one end closed and the other open. They showed that the first pressure pulse, due to the initial development of the fireball and its elongation, plays a dominant role and imposes a piston effect on the gases in the pipe. In particular, they observed that the smaller the diameter of the tube, the greater the effect of the size of the turbulent boundary layer in the tube on the results. Nevertheless, the turbulence induced by the compression wave in these tests remained very low. Superimposed on this general trend are pressure oscillations due to the acoustic resonance of the pipe. Their influence appears to be greater in smooth tubes (PMMA in this case) than in those with a certain degree of roughness (steel in this case). During these studies, a coupling between the pressure wave and the different acoustic frequencies in the tube, i.e. in the fresh gases (in front of the flame) and in the burnt gases (behind the flame front), was demonstrated. Despite the visible oscillations of the flame front, due to the acoustic effects, Daubech (2018) measured a constant self-acceleration of 130 m/s^2 with a stoichiometric methane-air mixture.

While all these mechanisms are individually known, at least qualitatively, we cannot explain their interactions nor their relative importance in the acceleration process. Insofar as there is currently no conceptual diagram describing this process, we also have no realistic prediction tools adapted to specific geometric situations.

3.5.4.2 Industrial situation

The reference situation in the industry rarely corresponds to the case of a straight pipe closed at one end and open at the other. We know that the presence of obstacles in the path of the flame can have a marked effect on the course of the explosion, as shown by work such as that carried out by the Montreal school in the 1980s (Lee, 1984). We can distinguish a priori four main types of situations (Proust, 1996):

- 1) *The isolated pipe, open near the point of ignition and closed at the other (Lewis & von Elbe, 1987):* the combustion products are evacuated to the outside, which considerably reduces the intensity of the flow in front of the flame front so that the acceleration mechanisms mentioned above are of little use. The levels of overpressure generated remain comparatively low. However, the flame can become extremely vibratory and develop a turbulent structure.
- 2) *The isolated pipe, open at both ends (Lewis & von Elbe, 1987):* the excess volume produced by combustion can be discharged at both ends so that the flame can move faster than in the previous situation with broadly the same characteristics. This situation is not very conducive to flame propagation and severe explosions.
- 3) *The isolated pipe, closed at both ends:* after an initial expansion phase in which the flame stretches strongly, the flame surface area decreases, resulting in a reduction in the pressure increase and the flame's spatial velocity (Phylaktou, 1991; Leyer, 1969). From this point onwards, an oscillatory propagation may appear with the formation of a "tulip" flame, the origin of which could be aerodynamic. The acceleration of the flame is, therefore, not continuous, and the speeds reached remain lower than in the following configuration:



Figure 30. Formation of a "tulip" flame in a $10 \times 10 \text{ cm}$ vertical tube with a 5.9% methane-air mixture; 20 ms between images; the red point visible at the bottom is the ignition point. (Proust, 2004)

- 4) *The isolated pipe, closed on the side of the ignition source and open at the other end:* some of the most precise work carried out on this subject includes that of Guénoche (1952), confirmed by others (Schmidt, 1951; Jones & Thomas, 1991), and more recent work by Ineris (Proust, 2014; Daubech, 2018; Lecocq, 2018). The flame generally accelerates, but sometimes in a "jerky" manner. When the flame makes several transient stops, it sometimes retreats along its path. The mechanism of oscillatory propagation is not yet clearly known, but it seems very likely to be linked to acoustics (Daubech, 2018). In any case, extremely severe explosion regimes can easily be reached.*

3.5.5 Case of an enclosure connected to a discharge pipe

The typical configuration is an enclosure located inside a building, away from walls, in which a deflagration may be triggered in the event of an accident. In this case, an exhaust duct can direct the hot gases from the enclosure to the outside of the building. The two flame propagation mechanisms specific elements of this network are likely to interfere. The nature of this interaction is still poorly understood, mainly because the mechanisms by which explosions propagate in pipes have yet to be discovered.

Several studies have been conducted since the early 1980s, proving that the presence of a vent duct for the explosion's products generally increases the explosion's severity compared with the situation encountered with a vessel vented directly into the atmosphere. It has been shown that the deflagration pressure can be in excess of a factor of 10 or more, as obtained in experiments involving direct discharge into the atmosphere (Bartknecht, 1981; Molkov, 1994). This is mainly due to the combustion dynamics inside the discharge pipe compared with that taking place in the enclosure. Despite numerous experimental studies and their findings (Bartknecht, 1981; Kordylewski & Wach, 1986, 1988; Molkov, 1994; Ponizy & Leyer, 1999), a full picture of the phenomenon affecting the maximum pressure in the enclosure remain uncertain. The myriad of interactions affecting gaseous combustion dynamics in the pipe and the enclosure, themselves dependent upon and influenced by geometric effects and multi-variable operating conditions are criteria that play crucial roles on maximum pressure. . In an insulated enclosure fitted with a vent, we have seen that the appearance of the pressure peak is directly linked to the competition between the production of gases by combustion and their evacuation through the vent. The presence of the vent influences the development of the explosion and, therefore, the maximum overpressure reached because it can affect both the discharge process and combustion in the vessel.

Various phenomena have been studied as possible causes of the increase in explosion violence in an enclosure connected to a discharge pipe (Russo & Di Benedetto, 2007):

- frictional head losses (Bartknecht, 1981; Ponizy & Leyer, 1999; Kordylewski & Wach, 1986, 1988; Ural, 1993);
- the inertia of the gas column in the pipe (Bartknecht, 1981; Ponizy & Leyer, 1999a; Kordylewski & Wach, 1986, 1988; Ural, 1993; Grégoire, 2014);
- acoustic oscillations (Kordylewski & Wach, 1988; McCann, 1985);
- combustion in the pipe (Molkov, 1994; Ponizy & Leyer, 1999a, b; Ural, 1993).

As a function of pipe characteristics, its diameter, length, roughness, and any singularities such as bends or cross-sectional deviations, frictional losses may present themselves. In one of the pioneering works on gas explosions in enclosures vented through a pipe, Bartknecht (1981) pointed out that the increase in the maximum explosion overpressure in the enclosure is strongly affected by fluid friction and the inertia of the gas column. Ural (1993) and Ponizy & Leyer (1999) reached similar conclusions. More recently, Grégoire (2014) observed that for confined organic dust explosions of moderate reactivity (class ST1), the flame acceleration effects in the duct are not significant, rather the essential influences on flame acceleration are dominated by inertial effects which consist not of conventional pressure drops but by delaying discharges through aerodynamic blocking mechanisms until the flame is out.

Even under an inert atmosphere in the pipe, acoustics influence it. This can be linked to a piston effect: gases are gradually accelerated in a tube. Depending on the length of the tube, the evolution of the explosion in the enclosure, or the possible presence of singularities in the pipe, the compression waves can accumulate, and a sonic blockage can be reached.

This occurs when the flow is shocked, which limits the mass flow and generates back pressure and oscillations between the enclosure and the pipe. The acoustic oscillations induced in the tube can generate pressure in the enclosure and thus modify flame propagation in the enclosure. (Ponizy & Veysière, 2000). However, according to Russo & Di Benetto (2007), who carried out a review of the state of the art on this subject, although acoustic oscillations can modify the behaviour of the flame in the enclosure, they do not explain the large differences in overpressure observed with the situation of an isolated vented enclosure without a discharge pipe.

An explosion in the pipe can affect both the propagation of the flame inside the enclosure and the rate of gas evacuation (as it creates a back pressure). The discharge rate is then reduced, stopped or even reversed at the vent opening, in which case gases are expelled from the pipe into the enclosure. Similarly, this change in flow due to the interaction between two connected enclosures (see paragraph 3.5.3), can cause an increase in the turbulence induced in the vessel, thus accelerating the combustion rate inside the enclosure. Molkov (1984) identified this phenomenon as the primary mechanism responsible for the increase in overpressure in the vessel. Molkov (1993) also found that extinguishing the flame in the pipe by spraying water droplets could considerably reduce the maximum pressure measured in the enclosure, thus confirming the major effect of combustion in the pipe. Other results from Bartknecht (1981) and Ponizy

& Leyer (1999) confirmed the role of combustion and reflux on the overpressure measured in the enclosure. This phenomenon was also indicated as dominant by Russo & Di Benedetto (2007) for confined gas explosions.

This work indicates that to estimate the overpressure produced by a gas explosion, in the case of an enclosure connected to a pipe, two coupled combustion problems in the enclosure and in the pipe must be solved. There are simplified limiting cases, such as that of a very short pipe, that are dealt with, for example, in the standards on the sizing of explosion vents, which in some cases make it possible to simplify the description of this problem. However, little is known about the overall phenomenon.

3.5.6 Effect of a pipe between 2 enclosures

Phylaktou and Andrew (1999) have shown that for equipment interconnected by pipes, the explosion can be transmitted from one piece of equipment to another, and propagation becomes very complex. A possible pattern of propagation between two enclosures can be described as follows (Figure 31): ignition in the first enclosure leads to an initial explosion (Figure 31-a) and a powerful, turbulent flow in the connecting pipe; (Figure 31-b) a powerful jet of reactants is subsequently injected into the second vessel; while the primary explosion, which is not yet complete, pressurises the second vessel.

After accelerating sharply in the pipe, the flame enters the second enclosure in an explosive atmosphere under pressure and highly turbulent. A second, very violent explosion can then occur (Figure 31-c). This combination of acceleration and explosion could produce a flashback in the pipe and into the first enclosure where combustion is not yet complete inducing a new and sudden increase in pressure (Figure 31-d). However, flashback could either be a result of an acceleration of the reaction (secondary explosion) or as a result of the expansion of the gases in the pipe towards this enclosure, given a sufficiently large volume (in the case of large pipes or large diameters).

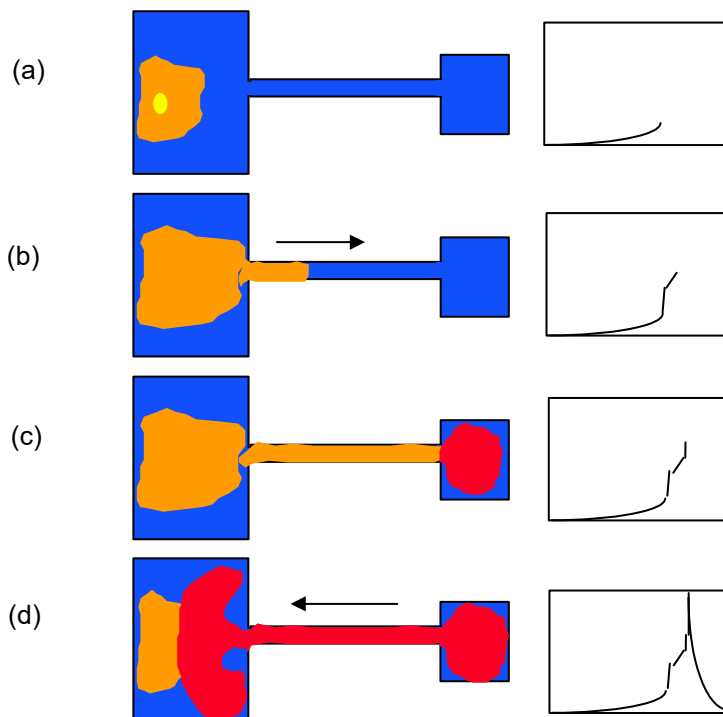


Figure 31. Schematic representation of the propagation of an explosion in interconnected enclosures (Proust, 2000)

This can lead to a situation where the velocity of the flames becomes so high that it is no longer possible to protect the connected enclosures from the effects of the explosion. In the industry, pipes are often steel cylinders with a circular cross-section. They are, therefore, reasonably resistant to explosion overpressure, unlike the equipment to which they are connected. For this reason, pipe explosion mitigation strategies consist of slowing down (with vents or explosion diverters) or stopping the flames (with flame arresters or insulation systems) to be able to protect the connected equipment rather than the pipes themselves.

3.6 Special case of flame propagation under detonation conditions

3.6.1 Phenomenology

When the reaction becomes faster, greater than the speed of sound in the medium, a shock wave is formed, reaching the supersonic regime. This wave compresses and heats the fresh reactants before convection can play a role. We then see an incident shock wave immediately followed by a flame front, that is, detonation. This detonation regime is a special case observed mostly with reactive mixtures such as hydrogen and acetylene, which appear after a strong initiation first explosion or a significant acceleration of the flames. The latter is typically linked to significant turbulence or particular confinement that favours flame acceleration. Detonations of this type appear to occur as transitions from deflagration to detonation, often referred to as DDT. The complexity of the mechanism of DDT and the conditions under which it occurs, is the subject of numerous research projects.

For the purposes of this report, DDT is possible and more likely to occur:

- with highly reactive explosive mixtures. For example, a stoichiometric hydrogen-air mixture will detonate more easily than a methane-air mixture under the same conditions;
- When turbulence is high, for example, during a massive leak from a highly pressurised gas tank (propane, hydrogen);
- when the containment has special characteristics, such as a very long pipe or one containing obstacles. The NFPA68 guide gives some practical limits on the maximum L/D ratio for pipes that must not be exceeded, to avoid DDT;
- when the initiation is particularly violent. For example, it is even possible to detonate aluminium dust clouds by igniting them with a condensed explosive.

In the case of a detonation, the thermomechanical effects of the explosion are contained behind the incident shock. The confinement, if sufficiently large⁴, does not affect the evolution of the reaction. In the case of a detonation in a confined space, we are often not interested in the propagation of the flame. The effects of the explosion can be estimated directly and with satisfactory accuracy using a thermodynamic model which omits any consideration of turbulence, flow or the volume of the enclosure. The two central representations are the Chapman-Jouguet (CJ) model and the Zeldovich, Von Neumann and Döring (ZND) model.

3.6.2 CJ and ZND models

The Chapman-Jouguet (CJ) theory is based on the following main assumptions:

- detonation is an infinitely thin discontinuity;
- the flow is stationary (the velocity of detonation is constant);
- the flow is one-dimensional, flat, and adiabatic;
- The gases are assumed to be ideal and γ constant.

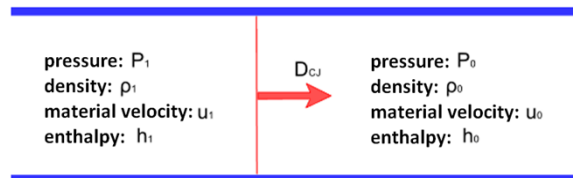


Figure 32. Diagram of a detonation in the CJ theory

W_0 and W_1 , respectively, are the velocities of the fresh gas and the products in the reference frame associated with the detonation wave:

$$\begin{cases} W_0 = D_{CJ} - u_0 \\ W_1 = D_{CJ} - u_1 \end{cases} \quad \text{Equation 33}$$

⁴ Detonation cannot propagate if the size of the confinement in the plane of the flame front does not exceed a certain critical diameter, which depends on the reactive mixture. In most cases (in industry) this condition is largely satisfied, as the diameter can be of the order of a few centimeters or even millimeters.

Through the discontinuity, we write three conservation equations:

$$\dot{m} = \rho_0 W_0 = \rho_1 W_1 \quad \text{Equation 34}$$

$$P_1 + \rho_1 W_1^2 = P_0 + \rho_0 W_0^2 \quad \text{Equation 35}$$

$$h_1 + \frac{W_1^2}{2} = h_0 + \frac{W_0^2}{2} \quad \text{Equation 36}$$

By noting $v=1/\rho$, the specific volume and using the conservation of mass equations (Equation 34) and momentum (Equation 35), we obtain:

$$\frac{\dot{m}^2}{v_0^2} = \frac{W_0^2}{v_1 - v_0} = -\frac{P_1 - P_0}{v_1 - v_0} \quad \text{Equation 37}$$

Equation 37 is known as the Rayleigh-Michelson (RM) line.

The reaction is assumed to be: "Reactants \rightarrow Products" with an overall heat release Q . The enthalpies are expressed as:

$$h(P, v, \lambda) = \frac{\gamma P v}{\gamma - 1} - \lambda Q \quad \text{Equation 38}$$

Where λ is the rate of reaction, which takes the value 0 in the fresh gases and 1 in the detonation products.

From this equation and the energy conservation equation (Equation 36), we obtain a second equation known as the "Crussard adiabetic".

$$\frac{\gamma}{\gamma - 1} (P_1 v_1 - P_0 v_0) - \frac{1}{2} (P_1 - P_0) (v_1 + v_0) = Q \quad \text{Equation 39}$$

The state of the reaction products is located at the intersection of these two curves, the Rayleigh-Michelson line and the Crussard adiabetic. Figure 33 shows the possible intersections between these two curves. The point (1.1) represents the 0 state before the reactive wave. We are interested in a zone where $P_1 > P_0$, this is the gas compression zone following the passage of the wave. Three cases are possible (and represented in Figure 33):

- The slope of the Rayleigh-Michelson line is too small; the curves do not cross, and there is no detonation.
- The slope of the Rayleigh-Michelson line and the Crussard curve intersect at two points, f and F. These are called strong detonations for F and weak detonations for f.
- the Rayleigh-Michelson line is tangent at a point CJ to the detonation or deflagration branches, respectively. This point corresponds to stationary propagation.

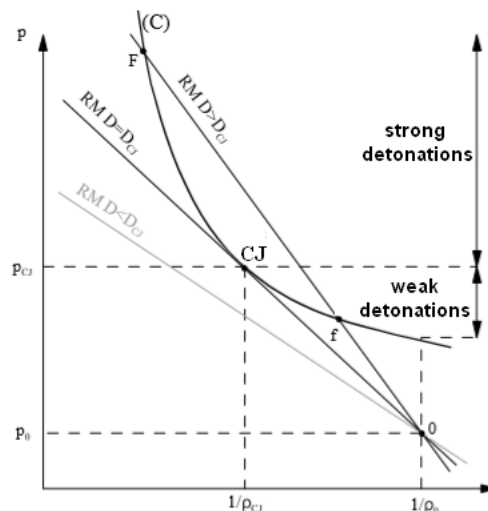


Figure 33. Rayleigh-Michelson lines and Crussard curve (Matignon, 2000)

We show that points f and F correspond to non-stationary regimes. Strong detonations have a relative velocity lower than the celerity of sound in the products, so the disturbances (F) in the downstream medium (expansion waves) will reach the front and weaken it. In the case of a weak detonation, for each point f there is a point that is thermodynamically more stable and therefore more likely to be close to the CJ state. So weak detonations in the f state have never really been observed. The stable position is characterised by the point CJ, known as the Chapman Jouguet point, for which the detonation wave is sonic in relation to the products (condition CJ: $D_{CJ} - u_{CJ} = c_{CJ}$), autonomous, stationary, and at a velocity, D_{CJ} .

For a given detonating mixture, there are tables in the scientific literature giving the parameters of the CJ state of the mixture during detonation. There are also simplified relationships for determining the CJ conditions for a polytropic gas obeying the law of perfect gases and Laplace's law, where $P \cdot V^\gamma = a \text{ constant}$, with γ , the ratio of specific heats at constant pressure and volume. These relationships apply to mediums initially quiescent, that is $u_0 = 0$, and where $D^2 \gg c_0^2$. In the applications considered here, there is a factor of about 10 given by the ratio of the squares, $D^2 : c_0^2$, where c_0 the speed of sound and D , the velocity of the detonation wave are approximately equivalent to ≈ 340 m/s and 1-2 km/s, respectively. Knowing the mass heat of reaction Q , we can determine the detonation velocity D by:

$$D = \sqrt{2(\gamma^2 - 1)Q} \quad \text{Equation 40}$$

Remarkably and reasonably well verified experimentally, this propagation velocity is independent of the physics of combustion and depends solely on the total energy released by the chemical reaction. The chemical reaction is instantaneous in this model, which is why it is unsuitable for deflagrations.

From D , we obtain the parameters CJ:

$$P_{CJ} = \frac{\rho_0 D^2}{\gamma + 1} \quad \text{Equation 41}$$

$$\rho_{CJ} = \frac{\rho_0(\gamma + 1)}{\gamma} \quad \text{Equation 42}$$

$$T_{CJ} = T_0 \left(\frac{\gamma}{\gamma + 1} \cdot \frac{D^2}{c_0^2} \right) \quad \text{Equation 43}$$

$$u_{CJ} = \frac{D}{\gamma + 1} \quad \text{Equation 44}$$

In 1900, Paul Vieille proposed another detonation theory, according to which a reaction zone of non-zero thickness follows a precursor shock. Building independently on Vieille's work, Zeldovitch, Von Neumann, and Doering (1940-1943) established the mathematical formulation of the problem (known as the ZND model). They consider detonation as an adiabatic compression of the reactants followed by a finite zone of chemical reactions. The two waves travel at the same speed, equal to the detonation velocity D . At the end of the reaction, the products are assumed to be in the CJ state. The results obtained in the CJ theory remain true and allow the velocity D to be calculated. At the shock front, it is assumed that the reaction progresses to zero. We obtain Hugoniot's equation (Equation 45), which, together with the Rayleigh-Michelson line, governs the propagation of shocks in a non-reactive medium:

$$\frac{\gamma}{\gamma - 1} (P_1 v_1 - P_0 v_0) = \frac{1}{2} (P_1 - P_0) (v_1 + v_0) \quad \text{Equation 45}$$

Schematically, the reaction can be represented as follows:

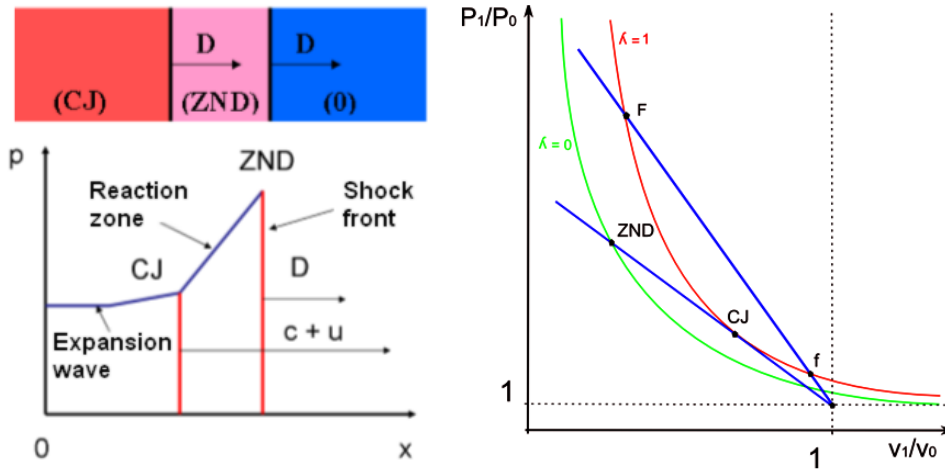


Figure 34. Diagram of the ZND model (left) and representation of the Rayleigh-Michelson lines and the Crussard and Hugoniot curves in the P, V plane

In short, when the shock passes, the reactive medium is brought almost instantaneously into a state called the ZND state (Von Neumann peak), with a pressure P_{ZND} and a temperature T_{ZND} much higher than the mixture's self-ignition temperature. In this case, the ZND pressure of the precursor shock is about 2 times the CJ pressure, while the ZND temperature is about half the CJ temperature. After the shock wave has passed through, a reaction zone is observed, bringing the shocked gases which retain their initial chemical composition towards the final equilibrium state at point CJ.

3.6.3 Piston model

The CJ and ZND models are fairly well suited to describe the flow state at the level of the detonation wave front, but it is often helpful to know the state of the gases behind this wave. In practice, the question of the occurrence of a detonation only arises in special cases of highly reactive, turbulent mixtures or in pipes. According to the Chapman Jouguet (CJ) model, detonation corresponds to a flat, stationary 1D case with constant detonation velocity, D_{CJ} and zero thickness at the reactive zone. This situation is equivalent to a 1D detonation plane moving in a closed-bottom tube. The model is, therefore, well suited to describing what can be expected in a pipe. In the CJ case, the expansion behind the wave is that of a Riemann expansion given by:

$$u_{CJ} - \frac{2}{\gamma-1} \cdot a_{CJ} = \text{Constante}, \quad \text{Equation 46}$$

where u_{CJ} and a_{CJ} are the material velocity and wave sound speed, respectively, at point CJ. We also can express the equation in terms of the constant detonation velocity, D_{CJ} :

$$u_{CJ} = \frac{D_{CJ}}{\gamma+1} = \frac{a_{CJ}}{\gamma} \quad \text{Equation 47}$$

Since the front of the CJ detonation wave is known we are now interested in the state of the burnt gases, b, as shown below in the diagram corresponding to this situation:

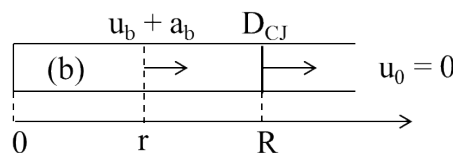


Figure 35. Diagram of the detonation wave propagation in gases at rest in a closed-bottom tube.

At a point in the tube upstream of the wave ($r < R$), we must therefore have:

$$u_{CJ} - \frac{2}{\gamma-1} \cdot a_{CJ} = u_b - \frac{2}{\gamma-1} \cdot a_b \quad \text{Equation 48}$$

If we look for the point from which $u_b = 0$, we have:

$$a_b = -\frac{2 \cdot a_{CJ} - (\gamma - 1) \cdot u_{CJ}}{2} = \frac{D_{CJ}}{2} \quad \text{Equation 49}$$

This corresponds to the distance $R/2$ between the expansion tail and the bottom of the tube, and is a uniform field or zone referred to sometimes as the "core". In the core, the burnt gases are at rest:

$$\begin{cases} u_b = u_N = 0 \\ a_b = a_N = \frac{D_{CJ}}{2} \\ P_b = P_N \\ \rho_b = \rho_N \end{cases} \quad \text{Equation 50}$$

The variable $Z = r/R$ is introduced into equation 49 with a value varying from 0.5 to 1:

$$\left. \begin{cases} u_b = \frac{2}{\gamma - 1} (a_b - a_N) \\ a_N = \frac{D_{CJ}}{2} \end{cases} \right\} \Rightarrow u_b(Z) = \frac{D_{CJ}}{\gamma + 1} (2Z - 1) \quad \text{Equation 51}$$

The same variable applies to pressure and temperature profiles:

$$\left. \begin{cases} \frac{P_b}{P_{CJ}} = \left(\frac{a_b}{a_{CJ}} \right)^{\frac{2\gamma}{\gamma - 1}} \\ a_{CJ} = \frac{\gamma}{\gamma + 1} D_{CJ} \end{cases} \right\} \Rightarrow P_b(Z) = P_{CJ} \left(\frac{\gamma - 1}{\gamma} Z + \frac{1}{\gamma} \right)^{\frac{2\gamma}{\gamma - 1}} \quad \text{Equation 52}$$

$$\frac{T_b}{T_{CJ}} = \left(\frac{a_b}{a_{CJ}} \right)^2 \Rightarrow T_b(Z) = T_{CJ} \left(\frac{\gamma - 1}{\gamma} Z + \frac{1}{\gamma} \right)^2 \quad \text{Equation 53}$$

For values in the core, we take $Z = 1/2$. These equations can often describe, with sufficient accuracy, the state of the gases at any point in the tube behind the detonation front. A graphical representation of these data is:

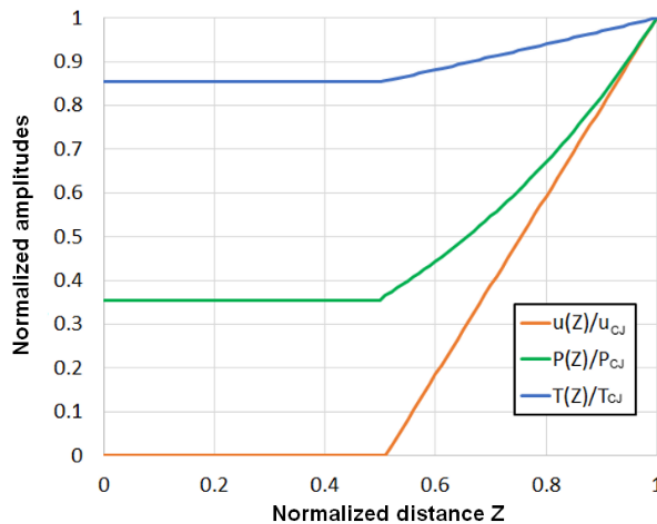


Figure 36. Pressure, temperature and gas velocity fields in the detonating piston model

The model assumes a plane flow and is well suited to pipes. For the detonation of a cloud, spherical coordinates will be used, leading to slightly modified profiles (as the mass conservation equation will involve an additional term in $2^* \rho^* u/r$).

3.7 Some specific features of explosions involving dust or hybrid mixtures

Much of the phenomenology described for gas explosions remains valid for dust explosions and hybrid mixtures (combustible gas and dust). We will limit ourselves here to mentioning a few specific aspects of the combustion of these two mixtures.

(The Omega 21 report focuses on confined dust explosions. It can be referred to for a better description of the phenomenon.)

The phenomenology of combustion remains similar to that of gases: the flame transforms fresh reactants into essentially hot gaseous products which expand. In confinement, expansion is partially blocked, and an increase in overpressure is observed. The mechanisms for generating pressure in enclosures and pipes are the same, although the reaction's amplitudes and timescales may differ significantly from those for gases.

However, dust combustion has several specific features compared with gas combustion. On a microscopic scale, it generally involves a fuel oxidized by oxygen in the air in an exothermic reaction. Surface reactions and the combustion of volatile species around the particles are observed on a mesoscopic scale. In simple terms, the solid fuel must first be heated to emit volatile species that can react with the oxygen in the air. The dynamics of this mechanism differ from gas combustion. Thermal conduction in a combustible particle propagates heat from the particle's surface towards its centre. A direct consequence is that greater energy input is required to ignite larger particles or those with a smaller specific surface area (surface area to volume ratio). The combustion of particles can also be affected by the radiation from the flame, which can, under certain conditions, contribute to the pre-heating of as yet unreacted particles, thus accelerating the propagation of the explosion.

For example, this phenomenon is inferred in the combustion of metallic particles such as aluminium. In most cases, particularly for organic materials used in the food industry, it is more difficult (but not impossible) to propagate explosions with suspensions of spheroidal particles with a diameter larger than 200 μm . On the other hand, with small particles or when they have a large specific surface area (e.g. wood fibres), explosions spread more easily. The chemical nature of the fuel also plays a role in these flame-particle interactions, so these phenomena can only be described in very general terms for this report.

As in the case of gases, combustion of the cloud of particles assumes that it is mixed with air in appropriate proportions. As the density of particles is typically on the order of 500 to 5000 times that of air, flow and turbulence are necessary conditions for the formation and explosion of the cloud. The particles' sizes, shapes and densities will play a role in combustion, as it is more difficult, for example, to keep a cloud of heavy spherical particles in suspension than small fibres of low-density material. Dust suspensions can be caused by the operating conditions of an industrial process or by a pressure wave generated by an explosion. A typical example are the fire-damp explosions in mines, where the ignition of a methane pocket suspends coal particles and then burns them.

The high-density ratio between gases and combustible particles means that the same proportional amount of energy as one encounters in fire-damp scenarios can be stored in a very small volume: a layer of one millimetre of dust over 1 m^2 is enough to generate an ATEX of 1 m^3 .

Although turbulence plays a key role, modelling it remains largely inaccessible for these multiphase mixtures. Because of their density, particles have more inertia than the air surrounding them. As a result, they have their own velocity field, which is different from that of the air, and they do not follow the same streamlines as the air around them. The size and shape of the particles will also have a significant impact on this. As far as the turbulent combustion of gas-particle clouds is concerned, the knowledge available on this subject is limited. Several experimental observations confirm that the greater the agitation of the medium, the more vigorous the combustion, but very few physical representations exist. The transport equations in these two-phase mixtures are not the same as those for gases either: depending on the particle concentration; the fluid may behave like an ideal gas or, on the contrary, when there are many particles, it may exhibit non-Newtonian behaviour, which can be extremely complex to describe.

Generally speaking, particles will absorb some of the fluid's momentum. However, the behaviour of a 1 kg/m^3 loaded fluid with 500 g particles per m^3 , is not equivalent to that of a fluid loaded at 1.5 kg/m^3 but is closer to that of gas alone. Finally, in the absence of a better solution, the turbulence and transport models established for gases are transposed to the case of gas-particle mixtures.

According to Andrews (2017), mixtures of combustible droplet aerosols in air (e.g. hydrocarbons) would behave partly like combustible air-dust clouds. Testing these clouds in a confined environment is complex because droplet aerosols tend to puddle when they encounter obstacles.

These fluid mechanics problems are general to combustible air-dust mixtures and hybrid mixtures (air - combustible gases - combustible dust). In terms of thermodynamics, there are other differences. It should be remembered that for combustible gases, concentration conditions of LEL, Lower Explosive Limit, UEL, Upper Explosive Limit and stoichiometry in air can be defined. and that the worst situation in terms of effect appears for a richness slightly greater than 1, around 1.05 - 1.15. It follows that for air-dust mixtures:

- There is also an LEL, generally around one hundred grams per cubic metre for the usual organic particles (flour, starch), but it can be as low as 30 g/m³ for wood fibres (Wilén, 1999). While for gases, the LEL is often of the order of half the stoichiometry, or even as low as 15 to 20% of the stoichiometry in the case of dusts;
- the existence of a UEL has not been clearly demonstrated, as its measurement often comes up against problems with the formation of the combustible cloud. INERIS has already demonstrated dust explosions at concentrations of several kg/m³;
- In most cases, the reaction optimum is well above a richness of 1. For wood dust, for example, the stoichiometry lies around 210 g/m³ (Wilén, 1999), and an optimum can typically be found in the 500 to 750 g/m³ range.

The phenomenon becomes even more complicated when combustible gases are mixed with air and combustible particles. A flammable gas can make a dust-gas mixture explosive at a dust concentration below the standard lower explosive limits for concentrations of dust and alone. These reduced LELs can also render explosive a cloud of dust made up of particles that are usually too large to propagate an explosion. The minimum explosive concentration, minimum ignition temperature and minimum ignition energy are all reduced, which in turn act to increase the rate of pressure rise. (Abassi, 2007). The energy contribution of particles can, therefore, drastically increase the energy yield of combustion.

3.8 Effects of the explosion on the enclosure where the explosion occurs

The main feature of a confined gas explosion is the transformation of cold reactants into hot products that expand. Therefore, thermal and mechanical effects due to overpressure can be expected in the enclosure where the explosion occurs.

In practice, the thermal effects are indirect. The explosion is caused by a fast-moving flame, whose velocity of a few m/s up to tens of m/s is increased proportionally by a 3-D expansion rate on the order of 2 to 10 depending on the gas concentration. This means that in the largest volumes, the explosion only lasts a few seconds. We can assume that a certain volume, V, of hot gases is obtained in an enclosure at ambient temperature. This is due to the relative longer times required for heat transfer from the gases to the enclosure. the characteristic times for heat transfer from the gases to the enclosure are very long compared with those of the explosion. Heat exchange between the mass of hot air and the walls is essentially by convection once the explosion is over.

To calculate an equilibrium temperature T_E between 2 isolated bodies A and B exchanging heat, we need to know their masses m_A and m_B , their initial temperatures T_A and T_B and their mass heat capacities c_A and c_B :

$$T_E = \frac{T_A \cdot c_A \cdot m_A + T_B \cdot c_B \cdot m_B}{c_A \cdot m_A + c_B \cdot m_B} \quad \text{Equation 54}$$

Heat capacity characterises a material's ability to store heat. A high heat capacity means that a large amount of energy can be stored with a relatively small increase in temperature. Air has a heat capacity of around 1000 J/K/kg, steel 450 J/K/kg and aluminium 900 J/K/kg. The orders of magnitude are equivalent at this level. However, this is not the case for the density of the materials: the density of the solids that make up the enclosure is around 1000 times that of the gases it contains. So, even if the enclosure walls seem thin, they can absorb a large amount of heat. Assuming a cubic box measuring 1 m³, with walls 1 mm thick, and containing gases at 2000°C, we obtain an equilibrium temperature of 130°C for steel and 170°C for aluminium. If the cube is 1000 m³ with 5 mm thick walls, the temperatures for steel and aluminium are 40°C and 50°C respectively. Irrespective of any consideration of the enclosure's resistance to explosion overpressure, the direct thermal effect does not appear to be a critical hazard for the enclosure. Enclosures subjected to explosions are themselves sources of fire propagation often owing to the escape of burnt gases rendering most thermal effects indirect.

The overpressure generated by explosions induces mechanical stress on enclosures. The behaviour of structures subjected to pressure waves depends not only on the intensity, that is maximum overpressure of the wave received but also on its duration and shape. In addition, the friable or ductile nature of the materials composing a structure along with the context of its industrial use are factors that determine whether an enclosure will or will not sustain an explosion as the first plastic deformities appear before complete rupture or tearing away of a wall. Overpressure, wave shape and duration present different effects on brittle materials such as concrete), thusly there can be major differences between the behaviour of friable and ductile materials, such as aluminium and steel.

The methods used to determine the resistance of structures to accidental actions are usually of three types:

- 1) empirical methods, which are the most frequently used for assessing effects. The most common methods are damage tables as a function of pressure level and P-I (pressure - impulse) diagrams. In the first case, thresholds are available in the scientific literature and are often derived from tests and feedback from accidents. In the second case, the P-I diagrams are hyperbolas which follow $1/X$ patterns providing better information about the behaviour of the structure in the face of pressure and time stresses . These diagrams also contain empirical data obtained from tests. A typical P-I diagram is shown below:

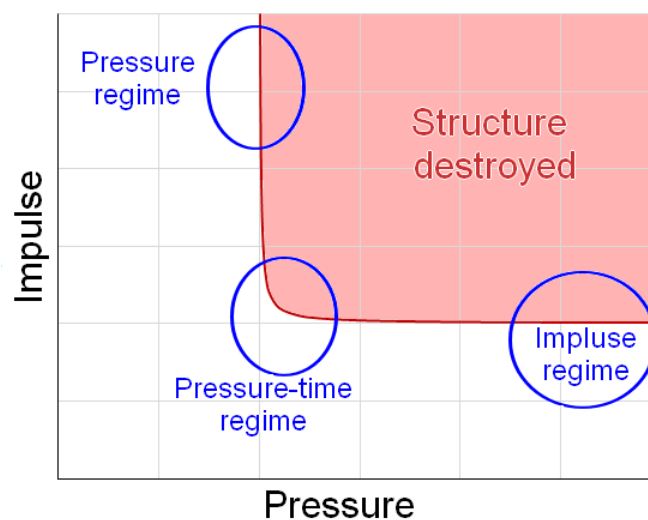


Figure 37. Diagram of a P-I diagram

The structure reacts differently depending on the load. For example, in the pressure regime, the impulse is of little importance, and only the pressure level is sufficient to indicate whether the enclosure is holding or not. A rule of thumb based on normative pressure levels is well suited in this case. The impulse regime is the opposite: the structure can well tolerate pressure variations as long as they are short. In the pressure-time regime, a dynamic calculation may be necessary.

- 2) analytical methods, which mainly use a mass-spring analogy to calculate a stress level in the structure, compare these calculated values with the stress at failure data to determine whether the structure remains intact;
- 3) Complete numerical methods which couple a CFD code that applies the pressure field to the structure with a finite element code that gives the structure's stress distribution. These more precise methods, which take into account the actual layout of the enclosure (fixings, materials, etc.), are costly in terms of calculation time and often require the use of parallelised computers.

In particular, structural behaviour when subjected to a pressure load of known amplitude, time, and shape is linked not only to the materials of which they are made but also to their dimensions and layout. Other factors such as the vibrational periods and modes of failure are undoubtedly important. For further information, see the Omega project on structures' resistance to accidental actions (Reimeringer, 2007).

3.9 External effects

When there are openings in the enclosure or group of enclosures where the confined explosion occurs, two types of external effects are expected: flames and pressure waves. These are manifested by a secondary explosion phenomenon, as described in paragraph 3.5.2.3, which contributes to the expansion of compressed gases from the enclosure into the air.

In the field of confined explosions, it is relatively rare for questions to be asked about the thermal radiation effects of the external fireball. It should be noted that although the temperatures reached can be very high, the duration of the fireballs is short (a few seconds for the largest clouds, outside a grain silo, for example) so that the dangerous thermal effects remain limited to direct contact with the flame, which can cause effects on humans (burns) or the environment (propagation of a fire). This is why thermal effects are determined based on the maximum flame length, generally estimated by empirical models.

Pressure waves transmitted into the atmosphere can be of several types:

- In the case of a total confinement that bursts, a shock wave is observed in the air. Its origin is mechanical and due to an almost instantaneous pressure gradient between the pressurised gases and the surrounding air.
- Shock waves are also transmitted through the air during a detonation.
- In the presence of permanent or progressive openings, or in the case of a secondary explosion, the pressure wave is of chemical origin. It is produced by the expansion of the fireball and ceases when it is extinguished. It is, therefore, a transitory phenomenon that propagates outwards at a velocity comparable to that of sound. As long as the flame is developing, the surrounding atmosphere and the interior of the fireball is put under pressure. An overpressure wave is emitted. When combustion stops, the fireball must depressurise and return to atmospheric pressure, which is achieved by an expansion wave that starts at the flame front and slows down the gas velocity both outwards and inwards. This explains why the blast wave comprises a pressure wave and an expansion wave, which most often take the form shown in Figure 38-a. This waveform is called an "N" wave. When the flame's propagation velocity reaches a speed of about 120 m/s, the overpressure wave generated is the composition of a shock wave and an N-wave (Figure 38-b). When the flame propagates sufficiently fast, typically at a speed comparable to that of sound, the different waves emitted during the development of the flame come together and merge to form a "steep front" typical of "shock waves" (Figure 38-c).

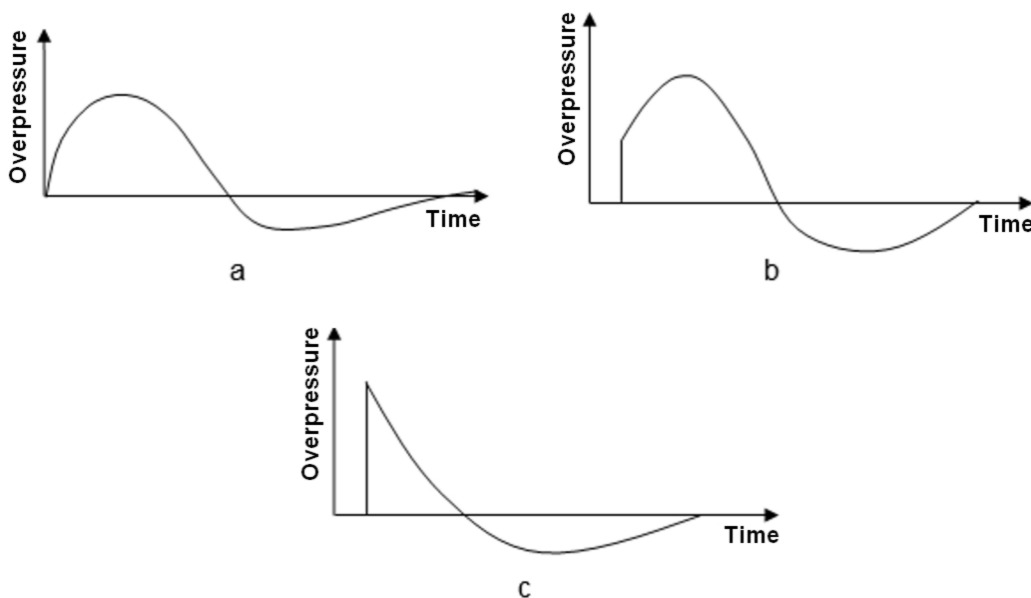


Figure 38. N-shaped waves (a, b) and shock wave (c)

Except for specific situations involving irregular reflections, the physics of shock waves in air is well known and obeys simpler laws than those of sonic pressure waves. They are also easier to produce and reproduce experimentally, so the charts or databases that provide damage levels as a function of overpressure are most often associated with shock waves.

Another difference between the two types of waves is whether they are isotropic or non-isotropic. Shock waves are disturbances that aim to re-establish equilibrium between the compressed medium and the atmosphere. They are isotropic, propagating at the same speed and amplitude in all directions, as long as they do not interact with obstacles. Progressive compression waves can have directional effects and are affected by the flow.

So, in front of a vent on the axis, at a certain distance d , there is more pressure than at the same distance d further away from the axis.

The aim of the methods used to assess the effects of overpressure is to estimate the external effects of a confined explosion on property and people. For this purpose, French legislation (the decree of 29 September 2005) uses the following thresholds:

For structures:

- 20 hPa or mbar: threshold for significant destruction of windows;⁵
- 50 hPa or mbar: threshold for slight damage to structures;
- 140 hPa or mbar: threshold for severe damage to structures;
- 200 hPa or mbar: threshold for domino effects;⁶
- 300 hPa or mbar: threshold for very severe damage to structures.

For people:

- 20 hPa or mbar: effects threshold delimiting the zone of indirect effects on humans through broken glass,
- 50 hPa or mbar: threshold for irreversible effects delimiting the "zone of significant danger to human life"
- 140 hPa or mbar: threshold for lethal effects, delimiting the "zone of severe danger to human life",
- 200 hPa or mbar: threshold for significant lethal effects delimiting the "zone of very severe danger to human life".

The effects on humans are indirect. In practice, the human body is a soft structure highly resistant to shock and can withstand several hundred mbar. Nevertheless, an airflow of 50 mbar already develops enough force to lift and accelerate objects that will become dangerous projectiles or throw a man to the ground.

⁵ The regulations specify that, "taking into account the modelling dispersions for low overpressures, an effect distance equal to twice the effect distance obtained for an overpressure of 50 mbar may be adopted for an overpressure of 20 mbar".

⁶ The regulations specify that this is "the threshold above which domino effects must be examined. Modulation is possible depending on the materials and structures involved".

4. Modelling and calculation of the pressure effects of confined explosions

4.1 The main categories of models

When modelling a physical phenomenon, two main tools are available: the empirical method and the formal method. The underlying idea is that in the first case, the result is obtained by direct comparison with an experimental observation. In contrast, in the second, a theoretical reflection is made based on axioms and equations that are assumed to describe precisely the physical behaviour being studied. In practice, these two methods are often combined in models of varying complexity, used to estimate the effects of a physical phenomenon. In the context of estimating the effects of hazardous phenomena, models are commonly classified into three categories according to their complexity or degree of representativeness of the physics of the phenomena:

- empirical models, which include simple presumptive methods (e.g. "windows break at 20 mbar overpressure") and any regression based on experimental observations, such as the calculation of a turbulent flame velocity S_t as a function of the laminar flame velocity S_{lad} , and the turbulence parameters u' and L_t (see paragraph 3.4.2). They form the basis of the models presented in this chapter.
- phenomenological models, which are mainly based on equations derived from the major theories of physics, such as the fundamental principle of dynamics. It is worth remembering that empirical equations can also be used in this model type (such as the turbulent velocity term in the previous section). The approach in chapter 3 of this report follows this type of description.
- CFD (Computational Fluid Dynamics) models, which are also constructed in the same way as phenomenological models but are admittedly more complex, particularly in terms of their data implementation and the volume of results produced. These models solve the Navier-Stokes equations (or the Euler equations where relevant) and use various methods to ensure the equations are closed (RANS, LES, DNS turbulence models, etc.). They assume a discretisation of the problem in space and time.

4.2 Reference situation

In this chapter, we return to the reference situation, the phenomenology of which was discussed in paragraph 3.5.2; that of an enclosure filled with a gas ATEX initially at rest, in the absence of obstacles and ignited by a source of ignition sufficiently strong to trigger the explosion without however reaching the detonation regime. The following paragraphs examine some of the most commonly used models for estimating an explosion's internal and external overpressure effects. The diagram of the typical overpressure profile described by Harris (1983) is recalled:

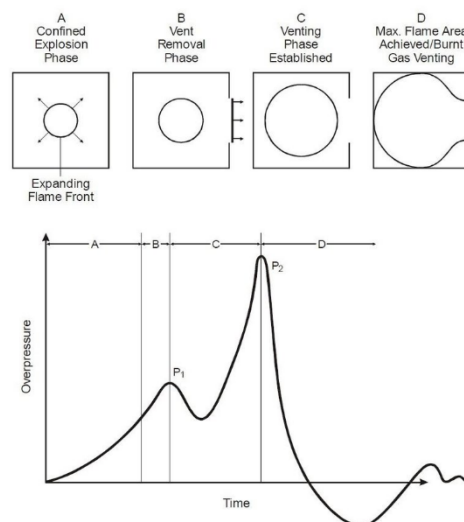


Figure 39. Illustration of the role of explosion vents, Harris (1983)

Therefore, given the reference situation and the over pressures profiles, the objective is to clearly define the issues to determine the value of the maximum overpressure reached at point P₂ and the evolution of the overpressure generated in the vicinity of the enclosure.

The empirical models typically used to describe the phenomenon are based on a set of variables specific to the industrial safety context. Some additional terms, therefore, need to be defined to facilitate subsequent understanding of the models:

- **A_v** is the physical vent area, i.e. the maximum real surface area of the open vent;
- **L** usually refers to the longest distance the flame can travel in the enclosure;
- **D** is the characteristic diameter of the enclosure;
- **P_{max}** is the maximum explosion overpressure, measured in accordance with standard EN13673-1;
- **K_g** is the gas explosivity constant, which is the maximum value of the rate of pressure rise per unit of time (dp/dt)_{max} during the explosion of a specific explosive atmosphere in a closed container under standardised test conditions and reduced to a container volume of 1 m³ by multiplying by V^{1/3}. It is defined in EN13673-2;
- **P_{stat}** is the static activation pressure of the vent: the overpressure at which the vent opens, with a maximum tolerance of 15%, under static conditions. It is defined in standard EN14797:2006;
- **P_{red}** is the reduced explosion overpressure: the maximum overpressure obtained in the enclosure by vent opening.

4.3 Multiphysics modelling, CFD approach

4.3.1 Foundations of the method

The science of explosion is based on several major areas of physics. Four branches of physics are particularly concerned with explosions: chemical kinetics, thermodynamics, fluid mechanics and structural mechanics. Thermodynamic laws dictate the behaviour of an explosion, while chemical kinetics determine its speed. The explosion generates flames and pressure. These effects are transmitted in the vicinity of the explosion according to the laws of fluid mechanics and interact with neighbouring structures within the framework of structural mechanics. During an explosion, these four principal domains interact to such an extent that modelling the complete multi-physics phenomena is only possible under a certain number of simplifications.

In the context of industrial safety, which is the focus of this report, the main interest is in the effects of explosions on people. As a result, greater importance is often attached to the mechanical aspects of explosions. Chemistry, for example, is often reduced to Arrhenius' law alone, with a law on species conservation where necessary. Thermodynamics is often reduced to simplifying a major principle, as in the case of entropy conservation, which is reduced to Laplace's law. The equation of state chosen for gases is usually that of perfect gases. The case of the rupture of structures is most often envisaged by simple presumptions. The aspect dealt with in most detail in an industrial safety context is fluid mechanics. The equations at the heart of the problem are the Navier-Stokes equations with which for a Newtonian fluid, we write:

$$\frac{\partial \mathbf{V}}{\partial t} + \nabla \cdot \mathbf{F}(\mathbf{V}) = 0 \quad \text{Equation 55}$$

$$\mathbf{V} = \begin{pmatrix} \rho \\ \rho \mathbf{u} \\ \rho e_t \end{pmatrix} \quad \text{Equation 56}$$

$$\mathbf{F} = \begin{pmatrix} \rho \mathbf{u} \\ \rho \mathbf{u} \cdot \mathbf{u} + p \mathbf{I} - \boldsymbol{\tau} \\ (\rho e_t + p) \mathbf{u} - \boldsymbol{\tau} \cdot \mathbf{u} + \mathbf{q} \end{pmatrix} \quad \text{Equation 57}$$

$$\text{Gaz idéal: } p = \rho \cdot r \cdot T \text{ et } e_t = \frac{p}{\gamma - 1} + \frac{\rho \cdot \mathbf{u}^2}{2} \quad \text{Equation 58}$$

where ρ is the density, \mathbf{u} the velocity field, e_t the total energy, \mathbf{I} the identity matrix, $\boldsymbol{\tau}$ the viscous stress tensor, \mathbf{q} a heat production term, T the temperature and γ the specific heat ratio.

These equations have two specific features that make them particularly difficult to solve:

- 1) they are non-linear so that minor disturbances in one area of the flow may have no effect at all after some time or may change the flow entirely;
- 2) they include a coupling term between the different directions of the flow, which implies non-isotropic wave propagation and disturbances that will evolve in 3 dimensions. In practice, disturbances due to turbulence manifest themselves as eddies on different scales in 3D. 2D simulations of turbulence are necessarily biased.

These equations are valid for inert flow. When there is a reaction, we must add the chemical model chosen for combustion allowing for the determination of \mathbf{q} for a species in the conservation equation.

4.3.2 CFD for explosions

4.3.2.1 Turbulence modelling

Direct resolution of the Navier-Stokes equations (known by the acronym DNS: Direct Numerical Simulation) is extremely costly regarding calculation time/resources and is more often applied by laboratories for analyses of small, cm, scales systems.

Industry has traditionally used the Reynolds-Averaged Navier-Stokes equations (RANS) approach technique to solve a set of averaged Navier-Stokes equations. This new set of equations is obtained by applying an operator that decomposes any physical parameter into two contributions: an average contribution and a contribution that fluctuates around this average and whose average is zero. This is known as the Reynolds decomposition. Averaging the Navier-Stokes equations after this decomposition reveals, due to the non-linearity of the equations, an unexplained quantity: the Reynolds tensor. A model is then required to determine this quantity. Here are some of the best-known models: $k - \epsilon$ (Launder, 1974), and $k - \omega$ (Wilcox, 2008), Spalart-Allmaras (1994).

The level of resolution of the physics is moderate since the entire turbulent spectrum is modelled by RANS in a confined closed environment. This approach places on the same plane large eddies and small eddies, both strongly affected in such confinement, and which arrive at a point of equilibrium between viscous and inertial forces.

Another technique used for moderate-scale technical applications (from tens of centimetres to metres) is Large-Eddy Simulation (LES). This approach involves solving filtered Navier-Stokes equations. The filter is linked to the mesh size used. The large scales of the turbulent spectrum are thus explicitly resolved on the mesh, and only the smallest scales are modelled. A resolution of 80% of the turbulent spectrum is often considered a criterion of good quality for an LES (Pope, 2004). This approach offers a higher level of physics resolution than RANS. On the other hand, it is more demanding in terms of computational resources, as the mesh sizes are smaller than those associated with a RANS calculation, and the discretisation schemes are potentially more complex and resource intensive. It is important to limit the spread of resolved scales. A sub-mesh model is required to quantify unresolved transport. Examples include the Smagorinsky model (Smagorinsky, 1963), the dynamic Smagorinsky model (Germano, 1991 and Lilly, 1992) and the WALE model (Ducros, 1998).

Other, more recent methods exist, which are often improvements (URANS) or hybrids of these models (RANS-LES, DES).

4.3.2.2 Combustion modelling

With the application of averaging or filtering operations, and the necessity to model chemical terms during turbulent combustion conditions there remains difficulties to take into account, The choice of the combustion model may be constrained by the choice of the turbulence model.

RANS approaches can, for example, model the propagation of the flame front by treating it as an interface, materialised by a gradient of the reaction's progress variable, propagating at a turbulent velocity made explicit by a correlation. This type of approach, used particularly in the FLACS tool (Arntzen, 1998), has the advantage of being simple in its formulation.

Other approaches, such as flame surface density models (Veynante, 2002), propose a closure of the source term that is similar in form to flame folding. The difference on the other hand, is that the flame surface density model is closed by solving a transport equation. The recent literature highlights work that takes up this type of approach and adapts it in an ad hoc manner to account for explosions (Tolias, 2018).

The EDC (Eddy-Dissipation Concept) model assumes that combustion takes place at the smallest characteristic scales of turbulence, leading to the closure of source terms with a slightly more complex shape (Rian, 2016).

The LES or VLES approach has led to explosion modelling based on algebraically closed surface density models. The closures can take complex forms because they incorporate phenomena that are not resolved by the system of transport equations or the mesh (Xiao, 2012).

The LES approach can also be coupled with the thickened flame model to account for an explosion (Quillatre, 2014). In this case, the flame front is artificially thickened to facilitate its resolution by the mesh. An efficiency function is used to model the loss of flame wrinkling due to the thickening effect.

4.3.2.3 Obstacle modelling

Limiting the examination to the case of industrial-scale explosions, two families of CFD codes emerge with regard to the treatment of geometry:

- an approach that resolves the obstacles using the mesh. The boundary layer needs to be modelled by either by choosing a wall law or by resolving it using the mesh, which can be very costly;
- a PDR (Porosity/Distributed Resistance) approach incorporating an additional level of modelling. This approach sub-models (in other words, does not solve) all the obstacles that may be present in the calculation domain, such as pipes with a non-negligible cross-section, for example. A porosity field represents the effect of these obstacles. Non-zero porosity, linked to a partial or total obstruction in a mesh by a geometric element, affects the flow and the flame. This additional level of modelling makes it possible to process large calculation domains (a few hundred metres on each side) while allowing a turnaround time of the order of a few minutes to a few hours for an office machine.

4.3.3 Example of CFD modelling of confined explosions

A CFD calculation is used to study an H_2 / air mixture explosion with a volume fraction of 21% in a 4 m^3 enclosure. This case is taken from an experimental campaign conducted at INERIS (Duclos, 2019). A diagram and photograph of the 4 m^3 enclosure are shown in Figure 40:

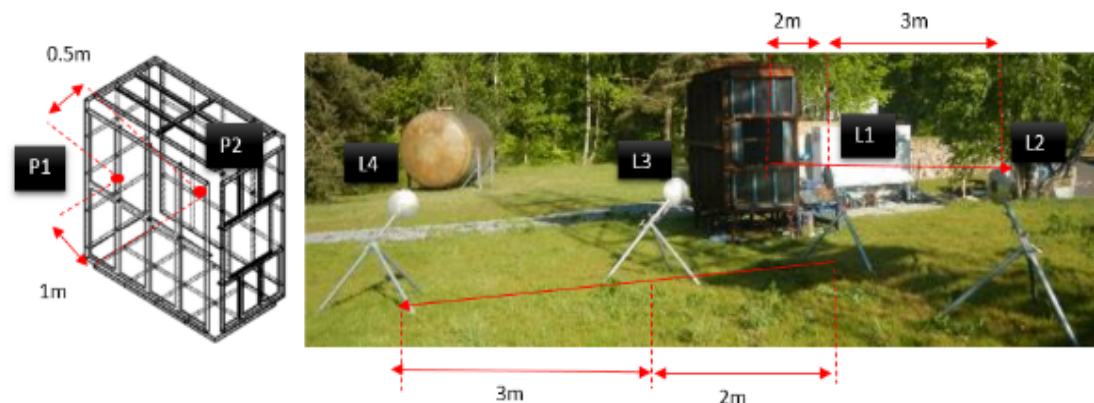


Figure 40. A diagram and photograph of the 4 m^3 enclosure, Duclos (2019)

The flammable atmosphere is contained in the enclosure. It is homogeneous in concentration, and its initial turbulence characteristics have been measured. The enclosure is fitted with an inertia-free vent (made of plastic sheeting) measuring $700 \times 700\text{ mm}$, with a static opening pressure of around 50 mbar. The ATEX is ignited at the bottom of the enclosure, on the side opposite the vent. There are two pressure sensors on two sides of the enclosure: P1 at the bottom and P2 at the center of one face. Outside, external pressure sensors L1 and L2 are placed at 2 and 5 meters from the vent along the axis. These are level with L1 but perpendicular to the L1-L2 line, with sensors L3 and L4 placed 2 and then 5 m from L1.

Images of the explosion of the 21% H_2 -air mixture initially at rest are shown in Figure 41:

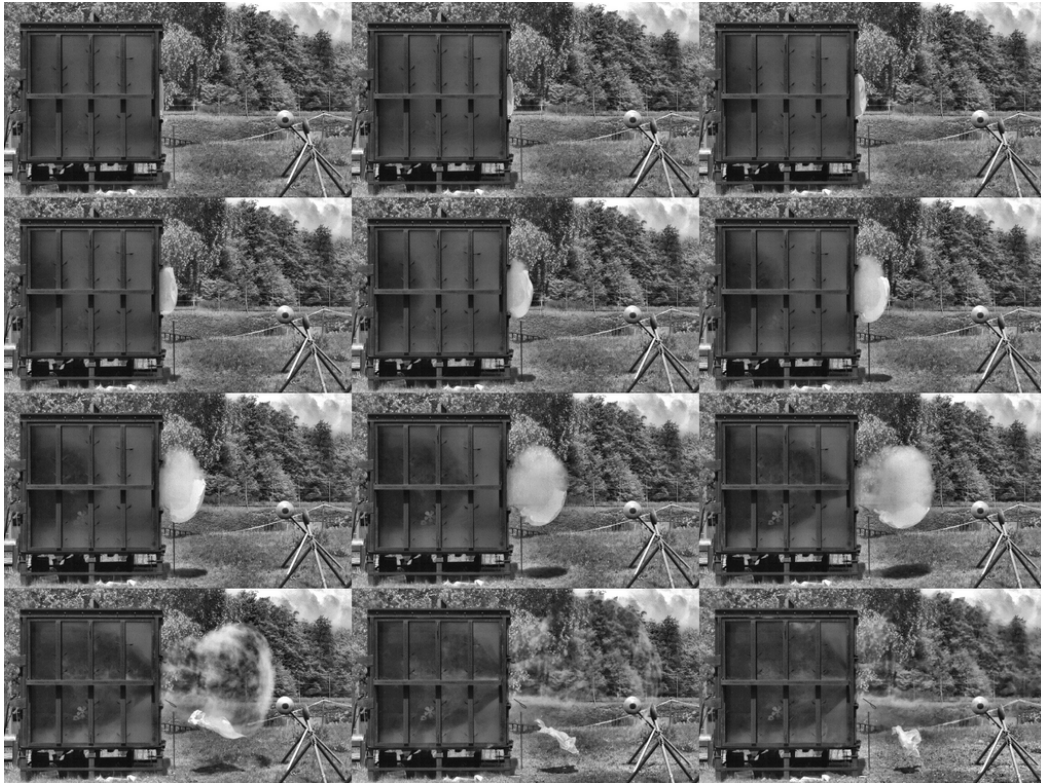


Figure 42. Images of the explosion of a 21% H_2 - air mixture, initially at rest, in a 4 m^3 enclosure fitted with a 0.49 m^2 vent. 20 ms between each image.

The Navier-Stokes equations are accompanied by equations for chemical species and energy to describe the explosion phenomenon. Additional modelling operations are required to solve these equations using computers:

- Since this set of equations cannot resolve all the turbulence, whether pre-existing before ignition or generated by the flame front movement, an averaging or filtering operator is applied (the classic LES or RANS approach);
- Filtered or averaged chemical source terms appearing in the transport equations must be modelled. This is known as turbulent combustion modelling.

In this case, the mesh comprises 5 million hexahedral cells spread over a calculation domain of the order of $20\text{ m} \times 20\text{ m} \times 10\text{ m}$. The mesh is refined inside the enclosure and in the pressure measurement zones.

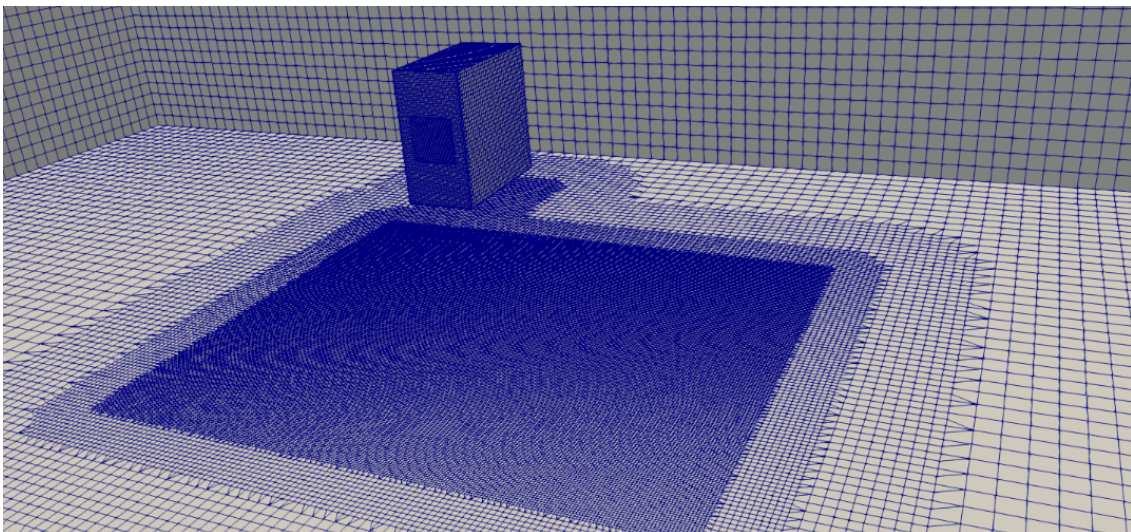


Figure 43. Representation of the calculation domain and mesh

The literature on H₂ air explosions includes various modelling strategies combining the choices of the turbulence and turbulent combustion model in conjunction with additional sub-models.

In this case, the following assumptions have been made:

- a turbulence model, k- ϵ , the best-known model for turbulence, developed by Jones and Launder (1972) gives a general description of turbulence using two transport equations: one for turbulent kinetic energy (k) and the other for dissipation (ϵ). The model is based on empirically derived coefficients;
- a pseudo-flame surface density model (Lecocq, 2011) for turbulent combustion. Briefly, a flame surface density model calculates an estimate of the pleated flame surface in the mesh cell volume, which is then multiplied by the laminar flame velocity to determine the combustion rate;
- the addition of an empirical correction to account for the propensity of H₂ - air mixtures to self-accelerate in the absence of initial turbulence. This is quantified using experimental measurements; in this case, it increases the laminar flame velocity by a factor of 3.

This strategy is very similar in its construction and choice of models to that recommended recently by DEMOKRITOS, for example (Tolias, 2018).

It is possible to take the vent into account, but this requires a model describing the displacement of the vent surface to be coupled to the equation of fluid motion with a displacement of the boundary conditions on the mesh as a function of time. In this case, the vent is modelled as a simple permanent opening.

The calculation results are compared with the high-speed videos and measured signals as presented below with generally good agreement. (Figures 43 and 44).

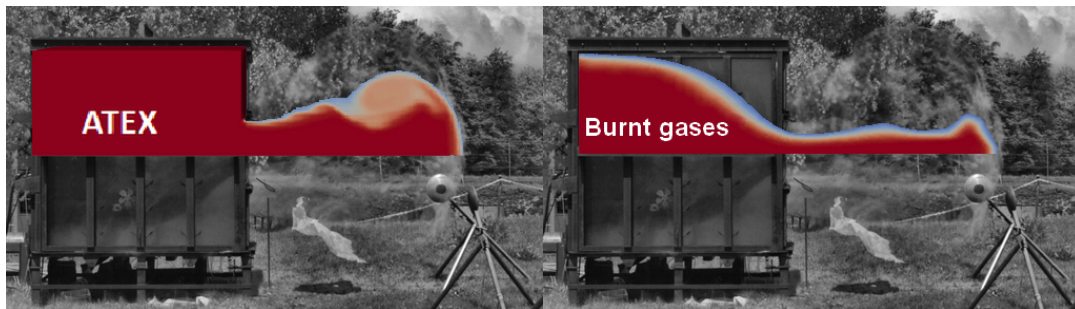


Figure 44. Position of the cloud and the flame when it reaches the edge of the cloud (ATEX refers here to the complete explosive cloud: all the reactive chemical species burnt)

The burnt gas advance along the axis of the vent and the position of the flame in the enclosure, as depicted in Figure 43 are well represented. Although it seems that in the real case, the radial expansion of the products and the flame are greater.

The following signals are measured and calculated in the enclosure:

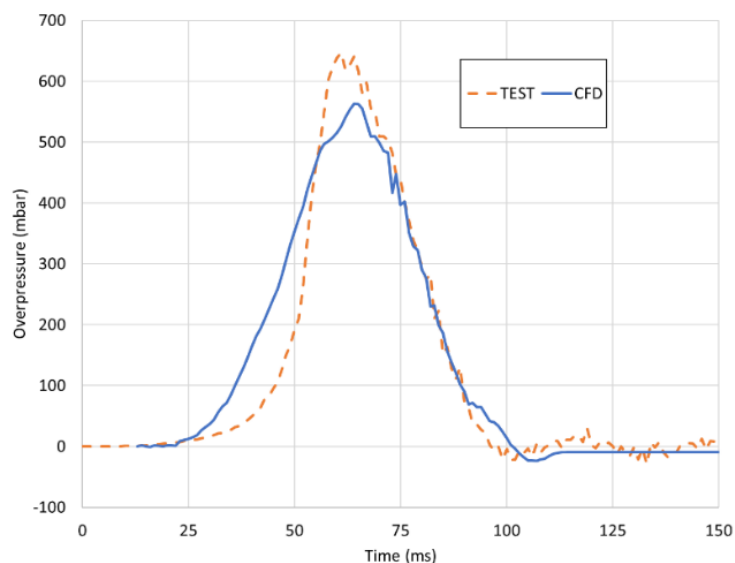


Figure 45. Pressure signals in the enclosure, measured during the test and calculated with the CFD tool

The simulation shows a rate of pressure rise that is initially faster than in the test. Although delayed, the experimental profile is steeper, and the maximum pressure level reached is ultimately greater than in the calculation. However, the order of magnitude of the maximum is well matched by the calculation, yielding 560 mbar compared with 650 mbar in the test.

Outside the enclosure, the results are as follows:

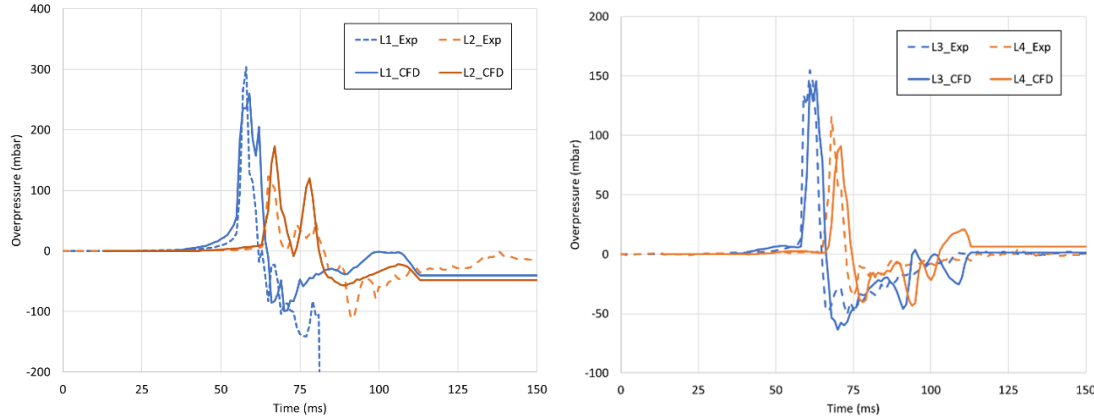


Figure 46. External pressure signals from sensors L1 and L2, then L3 and L4, measured and calculated

The CFD calculation generally matches the amplitudes and arrivals of the primary and secondary peaks well. During the test, the L1 sensor was damaged and drifted after the arrival of the overpressure peak, which explains the disappearance of the signal after $t = 80$ ms. By choosing the physical models appropriately, in line with the simulated phenomenon, the CFD calculation makes it possible to reproduce specific experimental observations, however, the exercise remains complex. For example, in this particular case, a relatively strong assumption was made about the explosion vent being replaced by a simple opening, the opening dynamics of which were therefore not modelled. Here, the vent represents only 3% of the internal surface of the containment and around 5% of the maximum flame surface measured. The use of a larger vent would probably have required a different approach.

4.3.4 Detonations

The case of detonation and air-borne shocks can be treated differently. As detonation is a very rapid process, molecular transport and viscosity phenomena are neglected. Thus, behind the detonation wave, the flow can be described by the unsteady, three-dimensional, compressible Euler equations of adiabatic flow, an equation of state $e(P, v, \lambda)$ and the laws of chemical kinetics, supplemented by the species conservation equation translating the transformation of the reactive gas into the detonation products. The physical problem is thereby simplified, and the RANS, LES or DNS considerations are no longer necessary.

The Euler equations (Equation 59 à Equation 61) and conservation of species (Equation 62):

$$\frac{\partial \rho}{\partial t} + \nabla \cdot (\rho \mathbf{u}) = 0 \quad \text{Equation 59}$$

$$\frac{\partial \rho \mathbf{u}}{\partial t} + \nabla \cdot (\rho \mathbf{u} \otimes \mathbf{u}) = -\nabla p \quad \text{Equation 60}$$

$$\frac{\partial \rho E}{\partial t} + \nabla \cdot (\rho \mathbf{u} \cdot (E + p)) = 0 \quad \text{Equation 61}$$

$$\frac{\partial \rho_{fuel}}{\partial t} + \nabla \cdot (\rho_{fuel} \mathbf{u}) = S_{fuel} - P_{fuel} \quad \text{Equation 62}$$

The equation of state is chosen according to the characteristics of the reactive medium, as are the chemical kinetics laws. The equations of state are either derived from theoretical models or are empirical or semi-empirical, in nature and employ tabulated databases. The most commonly used equation is the empirical Jones, Wilkins and Lee (JWL) equation:

$$P = A \left(1 - \frac{w}{R_1 V} \right) e^{-R_1 V} + B \left(1 - \frac{w}{R_2 V} \right) e^{-R_2 V} + \frac{we}{V} \quad \text{Equation 63}$$

V and e are known (the specific volume and internal energy); the other terms are constants specific to each explosive that can be found in tables or with other equations.

The above equations can be used to model the evolution of a detonation wave in a homogeneous reactive medium. However, when dealing with concrete problems, the stability of the calculation schemes is conditioned by the characteristic scales of the phenomena studied. For example, if we want to model the detonation of a 1 m³ gaseous sphere, the numerical treatment of these equations, even in one-dimensional spherical coordinates, requires powerful calculation tools. In the explosive, the thickness of the reaction zone will be of the order of 1 mm, and at least ten meshes would be needed to discretize the zone of the pressure peak of the detonation wave. Insufficient meshing inevitably leads to a curve smoothing, a diffusion of the shock, which is not physical and leads to an underestimation of the effects of the explosion. Whereas the peak is generally 10-20 bar for gases. In contrast, when the blast wave generated in the associated medium reaches a distance of 6-7 m from the charge, the incident excess pressure is of the order of 0.2 bar. Such distances require meshes that adapt to the calculation over time and a powerful computing platform. Eventually, during the explosion phenomenon, it is necessary to consider the reflections of the shock waves on various obstacles and the mixing of the detonation gases with the surrounding air. Ultimately, there are still very significant mesh requirements even if we gain computing capacity by switching to Euler's equations. Retaining the Navier-Stokes equations to deal with this type of problem would even be counter-productive if it were not justified, for example, by significant fluid-wall interaction, because these equations explicitly introduce viscosity terms that contribute to unjustified smoothing of the shock waves, which will therefore have to be corrected.

4.3.5 Modelling the deflagration to detonation transition (DDT)

In practice, the real problem is determining the potential for and risk of a gaseous deflagration transitioning to detonation. The problem is modelling the DDT. In this situation, the aim is typically to assess the risk DDT and to protect against it if it exists. The acceleration of a H₂-air flame in a pipe, which will transition to detonation if certain conditions are met. The first challenge is to determine the propitious conditions one of which is the formation of heterogeneities in the flow linked to turbulence, lending a stochastic component to the phenomenon. The challenge of the calculations is often determining a probable transition distance to detonation.

Detonations occur when local conditions in reactive gas mixture allow a spontaneous wave to form, evolving into a shock strong enough to sustain a detonation that can propagate outside the zone under consideration. This is one possible mechanism for generating a detonation, but others are possible (see, for example, the work by Liberman, 2010). A gradient mechanism for detonation formation, proposed by Zeldovich (1970) and since discussed and generalised by many researchers, indicates that a local reactivity gradient, which often appears near a hot spot, can generate a supersonic/spontaneous wave that can undergo a transition to detonation. If such a wave is produced, the result is a decoupled flame and a shock. In the simulation, a temperature or reactivity gradient will be sought (via, for example, the local expansion rate of the products defined as the ratio of the densities of the fresh and burnt gases).

To be maintained, detonation requires a minimum critical diameter, λ , corresponding to a detonation cell width, and an induction length of around 7 λ . The notion of a detonation cell has not been addressed in this report, yet its size remains an important factor. In a very simplified way, it will be remembered that the flame in the stable detonation wave has a cellular structure. The diameter λ of the cells depends on the nature and concentration of the reactive mixture.

If the cells are prevented from developing, for example by confining the explosion in too small a space, stable propagation of the detonation is prevented (unstable detonations can, however, propagate). For a H₂-air mixture at stoichiometry, λ is of the order of 1 to 2 cm; however, for less reactive gases such as methane or diluted mixtures, this value increases significantly, and cells of 50 cm are possible. For more information on the links between detonation cells and combustion properties, reference can be made to the work of Thomas (2012).

In CFD codes, the criteria used for the onset of detonation waves are linked to an acceleration factor and geometric considerations.

In practice, the main difficulty in simulating DDT arises from the scale factor. As previously discussed, simulations of reactive flows with the Navier Stokes equations rarely use a DNS approach. Instead, a model is used to estimate turbulence. The underlying idea of a turbulence model is to solve the large-scale mean fluid dynamics equations on a computational grid in which the smallest grid size is significantly larger than the scale at which viscous dissipation occurs. Next, the effects of turbulence and viscous dissipation at the sub-grid scale are modelled by calculating additional terms as a function of the turbulence model chosen. The desired effect is to model small-scale effects not resolved by the mesh, which often adds significant amounts of numerical diffusion. By diffusing numerically, we smooth out the values in the elementary volumes, making the extremums, decisive for the appearance of DDT, disappear.

This is why we consider that the main difficulty simulating DDT is the problem of scale. Solving the scalar problem requires information about the dynamics of the interactions between flames, shocks, boundary layers and turbulence. These highly non-linear interactions involve several physical and chemical processes that occur on spatial scales spanning many orders of magnitude. At the scale of a laboratory test, the thickness of the flame is typically 4 to 6 orders of magnitude smaller than the size of the system. The scales can differ by up to 10 orders of magnitude for industrial scenarios (Oran, 2007). This can be as extreme as spatial scales ranging from micrometres or millimetres (e.g. viscous dissipation scales, flame thicknesses) to kilometres (channel lengths) and time scales ranging from nanoseconds to seconds (e.g. chemical reaction times). The Nuclear Energy Agency (Breitung et al., 2011) has listed typical mesh sizes for different approaches commonly used in CFD modelling in an industrial safety context:

Type of calculation	Smallest resolved dimension
RANS	0.1 - 1 m
LES	0.01 - 0.1 m
DNS	10^{-5} - 10^{-2} m

By comparison, the thickness of a laminar hydrogen-air flame at stoichiometry is about 350 μm , and the thickness of the half-reaction zone of the detonation wave is around 150 μm (Gamezo, 2007). For a stoichiometric methane-air mixture, the laminar flame thickness is of the order of 1 mm, and that of the half-reaction zone of the detonation wave is around 250 μm (Kessler, 2012). In her work on DDT, Oran (2007, 2011) almost systematically uses adaptive meshes changing with time in the simulation to follow the flame front, in which the finest meshes measure only a few tens of μm .

4.4 Phenomenological modelling of internal effects: EFFEX

4.4.1 The EFFEX tool

4.4.1.1 General description

Integral codes, such as the EFFEX tool (Proust, 2000), are said to be phenomenological because they solve simplified physics equations without using complex mathematical methods such as an Eulerian description of the physical fields. Compared with CFD methods, this type of model is more accessible, and its results are often easier to interpret. Nevertheless, each code of this type is dedicated to a very specific situation, outside of which the results may be completely wrong. It is, therefore, important to identify the limitations of these codes with regard to the situations to be modelled.

The EFFEX code is dedicated to assessing internal overpressure effects and the projection distances of fragments produced by a confined gas or dust explosion. The rupture of the containment at the origin of the fragments is a consequence of the internal explosion. This is a phenomenological code based mainly on the equations described in Chapter 3. It has been developed and used at INERIS for around twenty years and is intended to be used in safety studies or for sizing protection solutions. This model is designed to provide orders of magnitude of the internal overpressure levels that can be predicted in the event of an explosion, as well as the velocity and distance of projection for a given fragment of the enclosure (surface, altitude, mass and angle given by the user).

The specifications and restrictions relating to the model are listed below:

- the enclosures modelled can be small (less than a litre) or very large (several hundred cubic metres);
- permanent openings such as open windows can be taken into account on the enclosure,
- frangible walls, such as explosion vents, may be present in the enclosure;
- only one opening of each type is permitted. Where the actual enclosure contains several openings, the total open areas of each type must be added together.
- the projected fragment is always a piece of the frangible wall selected as input data, it, therefore, leaves the enclosure when the frangible element is opened;
- the other walls are considered rigid, and the type of enclosure material (metal, composite, concrete, etc.) is not considered in the model;
- the enclosures must not exceed a length-to-diameter ratio of 5. This model is not suitable for modelling explosions in pipes;
- with regard to the effects of fragments, a characteristic dimension chosen by the user and the surface mass are used to estimate their trajectory. Assumptions must, therefore, be made about the fragmentation of the frangible wall;

- Explosive gas and dust atmospheres are treated similarly, with knowledge of a turbulent flame velocity and an expansion rate required to perform the calculation;
- the explosive atmosphere must be present throughout the volume. In the calculations, it is ignited at $t = 0$, then the flame propagates along the entire length specified for the enclosure and has a surface area equivalent to twice the cross-section of the enclosure (which corresponds to the largest hemisphere inscribed in the enclosure);
- no gas can enter the enclosure during the calculation.

As discussed in Chapter 3, other phenomena not taken into account by this tool can be generated by a capacity rupture, such as the formation of a fireball or a secondary explosion due to the discharge of a flammable cloud when the frangible wall ruptures. However, several variables are extracted automatically during the calculation, such as the mass flow rate of escaping reagents, which could be used in a secondary tool to model these effects.

4.4.1.2 Basics of the model

Therefore, The EFFEX tool comprises an overpressure prediction model (based on the Lewis and von Elbe (1987) equation, discussed in section 3.5.2 and recalled below) and a fragment projection prediction model.

$$\frac{1}{P} \frac{dP}{dt} = \gamma \cdot \frac{Q_+ - Q_-}{V} \quad \text{Equation 64}$$

Both models are based on a temporal discretisation of the governing differential equations according to an explicit and unconditionally stable Euler scheme. The two problems of the internal explosion and the projection of external fragments are solved in the same time step. The calculation does not end until both events are completed. In the context of this study, we are only interested in the generation of pressure in the enclosure, the calculation of which follows, for each time interval in the overpressure prediction model, the following stages:

- 1) examining the geometry of the structure by looking for open areas;
- 2) assessment of the gas flows produced Q_+ by combustion of the reactants using equation 21 in paragraph 3.5.1:

$$Q_+ = St \cdot Af \cdot (E - 1) \quad \text{Equation 65}$$

and evacuated Q_- (through leakage from orifices, see Equation 25 in paragraph 3.5.2):

$$Q_- = C_d \cdot S \cdot V_e \quad \text{Equation 66}$$

- 3) use of newly calculated flows to assess the variation in internal pressure (Equation 64);
- 4) adiabatic compression of the fresh mixture: following the pressure variation at the previous time step, the fresh gases are compressed according to Laplace's law:

$$\rho_{t+dt} = \rho_t \cdot \left(\frac{P_t + \Delta P_{dt}}{P_t} \right)^{\frac{1}{\gamma}} \quad \text{Equation 67}$$

- 5) assessment of the mass of reactants (U) and burnt products (B). It is assumed that the reactants are transformed into burnt products as the flame passes: a mass m_U of fresh gas thus becomes, at each time step, the same mass $m_B = m_U$ of burnt products. At the same time, certain quantities of products are ejected through the openings, and these must also be taken into account in the mass balance,

$$m_U(t + dt) = m_U(t) - m_{U, \text{burnt}} - m_{U, \text{ejected}} \quad \text{Equation 68}$$

$$m_B(t + dt) = m_B(t) + m_{B, \text{produced}} - m_{B, \text{ejected}} \quad \text{Equation 69}$$

- 6) determination of the volumes occupied by each phase. The flame is considered to be an interface separating the fresh gases from the burnt gases: the volume of the burnt gases is obtained by deducting the volume of the fresh gases from the total volume of the enclosure.

$$V_U(t + dt) = V_U(t) / \rho_{t+dt} \quad \text{Equation 70}$$

$$V_B(t + dt) = V_{total} - V_U(t + dt) \quad \text{Equation 71}$$

7) estimation of the flame velocity and position for the next step. In a reference frame attached to the flame surface, the reactant consumption velocity is the turbulent combustion velocity S_t . However, this is insufficient to describe the flame velocity U_f as seen by an external observer and referred to as the flame space velocity for two main reasons:

- firstly, because the burnt gases expand and the fresh reactive mixture compresses, the flame's spatial velocity is expected to increase by at least a factor of E (the expansion rate of the burnt products);
- secondly, if there is an opening in the enclosure, the fluid will be subjected to a pressure difference relative to the atmosphere, creating a flow proportional to the pressure difference between the inside and outside of the enclosure. As the flame is a massless surface, it is expected to follow this movement. To reflect this phenomenon, the volumetric flows of burnt gas $Q_{-,B}$ and fresh gas $Q_{-,U}$ at the openings are compared with the gas production flow at the surface flame A_f . The flame is accelerated by assuming the conservation of the volumetric flow on each surface. In the equations, this leads to:

$$U_f = S_t \cdot E + \frac{Q_{-,U}}{A_f} - \frac{Q_{-,B}}{A_f} \quad \text{Equation 72}$$

8) adjustment of the time step to avoid instant consumption of reagents in the next step or unnecessarily long calculations;

Several types of input data are required for the calculation:

- dimensional data linked to the geometry of the enclosure, such as volume, vent size, mass and opening pressure;
- thermodynamic data which are intrinsic to the mixture: the masses and densities of the fresh and burnt products and therefore the value of the expansion coefficient E ;
- data relating to the evolution of the reaction S_t the turbulent velocity of the flame and A_f its surface.

While the other data are reasonably well determined, this last point is more sensitive because, , estimating the turbulent velocity S_t and the flame surface A_f is more sinuous. In both cases, several approaches are possible.

4.4.1.3 Determination of the turbulent flame velocity S_t

The EFFEX code requires a turbulent flame velocity to be specified for the calculation. Two main options are currently being studied: one based on the Gülder correlation and the second on the INERIS correlation (Duclos, 2019). These models have already been explained in section 3.4.2.2 and we will only outline them here.

In both cases, it is necessary to estimate u' and L_t , the turbulence parameters. Empirical methods for determining these parameters based on simple dimensional considerations are available in the work of Hinze (1975) or Proust (2009). These are rough estimates but sufficient for the empirical models used here.

Gülder's model takes the form:

$$\frac{S_t}{S_{lad}} = 0,62 \cdot \left(\frac{u'}{S_{lad}}\right)^{0,75} \cdot \left(\frac{L_t}{\eta}\right)^{0,25} \quad \text{Equation 73}$$

The INERIS model is based on the composition of 2 instability terms:

- the Landau-Darrieus instability linked to the unstable expansion of the burnt products gives the velocity U_{LD} :

$$U_{LD} = \left[1 + 4E * \frac{(E - 1)^2}{(E^3 + E^2 + 3E - 1)}\right] * S_{lad} \quad \text{Equation 74}$$

- the Rayleigh-Taylor instability associated with the mixing of two fluids of different densities yields the velocity U_{RT} :

$$U_{RT} = 0.51 * \sqrt{\left(\frac{E - 1}{E} * \eta_{acc} * r\right)} \quad \text{Equation 75}$$

S_t is obtained by composing the two previously calculated velocity U_{RT} .

$$S_t = \frac{1}{E} \cdot \sqrt{U_{LD}^2 + U_{RT}^2} \quad \text{Equation 76}$$

4.4.1.4 Determining the flame surface A_f

Several ways of modelling the flame surface are possible. Intuitively, in a mixture initially at rest, in the absence of a vent, the flame is expected to grow spherically or hemispherically, depending on whether ignition occurs in the centre of the enclosure or against a wall. In most cases, the situation that maximises the length of the flame trajectory is the major one, which occurs upon ignition at the surface opposite the vent. We are, therefore, more interested in the case of the half-sphere.

However, in the presence of a vent, as soon as it is opened, the pressure difference between the atmosphere and the enclosure generates a flow that stretches the flame in the direction of the vent (see paragraph 3.5.2 or the CFD simulations in the previous paragraph). As a result, the flame surface increases and takes on an ellipsoid shape. Experimentally, when the vent opens shortly after the start of the explosion, we observe that the flame surface can be approximated by that of a cylinder surmounted by a half-ellipsoid (Figure 47):

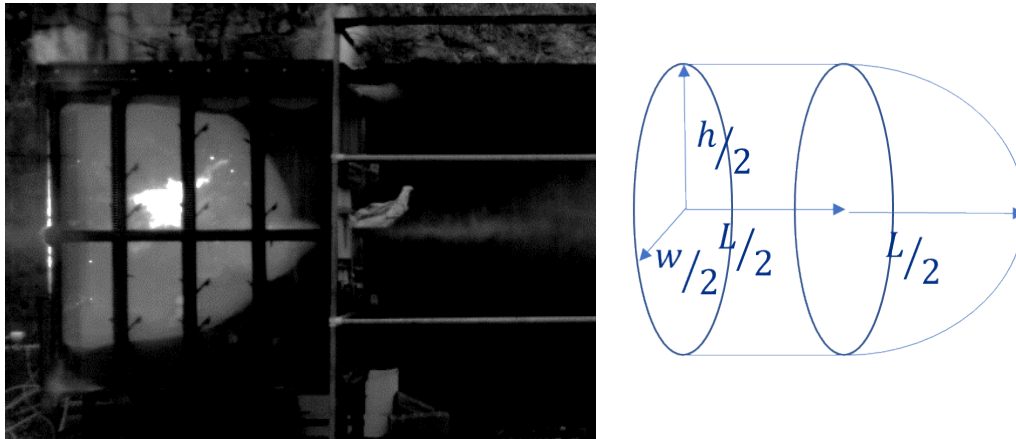


Figure 47. Approximation of the flame surface by a cylinder and a half-ellipsoid

The ellipsoid's surface is approximated by an empirical model proposed by Thomsen (2004). In equations, this becomes:

$$A_f = 2\pi \sqrt{\frac{h^2 + w^2}{4}} \frac{L}{2} + 2\pi \left[\frac{\left(\frac{L}{2}\right)^p \left(\frac{h}{2}\right)^p + \left(\frac{L}{2}\right)^p \left(\frac{w}{2}\right)^p + \left(\frac{h}{2}\right)^p \left(\frac{w}{2}\right)^p}{3} \right]^{\frac{1}{p}} \quad \text{Equation 77}$$

where L is the length of the enclosure, w is its width, and h is its height; p is a constant in Thomsen's formula (2004) and is equal to 1.6075. Calculating the growth of this surface area as a function of time is relatively easy. It requires a good knowledge of the enclosure's dimensions but allows us to remain relatively close to the experimental observation.

The enclosures where accidental explosions occur are often assimilated to cylinders of volume V , length L and diameter D (for example, in European standards on explosion vent protection). Proust (2000, 2005) indicates in this case that considering a flame with a constant surface area A_f equal to the surface area of the largest half-sphere inscribed in the enclosure and propagating along the length L , in the volume V , makes it possible to obtain a conservative estimate of the effects of confined explosions, provided that St is determined correctly.

This is the default assumption used in the EFFEX code, developed in an industrial safety context. It was specifically designed to provide conservative estimates rather than get as close as possible to the phenomenon's reality.

4.4.1.5 Outputs

At any point in the calculation, it is relatively easy to access:

- the proportions of reactants and products,
- the state of opening of the frangible walls,
- the mass and volume burnt or lost through the openings,
- to internal pressure,
- the velocity or position of the flame.

The advantage of these phenomenological codes is precisely that they provide simplified access and, therefore, optimum control and understanding of the phenomena.

Compared with a CFD code, using simplified equations with spatial discretisation enables a more straightforward coupling of physical phenomena, such as the mechanics of opening a frangible wall with the fluid flow through it. Typically, in the case of EFFEX, the fundamental principle of dynamics and the pressure in the enclosure are used to calculate the acceleration of the frangible wall once a pressure threshold chosen by the user in the enclosure has been exceeded. This type of wall condition is very complex to model in a CFD code.

Compared with an entirely empirical model (see next section), we obtain a greater diversity of results and often a better ability to evaluate these results. For example, here, we can compare the evolution of the internal pressure curve with the opening of a wall or estimate the quantity of fresh gas ejected from the enclosure before the flame emerges.

4.4.1.6 Example: Comparison with experimental data

The tests identified come from the literature or were carried out at INERIS. Comparing these experimental situations with the EFFEX tool results helps validate the tool and highlight its conservative aspect.

Bauwens (2012) has published work on the influence of hydrogen concentration on an explosion confined in a 64 m³ volume fitted with a 2.7 or 5.4 m² vent. The enclosure is 4.6 m long, 4.6 m wide and 3 m high. Ignition takes place on the side opposite the vent. This ignition point position maximises the flame path between ignition and exit through the vent, as well as pressure effects. The hydrogen concentration varies between 15 and 19% by volume in air. Turbulence in the explosion chamber is produced by 4 fans 0.5 m in diameter. The turbulent intensity generated is between 0.1 and 0.5 m/s.

Figure 48 shows a comparison of the overpressures calculated using the EFFEX tool and measured in the explosion chamber for 2 different vent surfaces (5.4 m² and 2.7 m²) and 8 different hydrogen concentrations.

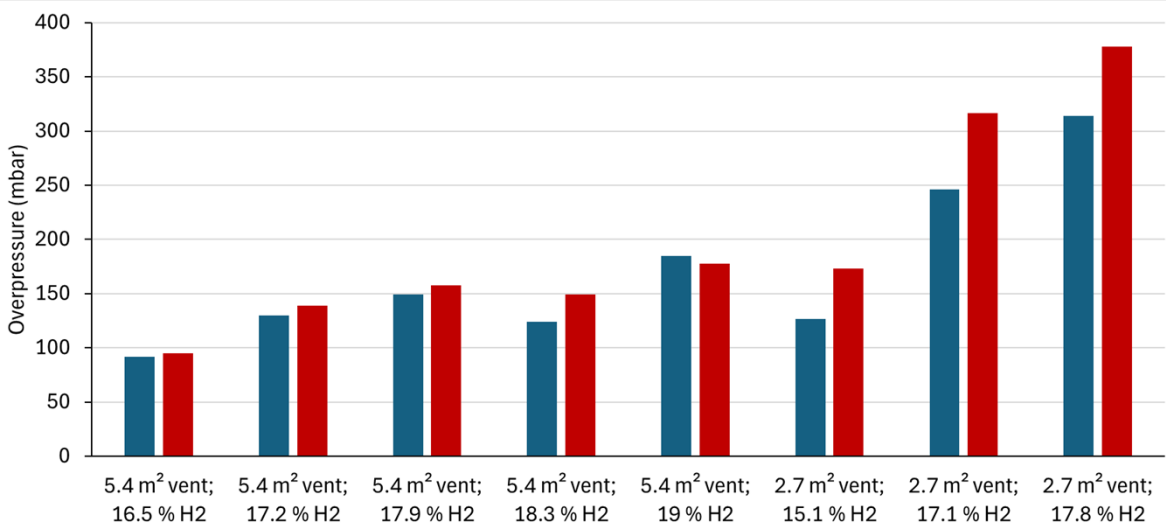


Figure 48. Comparison of overpressures calculated using the EFFEX tool and measured in the explosion chamber for 2 vent surfaces and 8 hydrogen concentrations - Bauwens, 2012

There is satisfactory agreement between the measured overpressures and the calculated overpressures, and the model gives a value that exceeds the real effects in most cases.

The influence of concentration on the effects of an explosion was also studied as part of the ANR DIMITHRY project. The explosion takes place in a 4 m³ enclosure (length: 2 m, width: 1 m, height: 2 m) fitted with vents with a surface area of between 0.25 m² and 0.5 m² (Figure 49).

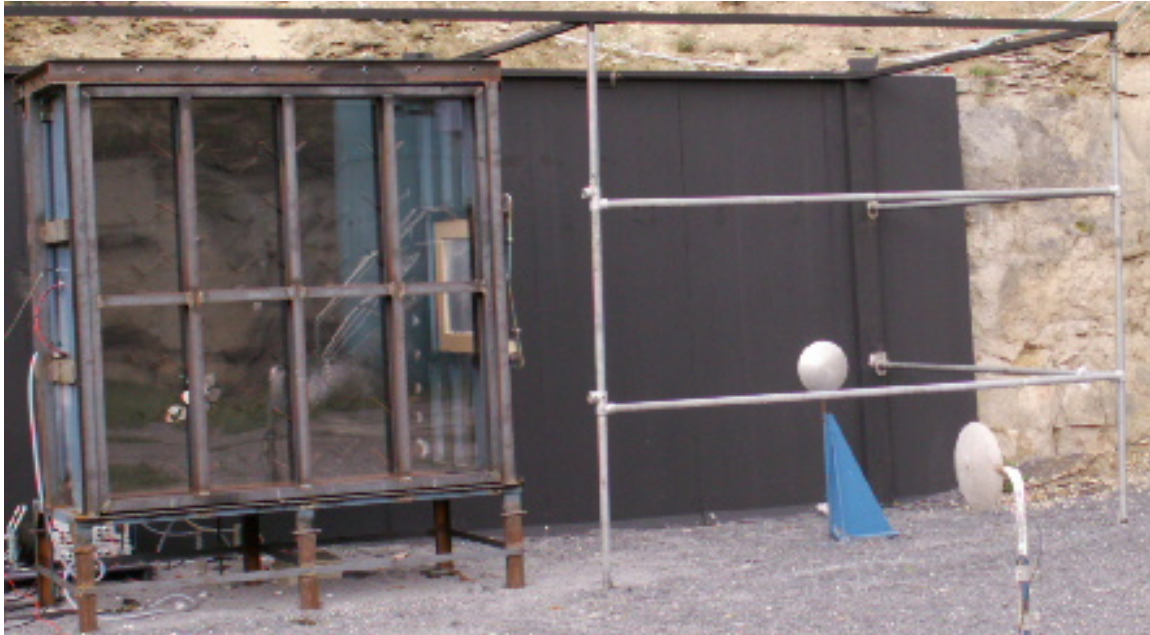


Figure 49. 4 m³ chamber used in the DIMITHRY project

The hydrogen concentration in air varies between 15 and 30% by volume. Two vent sizes were studied: 0.25 m² and 0.5 m². Figure 49 compares the overpressures calculated using the EFFEX tool with those measured during tests in the explosion chamber.

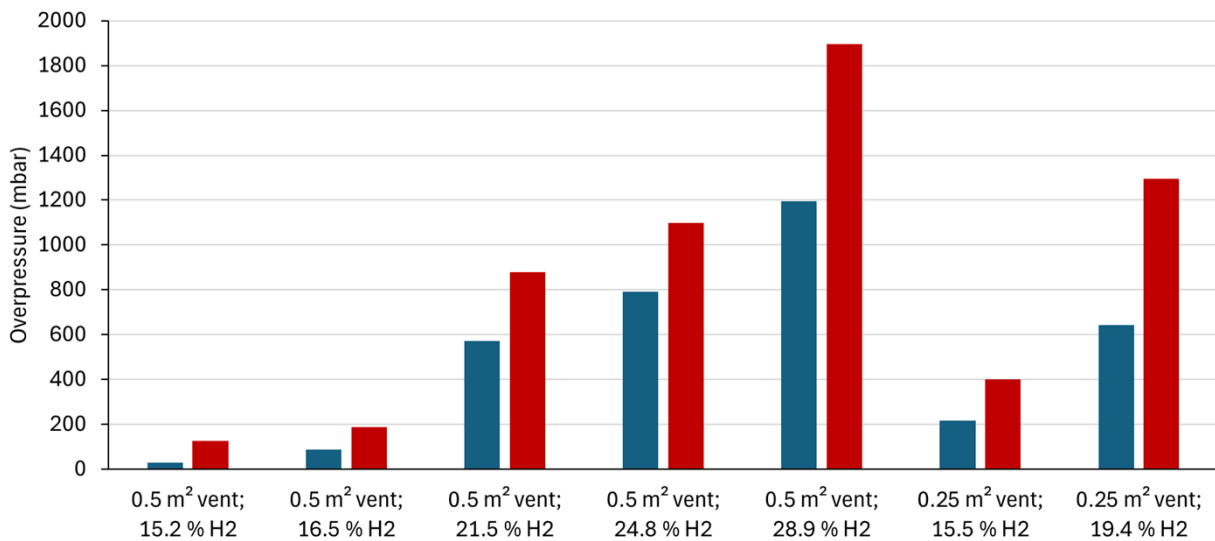


Figure 50. Comparison of overpressures calculated using the EFFEX tool and measured in the explosion chamber - 4 m³ chamber, ANR DIMITHRY project

In each case, the calculation overestimates the explosion overpressures, which underlines the conservative nature of the tool.

The results of this type of calculation are not limited to a maximum overpressure calculation. If we take the example of an ATEX explosion at rest, concentrated at 21.5% H₂ in air, EFFEX gives a curve showing the evolution of overpressure as a function of time:

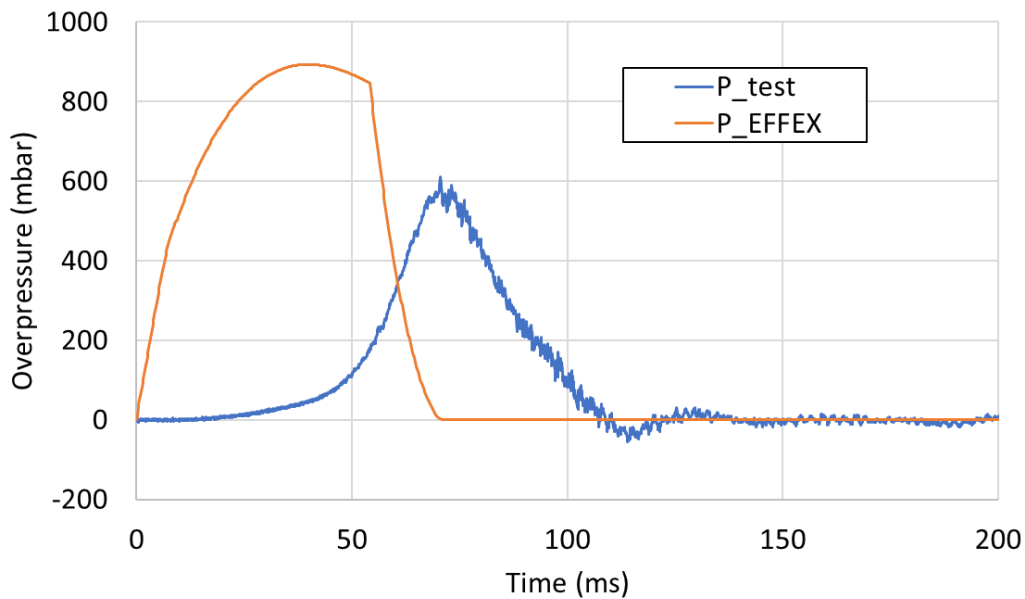


Figure 51. Comparison of overpressures calculated using the EFFEX tool and measured in the 4 m³ chamber with an ATEX of H₂ at 21% initially at rest and a 0.5 m² vent

If the foot of the curve is steeper in the simulation, this is because a conservative assumption is made of a constant flame surface, unlike in the test where the fireball grows progressively. Overall, the duration of the explosion is well established. It is also possible to access all sorts of other variables that evolve as a function of time during the calculation, such as the progressive opening of the vent or the gas production or evacuation rates during the explosion (Figure 52).

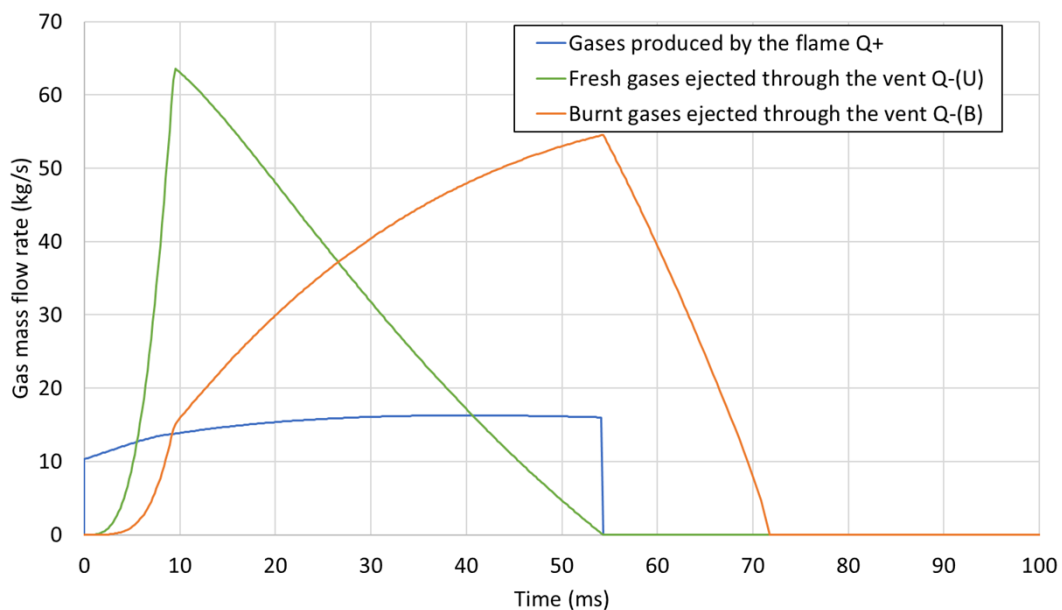


Figure 52. Comparison of overpressures calculated using the EFFEX tool and measured in the 4 m³ chamber with an ATEX of H₂ at 21% initially at rest and a 0.5 m² vent.²

This type of information can be used as input data for other calculations, for example, to simulate the effects of a possible secondary explosion. Easy access to the calculation variables also makes it easier to check the general behaviour of the models implemented in the code and sometimes to detect problems or potential limitations of the tool.

By way of illustration, some results obtained with the EFFEX code on randomly selected trials are compared with those of other models as shown in paragraph 4.5.5.3.

4.4.2 The SECEX tool

However, the EFFEX tool is not suitable for specific situations, as in the presence of secondary explosions, and more particularly when the vent opening pressure is low

The SECEX (SECOndary Explosions) model introduces a phenomenological description of the secondary explosion and external effects. It is based on a 5-step approach:

- 1) first, the maximum overpressure in the vented enclosure is estimated,
- 2) the expansion speed of the external vortex is estimated from this pressure value,
- 3) by applying the Lannoy model, an external explosion overpressure is determined,
- 4) finally, it is used to correct internal overpressure.

Step 1: Determining the internal overpressure P_{int} :

The internal overpressure corresponds to the competition between the rate of production of gases burnt by the flame Q_+ and the gas ejection rate by the vent Q_- . Its maximum is reached at equilibrium when $Q_+ = Q_-$.

The phenomenological model that the gas flows produce, Q_+ , by combustion of the reactants using Equation 21 in paragraph 3.5.1 are:

$$Q_+ = St \cdot Af \cdot (E - 1) \quad \text{Equation 78}$$

and the exhaust gas flow rate Q_- due to leakage at the orifices, Equation 25 in paragraph 3.5.2) is:

$$Q_- = C_d \cdot A_v \cdot V_{vent} \quad \text{Equation 79}$$

With A_v being the vent area, C_d being a discharge coefficient, and V_{vent} , the velocity of the gases discharged at the vent.

E is a thermodynamic parameter that depends on the mixture, while C_d and A_v depend on the structure's geometry. Therefore, it remains to determine St , A_f , and V_{vent} .

The calculation of St is based on the INERIS model developed by Daubech (2008) and based on the composition of Rayleigh-Taylor and Landau-Darreis instabilities (cf. paragraph 4.4.1.3).

For the flame surface, the ellipsoidal model presented in paragraph 4.4.1.4 which was explicitly developed for this case.

The velocity of the gases leaving the structure through the vent can also be determined in several ways. For example, using a simple Bernoulli equation of the type $V_e = \sqrt{2P/\rho}$ where P is the excess pressure and ρ is the density of the flue gas⁷. Another option is the leakage flow equation already presented in section 3.5.2.1 for the sonic case:

$$V_e = \left(\frac{P_2}{P_1}\right)^{1/\gamma} \cdot \sqrt{\frac{2 \cdot \gamma}{\gamma - 1} \cdot \frac{P_1}{\rho_1} \cdot \left(1 - \left(\frac{P_2}{P_1}\right)^{\frac{\gamma-1}{\gamma}}\right)} \quad \text{Equation 80}$$

Assuming the equilibrium condition $Q_+ = Q_-$, we find the maximum overpressure of the internal explosion P_{int} .

Step 2: Determining the expansion velocity of the external vortex of the secondary explosion

On the basis of the experimental correlation established by Proust and Leprette (2010), the expansion speed of the external vortex during the secondary explosion can be determined:

$$V_{exp} = 10 \sqrt{V_e} \quad \text{Equation 81}$$

⁷ It is assumed that at equilibrium between Q_+ and Q_- , it is essentially burnt gas that leaves the enclosure. Thus ρ_1 is the density of the burnt gases, which is close to that of the fresh gases divided by E .

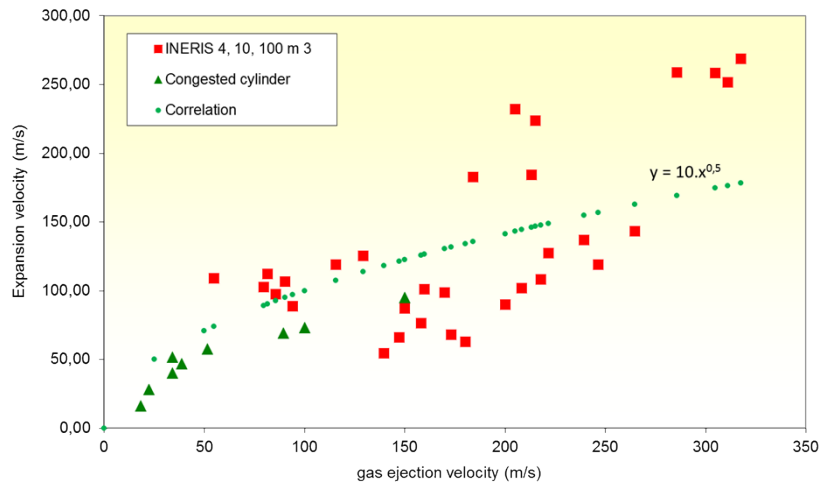


Figure 53. Cloud expansion velocity during the secondary explosion as a function of the gas exit velocity at the vent (Correlation by Proust and Leprette, 2010).

Step 3: Estimation of the violence of the secondary explosion using the Lannoy model (1984).

Lannoy (1984) proposed a model to estimate the effects of a gas explosion in a free field when the expansion velocity of the cloud is known. It takes the form:

$$\Delta P_{ext} = \frac{3}{2} \cdot \rho_0 \cdot V_{exp}^2 \quad \text{Equation 82}$$

Where ρ_0 is the density of air, approximately 1.2 kg/m^3 .

Step 4: Correction of internal excess pressure: from P_{int} to P_{red}

The external overpressure generated by the secondary explosion slows the discharge of gases and induces excess pressure in the enclosure. To reflect this effect, based on empirical observations, it is estimated that part of the pressure of the external explosion is added to the internal overpressure in proportion to the ratio of the vent area A_v to the cross-section of the enclosure A_s :

$$P_{red} = P_{int} + \frac{A_v}{A_s} \cdot P_{ext} \quad \text{Equation 83}$$

This model has been tested on published test cases or those carried out at INERIS:

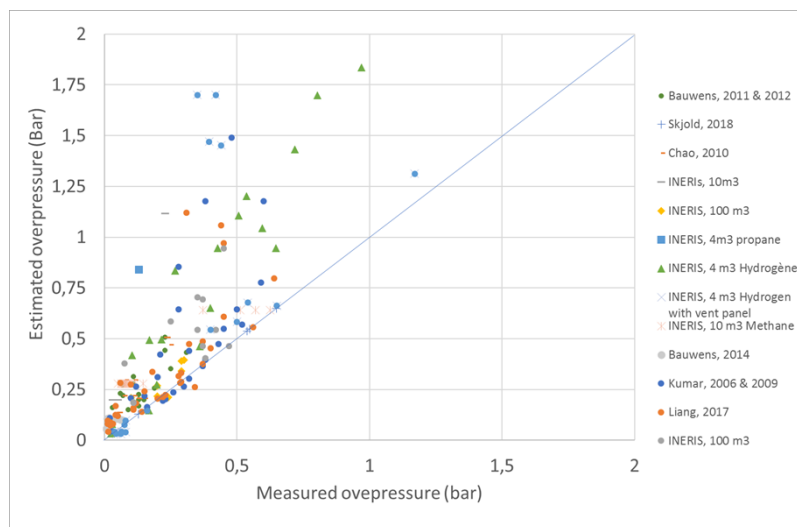


Figure 54. Pred prediction using the SECEX model for various tests published or carried out at INERIS (Duclos, 2019).

The agreement with experience is satisfactory. Moreover, the code remains conservative in the vast majority of cases.

4.5 Empirical modelling of internal effects

4.5.1 The Bartknecht model

Bartknecht (1981) showed that, for a given vent opening pressure P_{stat} , in order to maintain the same explosion overpressure P_{red} in enclosures of different volumes V , the vent ratio $f = A_v / V$ also follows a cubic law: $f \cdot V^{1/3}$ therefore, the vent ratio must be a constant. We sometimes use the coefficient $K = V^{2/3} / A_v$, which is the inverse of this value and must also be a constant.

Bartknecht (1981) verified this relationship in a series of experiments in a range of enclosures with L/D ratios <5 and volumes up to about 30 m³. He used plastic sheets with relatively high P_{stat} values, from 100 to 500 mbar, as vents. Mixtures of methane, propane, coke gas and hydrogen with air were tested. Based on these tests, Bartknecht produced nomograms for calculating a vent area A_v from P_{stat} , V , P_{red} and K_g . Although these nomograms refer to volumes of up to 1000 m³, they have only been verified up to around 30 m³. Therefore, the method should be cautiously applied, particularly with the largest enclosures, those with an L/D ratio in excess of 5 and in situations where significant turbulence may develop (British Gas, 1990).

Then, in 1993, Bartknecht re-evaluated several hundred gas explosion tests carried out over the previous 20 years. The nomographs were replaced by a formula valid for containers of cubic or almost cubic shape (L/D < 2), filled with stoichiometric and non-turbulent gas-air mixtures.

The formula is presented to determine the vent area A_v , which is often the data required by manufacturers. It can be reversed to determine P_{red} if A_v is known, in particular using a dichotomy calculation. A_v depends on the constant K_g characterising the reactivity of the flammable mixture, the maximum acceptable internal pressure P_{red} , the static vent opening pressure P_{stat} and the volume of the enclosure V according to the formula:

$$A_v = \left[\frac{0,1265 \cdot \log(K_g) - 0,0567}{P_{red}^{0,5817}} + \frac{0,1754 \cdot (P_{stat} - 0,1)}{P_{red}^{0,5722}} \right] \cdot V^{2/3} \quad \text{Equation 84}$$

Under the following conditions:

- 50 bar.m/s < K_g < 550 bar.m/s
- $P_{red} < 2$ bar
- $P_{red} > P_{stat} + 0.05$ bar
- 100 mbar < $P_{stat} < 500$ mbar
- $0.1 \text{ m}^3 < V < 1000 \text{ m}^3$

This is also the formula historically used in standard EN14994 on the sizing of explosion vents against gas explosions.

However, many reservations exist about using this formula. It is based entirely on Bartknecht's experimental work (1993) and ignores all other results after 1993. In addition, it has only been validated on Bartknecht's tests in free volumes (without obstacles) of 1 to 60 m³, whereas it is said to be applicable up to 1000 m³.

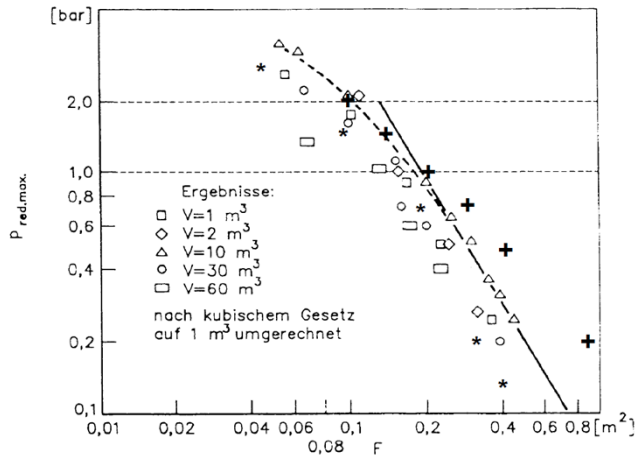


Figure 55. Original measurements by Bartknecht (1993) for the development of Equation 84 F is the ratio $A_v/V^{2/3}$.

In his doctoral thesis, Fakandu (2014) compared these data with other measurements as well as a model from the NFPA68 guide (cf. para. 4.5.2) for methane and propane tests:

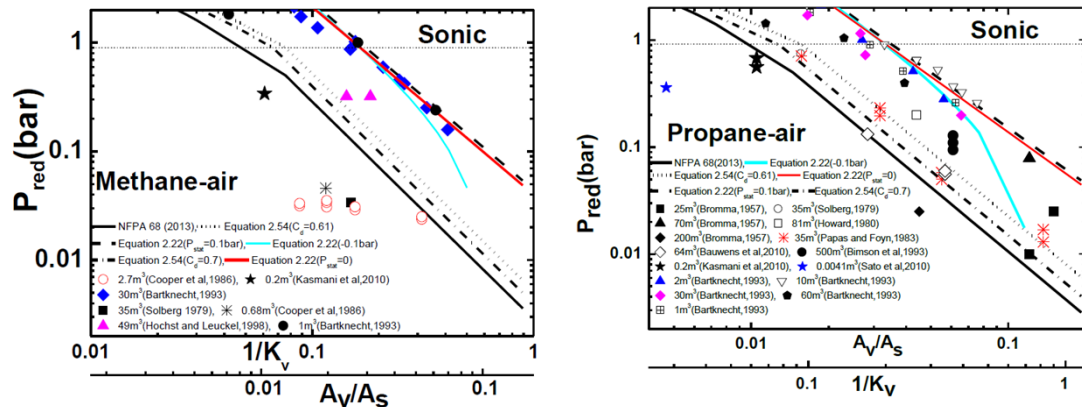


Figure 56. Original measurements by Bartknecht (1993) for the development of Equation 84 $F = A_v/V^{2/3}$. The red and blue lines correspond to Bartknecht's model, assuming $P_{stat} = 0$ for the blue line and 0.1 bar for the red line. The black solid line is the NFPA68 (2012) model, while the dots are experimental data.

It can be seen that the predictions using Bartknecht's model are very large for most of the cases and only really correspond to Bartknecht's data. In Bartknecht's publication, photographs of the experimental set-up show that the tank vents opened close to the ground. According to Fakandu (2018), who reproduced tests under similar conditions and with similar results, this produces a Coandă effect with the flame jet "sticking" to the ground, generating turbulence and leading to increased P_{red} .

Furthermore, this formula relies heavily on the K_g coefficient, which is most often measured in 20-litre spheres, whereas the formula is generally applied to industrial-scale enclosures with volumes in m^3 . As a reminder, the K_g is a standardised measure of the maximum rate of pressure rise of a gas during deflagration under specific, fixed operating conditions, which provides a reproducible and differentiating measure of the severity of the explosion of the gas tested. The link between this measurement and practical conditions is relatively empirical, as it is generally assumed that the K_g is proportional to the combustion rate. Flame theory is applied to practical cases to establish correlations and groupings of parameters. However, several studies (Lunn, 2003; Kasmani, 2006, 2010) have shown experimentally that the maximum value for the rate of pressure rise increases with volume, particularly for the most reactive gases, such as hydrogen (Fakandu, 2014). Ultimately, the opposite is observed in this case: the formula underestimates the effects of hydrogen explosions. Similar as yet unpublished observations have been made at INERIS. A formula based on the parameter S_u , the fundamental velocity of the flames, as in the NFPA68 (2017) guide, would, therefore, be more appropriate in this situation.

At present, in Europe, Bartknecht's results are still the basis of vent sizing standards for gas explosions (EN 14994). Although they lead in most situations (apart from the case of hydrogen) to a flagrant overestimation of P_{red} or a requirement for larger vent surfaces than necessary, this over-prediction can be considered a safety margin.

In paragraph 4.5.5.3, some results obtained using the formulae of standard EN14491 on randomly selected tests are compared with those of other models.

4.5.2 The NFPA68 guide model (2017)

The National Fire Protection Association (NFPA) guide to deflagration protection, NFPA 68, provides vent sizing models for gas mixture explosions. This standard is regularly updated, and the model can change radically from one version to the next. Here, only the latest one is considered (2017). As with the European standard, this guide proposes formulae for estimating a vent area A_v from a maximum acceptable internal pressure P_{red} , in/an enclosure fitted with a vent. Two formulae are proposed, depending on the level of overpressure P_{red} expected.

If the reduced overpressure P_{red} is less than 0.5 bar, the formula is:

$$A_v = \frac{S_{lad} \rho_u}{2 G_u} \frac{\lambda}{C_d} \left[\left(\frac{P_{max} + 1}{P_0 + 1} \right)^{\frac{1}{\gamma_b}} - 1 \right] (P_0 + 1)^{\frac{1}{2}} \frac{A_s}{P_{red}^{1/2}} \quad \text{Equation 85}$$

Otherwise, use :

$$A_v = A_s \frac{\left[1 - \left(\frac{P_{red} + 1}{P_{max} + 1} \right)^{\frac{1}{\gamma_b}} \right]}{\left[\left(\frac{P_{red} + 1}{P_{max} + 1} \right)^{\frac{1}{\gamma_b}} - \frac{\left(\frac{P_{stat} + 1}{P_0 + 1} \right)^{\frac{1}{\gamma_b}} - 1}{\left(\frac{P_{max} + 1}{P_0 + 1} \right)^{\frac{1}{\gamma_b}} - 1} \right]} \frac{S_{lad} \rho_u}{2 G_u} \frac{\lambda}{C_d} \quad \text{Equation 86}$$

With:

- As the internal surface of the enclosure
- P_0 the pressure in bar before ignition,
- S_{lad} flame velocity
- ρ_u the density of the fresh gas
- G_u the leakage mass flow rate of fresh products, per unit area ($G_u = 230.1 \text{ kg.m}^{-2} .\text{s}^{-1}$)
- λ a flame-pleating coefficient due to turbulence and instabilities
- γ_b the ratio of the specific heats of the flue gases (of the order of 1.1-1.2)
- C_d a discharge coefficient (equal to 0.8).

The implementation of these formulae relies on the definition of a flame wrinkling coefficient λ , the calculation of which is complex and relies on other empirical considerations. For more information on this point, reference can be made to the work of Rodgers and Zalosh (2013).

These relationships involving the laminar flame velocity appear to be closer to the actual physics of the explosion than the formula chosen in European standard EN14994, which is based on the K_g term corresponding to specific flow and environmental conditions. Nevertheless, it is also a tool developed to provide conservative estimates for industrial safety applications. In practice, this method provides results generally close to those obtained with the Bartknecht model. Yet, Bartknecht's formula rests unsuitable for turbulent media or when the P_{stat} of the vent is low, that is less than 100 mbar. Zalosh (2008) and Rodgers and Zalosh (2013) examined the performance of the NFPA guide models by comparing them with tests and also with the results of calculations carried out using phenomenological and CFD codes. They concluded that in the vast majority of test cases with large enclosures and no obstacles, these formulae predict vent areas equal to or greater than those from experience. According to them, the NFPA guide formulae also

perform well in a large number of cases when large obstacles are present, but they fail to predict correct vent areas when the obstacles are small and numerous, such as in a duct network. By way of illustration, some results obtained with these formulae on randomly selected tests are compared with those of other models in paragraph 4.5.5.3.

4.5.3 Molkov models

Empirical models are intrinsically complex, as illustrated by the Molkov Model. In 1999 he published a series of models that consider various modes of flame wrinkling during the explosion.

This aspect is addressed using the laminar (Br) and turbulent (Br_t) Bradley numbers (Bradley & Mitcheson, 1978). The turbulent Bradley number depends on the degree of interaction (DOI) between the creation of turbulence due to the flow of unburnt gases through the vent and the internal explosion of said unburnt gases through the vent. A number of ancillary parameters need to be adjusted based on existing experimental data. As the amount of data has increased over time, various versions of this model have been proposed (1999, 2001, 2008). The correlations are given in the following table:

Bradley number	$Br = \frac{A_v}{V^{2/3}} \cdot \frac{c}{S_{lad}(E-1)}$	Equation 87
Degree of interaction (DOI)	$DOI = \alpha \left[\frac{(1 + eV^g)(1 + 0.5Br^\beta)}{1 + \pi_v} \right]^\delta P_0^\omega$	Equation 88
Turbulent Bradley number	$Br_t = \frac{\sqrt{E/\gamma}}{\sqrt[3]{36\pi}} \frac{Br}{DOI}$	Equation 89
Molkov model from 1999	$P_{red} = Br_t^{-2.4} \text{ (if } Br_t > 1; P_{red} < 1)$ $P_{red} = 7 - 6 * Br_t^{0.5} \text{ (if } Br_t < 1; P_{red} > 1)$	Equation 90
Molkov model from 2001	$\frac{P_{red}}{P_v^{2.5}} = 5.65 * Br_t^{-2.5} \text{ (if } Br_t > 2; \frac{P_{red}}{P_v^{2.5}} < 1)$	Equation 91
2008 Molkov model	$\frac{P_{red}}{P_v^{2.5}} = 7.9 - 5.8 * Br_t^{0.25} \text{ (if } Br_t < 2; \frac{P_{red}}{P_v^{2.5}} > 1)$	Equation 92

Table 4. Definition of Bradley numbers (Br and Br_t), DOI and Molkov models from 1999, 2001 and 2008

With E the expansion rate, S_{lad} , the laminar flame velocity, γ the ratio of the specific heats of the fresh gases, c the speed of sound in the fresh gases, P_0 the initial pressure of the mixture and $P_v = (P_{stat} + P_0) / P_0$, a dimensionless static vent opening pressure. The ancillary parameters for calculating the DOI vary with the model:

Model:	1999	2001	2008
α	0.9	1	1
β	1	0.8	0.8
δ	0.37	0.4	0.4
e	10	10	2
g	0.33	0.33	0.94
ω	0	0.6	0

Table 5. Ancillary parameters for DOI calculation

Although flame instabilities and turbulence are incorporated into these correlations to a certain extent, they are taken into account entirely empirically.

In 2013 and then 2014, Molkov proposed a new way of estimating the DOI for hydrogen gas based on the results of CFD calculations under the assumption of large eddy modelling (LES). This model would a priori be less empirical and more general. The DOI is now defined as a product of flame wrinkling factors Σ :

$$DOI = \Sigma_K * \Sigma_{LP} * \Sigma_{FR} * \Sigma_{u'} * \Sigma_{AR} * \Sigma_O \quad \text{Equation 93}$$

Σ_K is the flame fold due to Landau-Darrieus instabilities, obtained by :

$$\Sigma_K = 1 + \left(0.75 \cdot \frac{E-1}{\sqrt{3}} - 1 \right) * \left[1 - \exp\left(-\frac{R}{R_0}\right) \right] \quad \text{Equation 94}$$

With R the flame radius and R_0 a critical radius which depends on the volume concentration of hydrogen gas:

X_{H_2} (vol.)	R_0
4%-29.5%	$4.3478 * X - 0.2826$
29.5%-75%	1

Table 6. Ancillary parameters for calculating the DOI for hydrogen

Σ_{LP} is the wrinkling factor due to flame deformation towards the open vent

$$\Sigma_{LP} = 1 + \frac{(\Sigma_{LP}^{max} - 1) * 2R}{R_0} \quad \text{Equation 95}$$

$$\Sigma_{LP}^{max} = 6.353 * X_{H_2}^2(\%) - 7.525 * X_{H_2}(\%) + 3.002; \quad \text{Equation 96}$$

Σ_{FR} is the folding factor due to the growth of fractals linked to Rayleigh-Taylor instabilities:

$$\Sigma_{FR} = \left(\frac{R}{R_0} \right)^{0.33} \quad \text{Equation 97}$$

Σ_{AR} is the folding factor due to the shape of the enclosure:

$$\Sigma_{AR} = \frac{A_{EW}}{A_S} \quad \text{Equation 98}$$

with A_{EW} the internal surface and A_S the surface of the sphere inscribed in the enclosure;

Σ_O is the wrinkling factor due to obstacles. It is 1 if no obstacles exist between the flame and the vent and 3.5 if there are obstacles present;

finally $\Sigma_{u'}$ is the wrinkling factor due to the initial turbulence in the enclosure, and is a function of the laminar flame velocity S_{lad} :

$$\frac{1}{X} = S_{lad} * \Sigma_K * \Sigma_{LP} * \Sigma_{FR} * \Sigma_{AR} * \Sigma_O \quad \text{Equation 99}$$

If $u' = 1$ m/s then:

$$\Sigma_{u'} = -4.420 * 10^{-3} * X^2 + 6.859 * 10^{-1} * X + 8.833 * 10^{-1} \quad \text{Equation 100}$$

If $u' = 0.1$ m/s then:

$$\Sigma_{u'} = 1.321 * 10^{-3} * X^2 + 2.291 * 10^{-2} * X + 9.937 * 10^{-1} \quad \text{Equation 101}$$

If Σ_u is greater than 1, then all other folding factors are taken to be equal to 1. With the new definition of DOI, new correlations have been proposed; the most recent are for:

- Those that give a better match with experience:

$$P_{red} = 0.23 * Br_t^{-1.06} \quad \text{Equation 102}$$

- and for a more conservative form:

$$P_{red} = 0.91 * Br_t^{-1.06} \quad \text{Equation 103}$$

Rocourt (2013) and Jallais and Kudriakov (2013) studied the effectiveness of these models in real cases. They concluded that the 1999 model gave better results than those of 2001 and 2008. More recently, Duclos (2019) compared the 1999 model with those of 2013 and 2014 in tests carried out at INERIS and others published in the scientific literature and concluded that the 1999 and 2014 models were more effective. An illustrative result is shown in Figure 57:

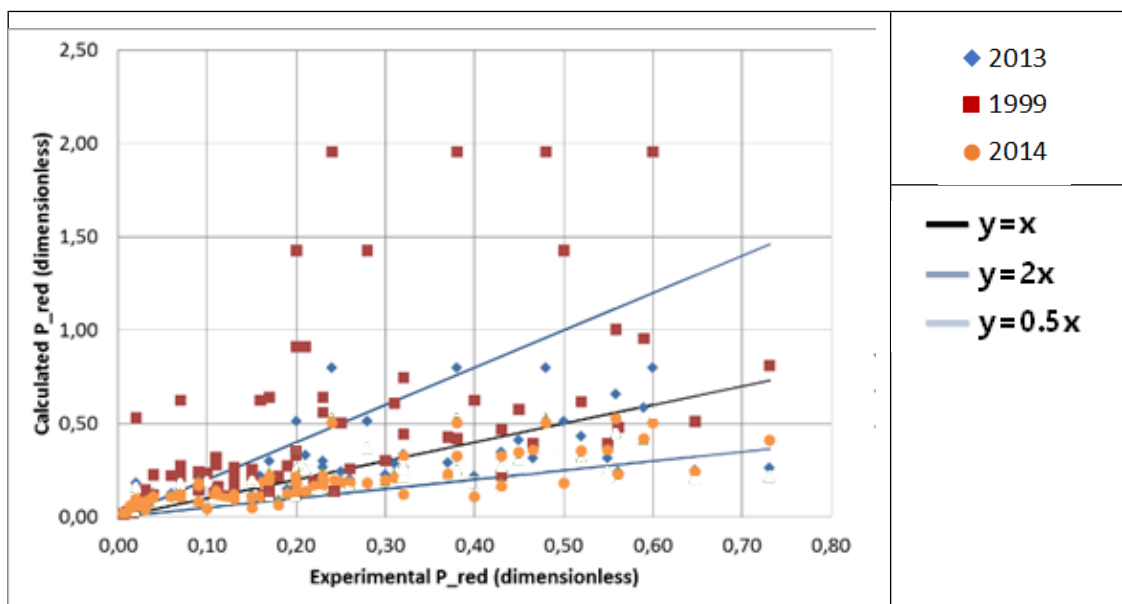


Figure 57. Comparison of Molkov model predictions with published trial data (Duclos, 2019)

4.5.4 Bauwens model

Bauwens (2012) proposed a formula for estimating several major pressure peaks P identified in the experiments. We recall the general graph of the pressure signal during the explosion proposed by Cooper (1986):

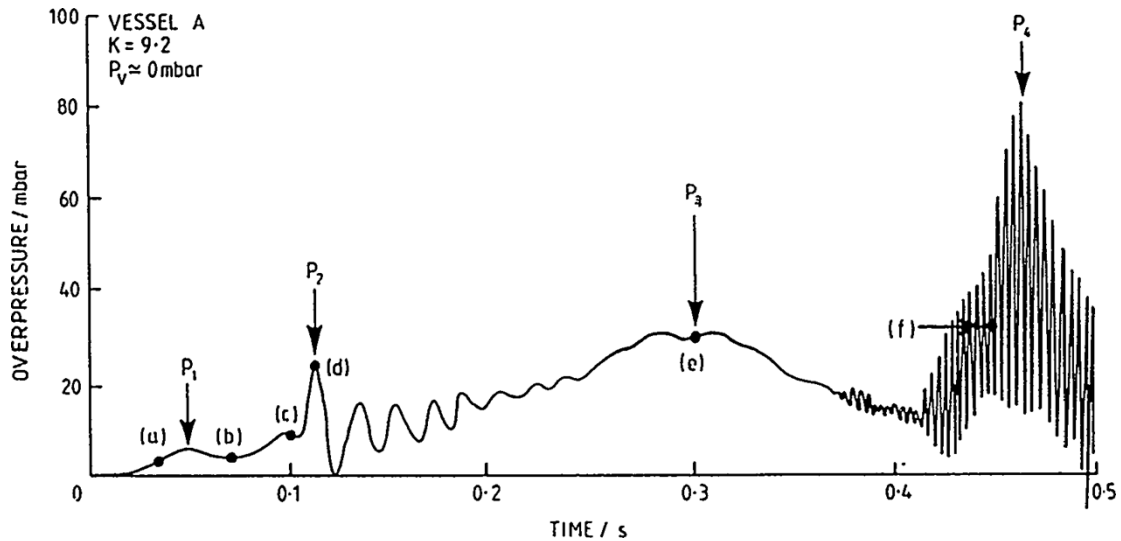


Figure 58. Experimental signal and analysis by Cooper, 1986

The Bauwens model aims to determine the following:

- the maximum "P₂" when the external explosion occurs
- the point P₃, corresponding to the maximum flame surface obtained as a result of the interaction of the flame with the external explosion (remember that in the general case, P₂ > P₃; see paragraph 3.5.2.2).
- the P₄ peak corresponding to the acoustic resonance

A single expression is used to estimate these 3 peaks:

$$\frac{P_i}{P_0} = \frac{P_e}{P_0} \left(1 - \frac{\left(\frac{\gamma+1}{2}\right)^{\frac{\gamma}{\gamma-1}}}{(A_v^*)^2} \right)^{-1} \quad \text{Equation 104}$$

with

$$A_v^* = C_D \cdot \left(\frac{R \cdot T_v \cdot \gamma \cdot (\gamma + 1)}{2 M_v} \right)^{\frac{1}{2}} \cdot \frac{a_{cd} \cdot A_v}{S_u \cdot A_f \cdot (E - 1)} \quad \text{Equation 105}$$

With:

- P_i the pressure of peak i;
- At the vent surface;
- A_f and S_u specific flame surface and velocity parameters, calculated later in the model;
- indices 0, e, f and v corresponding to ambient, external, flame and vent conditions, respectively;
- E is the expansion rate;
- γ the specific heat report;
- C_d, the vent discharge coefficient, generally around 0.6;
- R is the universal gas constant, 8.314 J/kg/mol;
- a_{cd} is the speed of sound of the gases discharged through the vent;
- T_v the exhaust gas temperature;

- and M_v the molar mass of the evacuated gas.

The external explosion overpressure P_e is determined by:

$$\frac{P_e}{P_0} - 1 = \frac{20 \cdot \gamma_r \cdot (E - 1) \cdot E \cdot S_u \cdot R_e \cdot \sqrt{k_T a}}{a_0^2} \quad \text{Equation 106}$$

Where R_e is the radius of the outer cloud at the moment it is reached by the flame, k_T is an adjustment coefficient (cf. Table 8), a_0 is the celerity of sound in air, γ_r is the ratio of the specific heats of the reactants. a is defined by:

$$a = \frac{2 \cdot (E - 1) \cdot E \cdot S_u^2}{\sqrt{A_v}} \cdot \frac{A_f}{A_v} \cdot \left(\sqrt{\frac{E \cdot \gamma_p \cdot (\gamma_p - 1)}{\gamma_r \cdot (\gamma_r - 1)}} - 1 \right) \quad \text{Equation 107}$$

With γ_p , the ratio of the specific heats of the products burnt.

The various values of P_i are estimated by selecting the correct values for the flame area A_f and the flame velocity S_u , using the equations in Table 7 (assuming ignition at the wall opposite the vent, A_f values may differ in other cases):

Pressure peak	A_f	S_u
P_2	$A_{f(P1-BW)} \sim 2\pi \left[\frac{L^p h^p + L^p w^p + w^p h^p}{3} \right]^{\frac{1}{p}}$	$S_u \sim \frac{0.9}{Le} S_{lad}$
P_3	$\frac{A_{f_{obst}}}{A_f} = \left(1 + \frac{4}{3} \sigma^{1-\alpha} (BR)^{\frac{1}{2}} N^\alpha \right)^2$	$S_u \sim \frac{0.9}{Le} S_{lad}$
P_4	$A_{f(P2)} = 0.9 (A_{cw} - 0.9 (A_{BW} - A_v))$	$S_u \sim \Sigma_A S_{lad}$

Table 7. Calculation of A_f and S_u for the various P_i peaks

Where:

- $p = 1.6075$ and $\alpha = 0.63$;
- L is twice the length of the enclosure, w its width and h its height;
- A_{cw} is the internal surface of the enclosure;
- BR is an average blocking rate;
- N is the average number of obstacles in the path of the flame;
- Le is the Lewis number;
- Σ_A is a flame wrinkling constant (cf. Table 8).

Study	k_T	Σ_A
Bauwens (2012)	3.21	3.2
ICHS 2013 n°135	9.26	1
ICHS 2013 n°176	10.78	3.17
DIMITRHY benchmark Air Liquide (Jallais, 2013)	9.26	3.28
DIMITRHY benchmark CEA (Jallais, 2013)	12.2	3.7

Table 8. k_T and Σ_A parameters from various studies

A recognised advantage of the Bauwens model is that the physics is better represented than in the Molkov models. However, Jallais and Kudriakov (2013) have shown that, in the presence of obstacles, some of the model's predictions are not conservative, with an overestimate observed by a factor of 2 on the experimental measurements of Daubech (2013). This model is also poorly suited to small enclosures where it tends to estimate overpressures close to the maximum adiabatic overpressure (10 b), which is unrealistic.

Duclos (2019) compared the performance of this model with that of the Molkov model in its most recent version (2014):

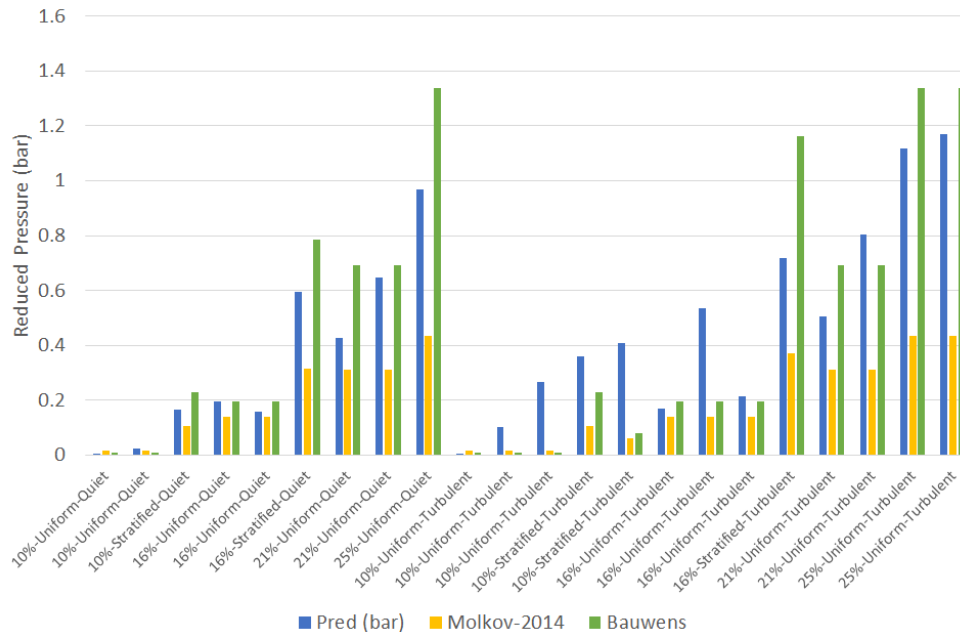


Figure 59. Comparison of model predictions by Molkov (2014) and Bauwens (2012) with published test data (Duclos, 2019). H_2 -air explosions in vented enclosures, bottom labels summarise H_2 volume concentration and degree of turbulence

Information on the test conditions can be found in Duclos's work (2019). At this stage, it should be noted that Molkov's model sometimes considerably underestimates the effects of overpressure. The Bauwens model is clearly the most suitable, particularly for lean mixtures (less than 20% H_2 vol.). Sometimes, this model also significantly underestimates the effects of the explosion, particularly for some tests carried out with higher turbulence,

4.5.5 Example of the use of a neural network

4.5.5.1 Description

. INERIS has examined a new approach that is closer to empirical tools. It is based on using an artificial neural network (ANN). From automotive technologies to financial forecasting and climate modelling, AI-based algorithms are gradually emerging in all scientific fields. They provide rapid estimates or classifications, often with acceptable accuracy. Above all, they promise an extreme ability to perform regressions on virtually any dataset (Karpathy, 2015). It is this ability that we wanted to test here.

Simulating a relatively simple gas explosion model in a vented enclosure is highly complex necessitating the creation of elaborate models despite rather simple reference situations. A wide range of models are proposed in the scientific literature, and this reference situation is still the subject of in-depth research.

An MPL (Multi-Layer Perceptron) type network is chosen, consisting of several series of densely connected layers of artificial neurons. This neural network architecture is chosen because it is particularly well suited to regression problems (Cybenko, 1989). An artificial neuron can be seen as a linear combination that takes several values as input and returns only one number. Its use as a computer requires a training phase in which the neuron is given input data and the corresponding output. The neuron must then adjust its internal coefficients to obtain the correct output value. Training takes place at the entire network level, with a large number of input/output pairs. Using the network to make predictions requires only the input data, using the same formatting as for training, and in this MPL architecture, there is no more adjustment during this so-called prediction phase. Here it is the modelling paradigm that is changed: we are no longer interested in obtaining a model or describing physical phenomena, but in seeking advanced mathematical regression, which broadly disregards the laws of physics.

4.5.5.2 How it works

The references are based on work published in the scientific literature and INERIS test data. The experimental data from works published by Bauwens (2011; 2012 and 2014); Chao et al (2011); Daubech J. (2011); Fakandu (2013); Kumar (1989; 2006 and 2009); Liang (2017); Pasman (1974); Skjold (2019); Sun (2018); Wang (2018) and Yao (1974) represent 202 tests, plus 60 tests carried out at INERIS. From the outset, we randomly exclude 26 tests (i.e. 10%) from the results of our database, the remaining tests will be used to evaluate the predictive capacities of the trained neural network.

An extract from the database is presented in the following two tables:

Essay #	Author	Year	Fuel	%vol	L (m)	W (m)	H (m)
2	Bauwens	2011	Hydrogen	16.5	4.6	4.6	3
69	Daubech	2011	Hydrogen	14	5.5	1.6	1.6
102	Kumar	1989	Hydrogen	10	1.18	1.18	1.18
155	Liang	2017	Hydrogen	6.2	4.5	4	3
171	Skjold	2018	Hydrogen	15	5.867	2.352	2.385
197	Wang	2018	Hydrogen	34	1.8	1	0.55

Table 9. Randomly selected trials in the database, left-hand side

Test #	V (m3)	Shape	Av (m2)	Ignition	Pstat (bar)	u' (m/s)	Pred (bar)
2	63.7	Rect.	5.4	Centre	0.005	0.1	0.03
69	10.5	Cyl.	2	Background	0.005	0	0.03
102	6.85	Sphere	0.0491	Centre	0.1	0	0.9
155	57	Rect.	0.55	Centre	0.01	1	0.05
171	33	Rect.	5.56	Background	0.005	0	0.03
197	1	Rect.	0.2	Centre	0.005	0	0.95

Table 10. Randomly selected trials from the database, right-hand side (Rect.: parallelepipedic shape; Cyl. cylindrical shape; "Bottom" means ignition at the bottom of the enclosure, opposite the vent; u' is the turbulent velocity just before ignition)

In total, the database contains the results of:

- 22 different studies by 12 authors between 1974 and 2019;
- tests carried out in 18 different volumes:
 - ranging from 10 l to 120 m³;
 - parallelepiped, cylindrical or spherical;
 - with vents with a static opening pressure P_{stat} of up to 300 mbar, but with the vast majority (259 out of 268) below 100 mbar, including 200 tests with P_{stat} below 20 mbar;
- tests carried out mainly with hydrogen (180) and methane (60), but also including tests with propane (9) and ethylene (19);
- mainly in fluids at rest, since 185 out of 168 tests were carried out with a turbulent velocity u' of less than 0.1 m / s;
- with P_{red} recorded up to 2 bar, but nearly 60% of tests in the 0-200 mbar range (and 90% of tests below 1 bar).

If the data is grouped by study (author and year), fuel and enclosure volume, 30 independent data groups can be formed.

Various parameters are used as input data, such as gas type, concentration, pre-ignition turbulence velocity u', mixture expansion rate, and enclosure or vent dimensions. The selected data consists only of variables directly relevant to the test configuration that can be accessed prior to performing the explosion vent test in a given configuration. In particular, it does not include data from the scientific literature or ancillary modelling such as flame velocity S_{lad} or S_t or expansion rate E. We use a categorical classification for textual data such as the gas used (i.e. we have a column for each gas which is 1 or 0 depending on whether it is the gas used or not). The neural network is used to estimate the reduced explosion pressure P_{red} .

Before training the neural network, data volume which does not include the 26 verification tests was increased by a factor of 10 using methods from the field of image processing. For example, if a variable X can be wrong by 5%, a test with the input data 1.05 X or 0.95 X should produce the same result. This method increases the robustness of the neural network and is more commonly used in image processing using neural networks.

4.5.5.3 Results

For 26 randomly selected tests, the network predictions are as follows:

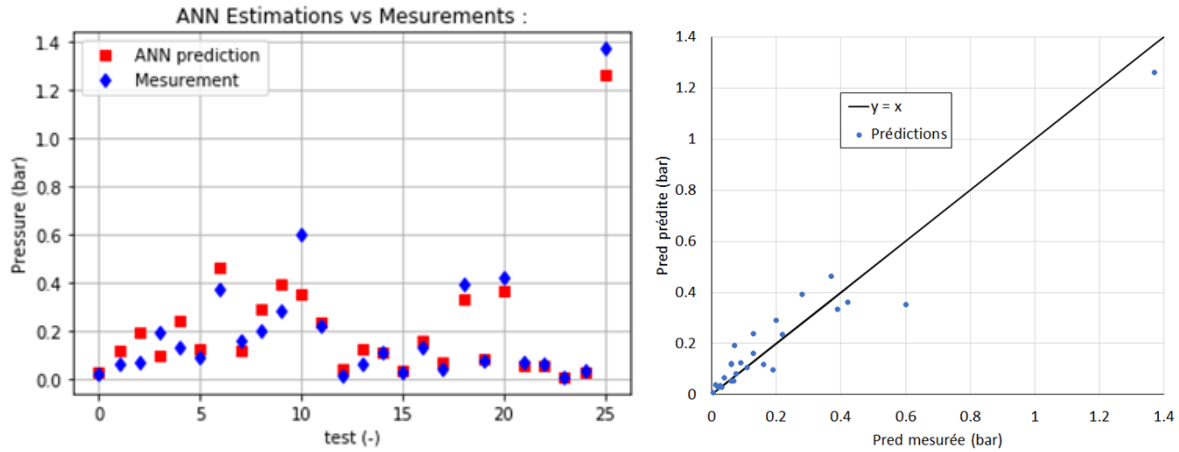


Figure 60. Comparison of neural network predictions with 26 trials randomly selected from the database

The neural network predictions are close to the measurements, with an average error of no more than 55 mbar and a maximum of 250 mbar. These results were compared with an empirical method and the INERIS EFFEX code (see paragraph 4.4.1) based on the models presented in 3. The neural network gave the closest estimate⁸ of the real case in 19 of the 26 cases, compared with 5 for the phenomenological tool and 2 for the empirical tool. Of these 26 randomly selected tests, only 13 are sufficiently documented to be able to estimate the overpressure P_{red} using the formulae in standard EN14994, the NFPA68 guide, Bauwens and Molkov from 1999 and 2014, and the EFFEX phenomenological model:

Test	Author	Year	%vol	I	L	D	V	Av	u'	S_{lad}	E
A	Bauwens	2011	14.9	0.5	4.6	3,63	63.7	5.4	0.1	0.83	4.6
B	Bauwens	2011	18.1	0.5	4.6	3,63	63.7	5.4	0.1	1.3	5.2
C	Bauwens	2011	19	0.5	4.6	3,63	63.7	5.4	0.1	1.4	5.4
D	Bauwens	2011	18.3	1	4.6	3,63	63.7	5.4	0.1	1.32	5.25
E	Bauwens	2011	19	1	4.6	3,63	63.7	5.4	0.1	1.4	5.4
F	Bauwens	2011	15.1	1	4.6	3,63	63.7	2.7	0.1	0.85	4.6
G	Bauwens	2011	18.3	0.5	4.6	3,63	63.7	5.4	0.1	1.3	5.2
H	Bauwens	2011	18.5	0.5	4.6	3,63	63.7	5.4	0.1	1.35	5.3
I	Daubech	2011	27	1	1.66	0.94	1	0.13	0	2.5	6.6
J	Kumar	2006	11	1	10	3.43	120	0.55	0	0.36	3.65

⁸ which in an industrial safety context is not the best estimate, because it is not necessarily conservative.

Test	Author	Year	%vol	I	L	D	V	Av	u'	S _{lad}	E
K	Kumar	2009	10.2	0.5	10	3.43	120	0.55	1	0.27	3.42
L	Kumar	2009	8.8	0.5	10	3.43	120	1.1	1	0.19	3.1
M	Duclos	2019	16	1	2	1.33	4	0.49	0	1	4.8

Table 11. List of tests randomly selected from the database to check the operation of the neural network and for which sufficient data is available to estimate the overpressure using the Bauwens (2012) and Molkov (1999, 2014) models. I refers to the ignition point: it is 0.5 if ignition takes place in the centre of the enclosure and 1 if it takes place at the opposite the vent. S.I. units

Table 12 shows the results of the calculations using the different models:

TEST	Pred	ANN	EN14994	NFPA68	Bauwens	Molkov - 1999	Molkov 2014	EFFEX
A	20	30	765	365	40	65	35	95
B	60	120	765	425	170	180	100	200
C	70	120	765	440	235	230	135	235
D	130	140	765	425	80	190	110	205
E	190	95	765	775	100	230	135	235
F	130	240	2510	945	30	205	90	200
G	90	125	765	425	180	190	110	200
H	90	115	765	430	195	200	115	215
I	1440	1310	3970	1965	3265	1675	485	4340
J	280	395	835	5850	100	1515	255	1010
K	590	630	835	5135	180	1270	190	965
L	220	235	420	1995	30	320	45	230
M	195	575	1335	535	195	370	140	270

Table 12 Experimental measurement and results of predictions or calculations for the tests listed in Table 11

Graphically, these same results can be displayed as follows:

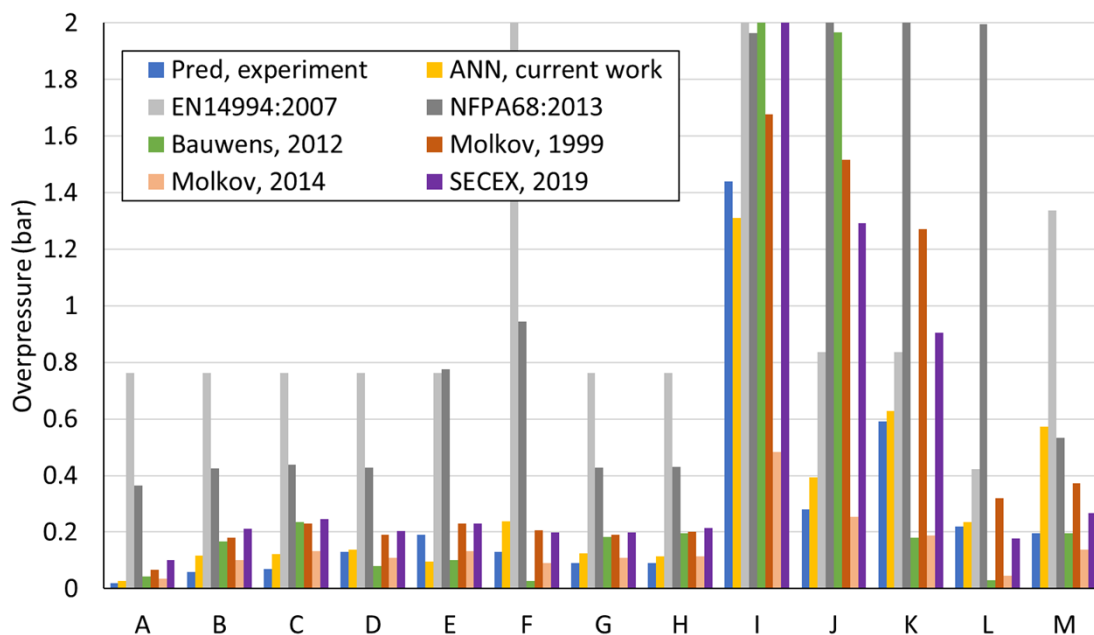


Figure 61. Comparison of neural network predictions with 26 trials randomly selected from the database. Values above 2 bar are not displayed.

The best performance of the neural network is unequivocal. Since the agreement is very satisfactory, considering that the computation cost is negligible, requiring only a few minutes on a conventional CPU, prompt utilisation and application of this type of code is an advantage. use Visual programming with few or no lines of code reduces the implementation period, where more time is also saved as the neural network simplifies and minimizes the time spent studying the physics of the explosion.

However, if the model can be seen as a kind of fit to the dataset, then close configurations can be expected to produce results close to those used for regression. The other definite advantage is that this neural network-based model implicitly takes into account (and could be used to detect) as yet unknown unknowns of the problem, which, in time, could help to improve our understanding of the physics involved.

Apart from the small number of cases analysed, which at least have the merit of having been chosen entirely at random, this selection of 10% of the results may not be statistically representative of the consistency of the data. Nevertheless, the aim was to illustrate how the method works rather than seek the best possible performance.

4.5.5.4 Limits

The representativeness of the predicted situation with respect to the data used to train it is the main limitation. Two major problems have been identified:

- 1) the extreme tendency of these tools for regression,
- 2) the absence of physical constraints on the predictions relative to the initial data set.

To study the first of these two problems, the exercise carried out in the previous paragraphs has been reproduced with one error. The 26 validation tests are the same, but this time, all the overpressures in the initial table (i.e. the last column of Table 10), with the first value in the table arbitrarily replaced by the last. This "accidental" shift in the output column could be due to a user error during coding. The network was then trained with the corrupted augmented data. The code gave the following results:

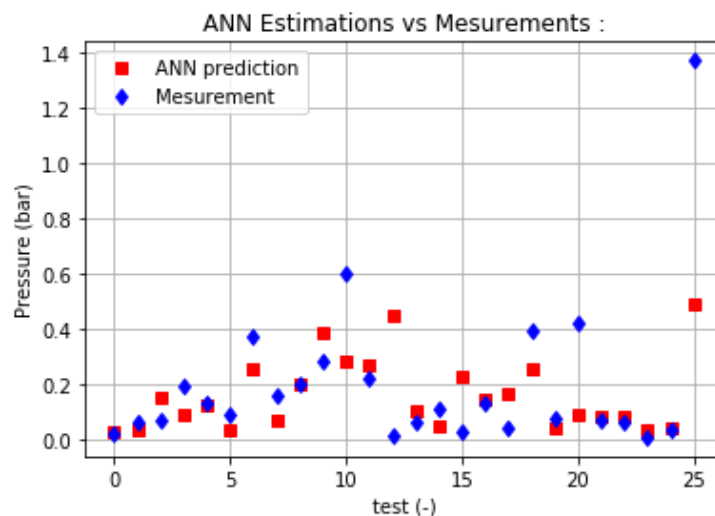


Figure 62. Comparison of neural network predictions with 26 trials randomly selected from the database

There are indeed more errors than in Figure 59, but an uninformed user may find this result acceptable. In practice, it is only slightly more difficult for the network to converge, and the user is not warned of any inconsistencies in the result. Therefore, data control is a key issue in this approach.

For the second point, we sought to test physical laws with the correctly trained network. Two configurations, well represented in the database, were chosen:

Comb.	Flight	L (m)	Dh (m)	V (m ³)	Ignition	Av (m ²)	Pstat (bar)	u' (m/s)
H ₂	19	4.6	3.63	63.7	Centre	5.4	0.005	0.1
CH ₄	10	4.6	3.63	63.7	Centre	5.4	0.005	0.1

Table 13. Two of the most common configurations in the database

On this basis, the trained network was asked to predict P_{red} for gas volume concentration values ranging from 0 to 80%. Maximum effects are expected for a gas content slightly greater than 1, i.e. around 30% for hydrogen and 10% for methane. In the database, methane tests were carried out in the 8-13% range, with the vast majority of tests around 10%, while hydrogen tests were carried out in the 5-34% range, with the vast majority of tests around 20%.

The result of the predictions is as follows:

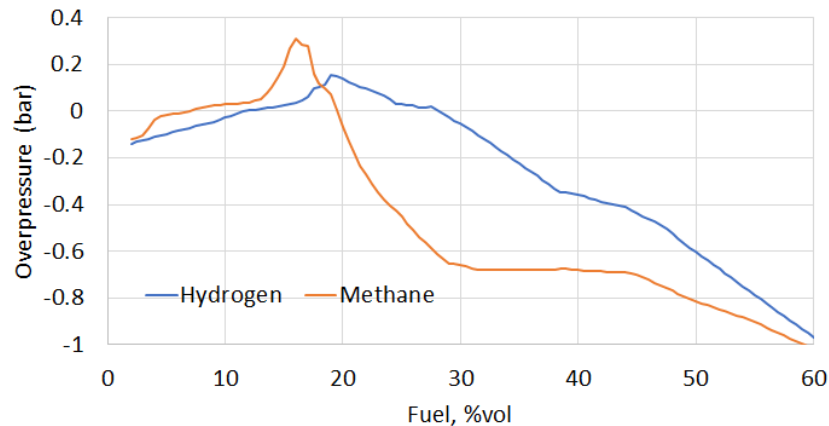


Figure 63. Predictions of the neural network by varying the gas concentration

There are several problems, the first being that the code makes physically false assertions. For example, it may predict maximum overpressures lower than the vent opening overpressure (by a few mbar). The errors are particularly recurrent outside the zones covered by the data range. However, these marginal errors are of little concern in this case because they are easily identifiable. There are ways of correcting these particular aspects by working on the neural network algorithm.

For hydrogen, we also note that the model does not give physical results in the 20-35% range despite the existence of tests in the database with a volume fraction of up to 34%. However, these tests were not carried out on the 63.7 m³ tank studied here. This could indicate another flaw in the network's ability to generalise predictions. Its range of validity cannot be defined simply by looking at the minimum and maximum tested for each variable. Therefore, the density of the training data is also of great importance.

Despite its simplicity of implementation, this type of calculation is far from trivial. The results of simulations carried out with this type of model must be examined carefully. If the code is intended to be empirical, the critical analysis of the results it produces can be highly complex because:

- the data: the multiplicity of assumptions that can be made about the training data is a first complexity (if, for example, as here, we rely on data from very different sources, more or less well documented, from which we choose a certain number of parameters that seem representative, and/or we add assumptions about increases in the data);
- the structure of the network: There is a wide variety of possible neural architectures. We did not focus on this point because it was not the object of the study. However, the construction of the network is based on choices about the number of neurons, layers of neurons, minimisation criteria, convergence, a certain number of iterations, or output parameters;
- the choice of outputs: We have chosen P_{red} here, but we could just as easily have asked for the four pressure peaks of Cooper's model, a pressure signal, or a physical parameter such as a flame velocity term to be used later in other models.

4.6 Modelling external effects

4.6.1 Preamble: Thermal effects

In the field of confined explosions, the thermal effects associated with flames are usually considered to be contained within the volume of the flame. European standards give several formulae for estimating flame lengths in front of a vent. Typical orders of magnitude are given below:

- In front of the vent, you can expect a fireball with a diameter equal to 2 times the largest dimension of the vent or 2.8 times the volume at 1/3 power (according to standard EN14491 on dust explosions);
- On the vent's axis, flames as long as 10 times the enclosure's volume can be seen at 1/3 power.

For confined explosions, the external effects are essentially pressure effects.

4.6.2 External overpressure wave calculation charts

4.6.2.1 Principle

As indicated in paragraph 3.9, the pressure wave emitted into the air can be sonic or supersonic, in which case it is referred to as a shock wave. Strictly speaking, solving the Navier-Stokes equations in air is necessary to describe their propagation. The complexity of this approach makes it difficult to apply to industrial situations. Numerous other methods exist for estimating, for a given explosion, the pressure levels that can be expected at different distances from the centre of the explosion. In most cases, the local effects of the explosion are "converted" into energy, which is then used as input data for empirical tables.

With the exception of specific situations involving irregular reflections, the physics of shock wave propagation in air is well-known and obeys simpler laws than those for sonic pressure waves. A particularly interesting feature of sonic pressure waves is that we can make the simplifying assumption that their general shape does not change as they propagate through the air. They are also easier to produce and reproduce experimentally, so the charts or databases that provide damage levels as a function of overpressure are most often associated with shock waves.

On the other hand, pressure waves generated by explosions in air are sonic pressure waves with an N-shaped signal that changes over time. Their modelling is relatively complex, and few charts are available to represent them. Moreover, these require knowledge of the wave profile to be propagated in the air. For example, in the Multi-Energy method (paragraph 4.6.2.2), assumptions are made about an explosion violence index before studying the distribution of the various thresholds of interest. In addition, in the case of a confined explosion, it is often assumed that a vent or wall will open instantaneously, bringing a pressurised medium into contact with another, which is not, and should therefore lead to the emission of a shock wave. Therefore, we are mainly interested in the emission of shock waves into the air.

4.6.2.2 Multi-Energy method

TNO proposed the Multi-Energy method (van den Berg, 1984) following major test campaigns carried out in the 1970s and 1980s, as well as developments in the theory of hemispherical gas deflagrations. Therefore, it is a priori well suited to the present case because it is based on ground-level gas explosions (surface explosions). It should be noted, however, that it is based on calculations using a CFD-type code (BLAST, developed by TNO). It takes into account several parameters that influence the velocity of flame propagation, including the following:

- the density of obstacles,
- the degree of containment,
- the shape and size of the flammable cloud,
- the fuel reactivity,
- the energy and position of the ignition source,
- and the turbulence of the reactive mixture before ignition.

However, the containment in question here refers to a congested industrial site rather than a closed enclosure fitted with a vent. The application of the Multi-Energy method is based on qualifying the violence of the explosion by choosing a violence index between 1 and 10, corresponding to a maximum level of overpressure. Finally, the maximum levels and the attenuation curves of the overpressure as a function of distance are given for each index on abacuses (*Figure 64*).

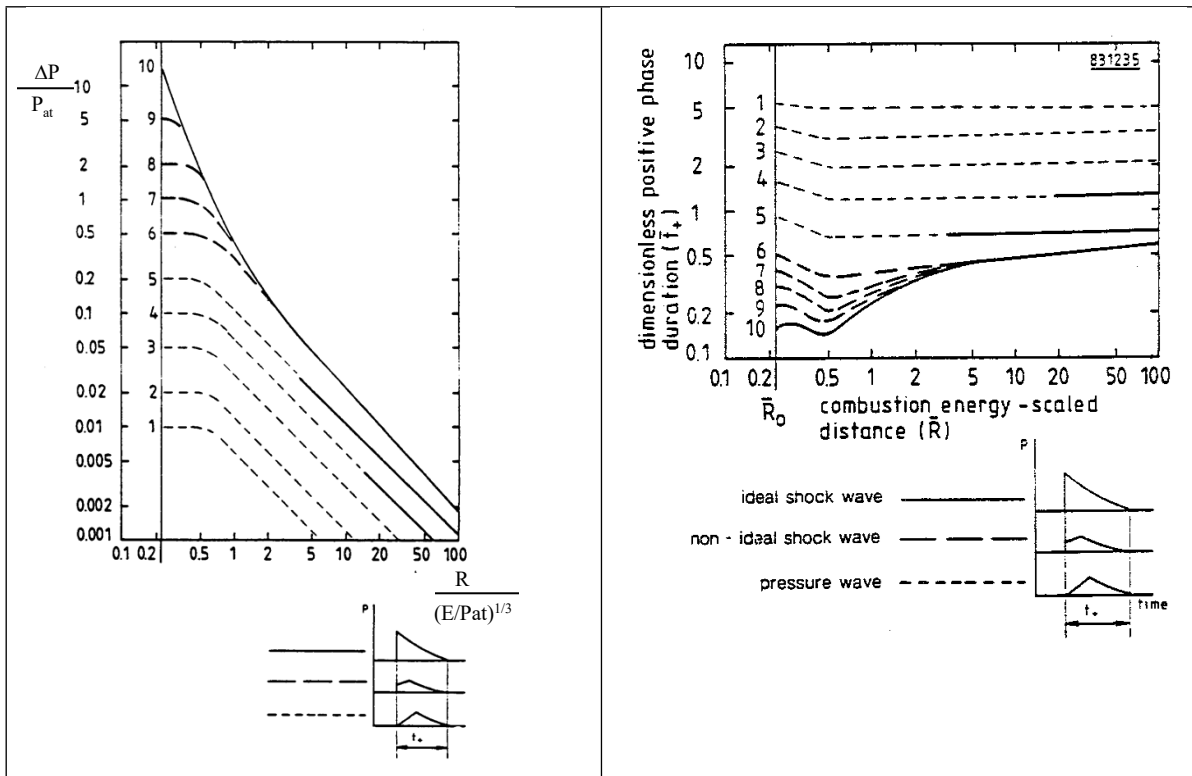


Figure 64. Overpressure and duration of the positive phase as a function of the reduced distance - from (van den Berg, 1984)

One of the problems of a confined explosion in an enclosure fitted with a vent is the difficulty of assigning a reduced explosion index to implement the Multi-Energy method. As no rule has been established to consider the effect of the progressive opening of a vent, it is assumed that the enclosure undergoes a burst, and the index used must be 10, the most severe. This is a major assumption which leads to the modelling of a shock moving isotropically through the air. Both the phenomenology and the experiments indicate that sonic pressure waves propagate, so an index of 1 to 9 would be more appropriate. For regulatory effects, indices from 6 to 10 lead to the same results.

Apart from the starting model being a gas explosion, another interesting aspect of the method is that the reduced distance is deduced from a "Brode energy". Brode energy is a parameter used to estimate the mechanical energy contained in a pocket of pressurised air before it expands into the atmosphere. The Brode energy of the explosion can be obtained by:

$$E = \frac{\Delta P \cdot V}{\gamma - 1} \quad \text{Equation 108}$$

This model uses V as the volume of the explosion, ΔP the maximum overpressure achieved, and γ the ratio of the specific heats of the burnt gases. It is more practical for this study because V is readily available, and ΔP is a primary variable of interest in the confined explosion problem.

The overpressure at a selected reduced distance can then be determined directly by graphical reading. (Note: below a reduced distance of 0.25, the model gives no information on the wave's parameters —this is the near-field zone.)

More details on the implementation of the Multi-Energy method are presented in the Omega report on UVCE.

4.6.3 Prediction of pressure effects using the method of European standards EN14994 or EN14491

According to EN14994, the pressure and blast effects produced outside a vent come from pressures produced by the explosion inside the enclosure and also by the external explosion of the cloud of combustible gas formed outside, near the vent.

A formula is proposed for gas and dust explosions to determine the external effects as a function of distance R and angle α :

$$P_{ext} = \frac{1,24 \cdot P_{red} \cdot \left(\sqrt{A_v/R} \right)^{1,35}}{1 + (\alpha/56)^2} \quad \text{Equation 109}$$

With A_v , the vent area, and P_{red} , the maximum pressure in the enclosure.

This formula is only valid under certain conditions:

- it only applies to enclosures without elements that encourage turbulence,
- with a volume of between 100 l and 250 m³;
- with vents with a static activation pressure less than or equal to 100 mbar;
- for an explosivity constant K less than or equal to 200 bar.m/s;
- an enclosure length-to-diameter ratio of less than 2;
- for gas explosions: a maximum external overpressure of between 200 mbar and 1 bar;
- for gas explosions: the angle between the connection line and the perpendicular to the centre of the vent orifice from 0 to 90°.

Note the pressure decay along the axis of the vent at $1/R^{0,675}$, which after a distance of 1 m is slow compared with the decay rates typically encountered in wave expansion problems (usually close to $1/R^{1,5}$). Not only are the gases discharged towards the perpendicular to the vent, but they are also expelled with greater force than if they were simply expanded isotropically, which induces a directional effect. This method of calculation results in effects along the axis of the vent that are sometimes greater than those predicted using the Multi-Energy method.

For dust explosions, the equation is the same, but the conditions are slightly modified:

- the angle α can only vary from 0 to 90°,
- the maximum explosion pressure must not exceed 9 bar,
- the reduced overpressure P_{red} must be between 100 mbar and 1bar
- the distance R must be greater than R_s equal to a quarter of the flame length outside the enclosure.

$$R_s = 0,25 \cdot L_f = 2,5 \cdot V^{1/3} \quad \text{Equation 110}$$

For dust explosions, the external effects model is supplemented by two formulae (which do not exist in the gas explosion standard EN14994) to describe the effects of the external explosion:

$$P_{ES,max} = 0,2 \cdot P_{red} \cdot A_v^{0,1} \cdot V^{0,18} \quad \text{Equation 111}$$

$$P_{ES,R} = P_{ES,max} \cdot \left(R_s/R \right)^{1,5} \quad \text{Equation 112}$$

Interestingly, this formula assumes that the secondary explosion generates isotropic effects in the air, which is not the case for the discharge of gases through the vent.

Furthermore, according to this model:

- In general, this model for dust explosions indicates that the overpressure generated outside the enclosure during the secondary explosion is less than the internal overpressure P_{red} . The absence of a limit on the minimum value of R in Equation 109 for the expansion of gas explosions leads to a zone of overpressure greater than P_{red} if $R < A_v$ and unrealistic, which tends towards infinity when the vent is approached;

- the secondary explosion modelled by Equation 112 decays faster than the expansion of Equation 109 (decay in $1/R^{1.5}$ or $1/R^{0.675}$);
- for a fixed ventilation rate (ratio $A_v/V^{2/3}$) and a fixed P_{red} , increasing the volume increases the effect distances. However, the relative importance of the secondary explosion is not changed compared with the vent discharge;
- for a fixed volume and opening ratio (ratio of vent surfaces to enclosure cross-section), increasing the P_{red} increases the external effects. However, this is more visible for the secondary explosion, which can become dominant (over the external effects);
- for a fixed volume and P_{red} , increasing the opening ratio reduces the importance of the secondary explosion compared with that of the discharge of gases through the vent. On the other hand, a small opening ratio can lead to an external explosion, which has stronger external effects than the internal explosion. In both cases, the external effect distances are increased, but the increase is proportional to $A_v^{0.675}$ for the gas discharge and $A_v^{0.1}$ for the secondary explosion.

4.6.4 The SECEX model - external module

The SECEX tool described in section 4.4.2 can be used to calculate the maximum overpressure generated by the external explosion. This result can be coupled with a law of expansion of the overpressure in air to estimate the effects of the explosion at different distances.

The air overpressure ΔP_L at a distance L can be obtained from this by using the acoustic law in the form

$$\Delta P_L = \Delta P_{max} * \frac{r_f}{L} \quad \text{Equation 113}$$

Where r_f is the outer radius of the fireball, which is generally about twice the diameter of the vent.

It is quite challenging to find standardised information in the literature on a large number of tests on the external overpressures generated by confined explosions. For this reason, this last part of the model has mainly been compared with INERIS results rather than with measurements published by other laboratories.

In the case of the 4 m³ enclosure, there were 4 external pressure sensors (see paragraph 4.3.3):

- L1 and L2, which are placed on the axis of the vent at 2 and then 5 m from the vent;
- At L1 level but perpendicular to the L1-L2 line, sensors L3 and L4 at 2 and then 5 m from L1.

The results are as follows:

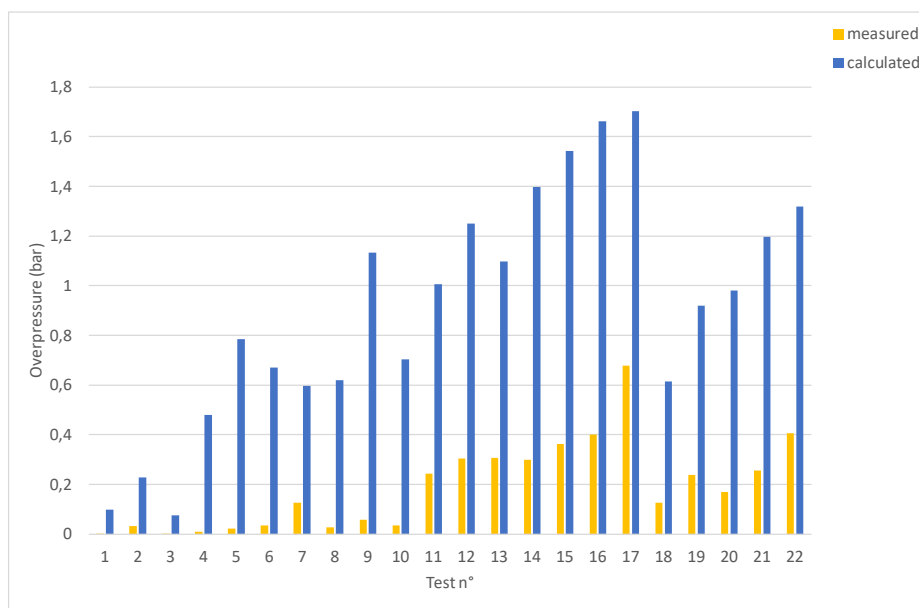


Figure 65. External overpressure prediction compared with tests carried out at INERIS (Duclos, 2019) at the L1 sensor located 2 m along the vent axis

At this level, the pressure in the fireball is greatly overestimated. This may be due to the acoustic approximation when the flame velocity is high.

On other sensors, the result is better:

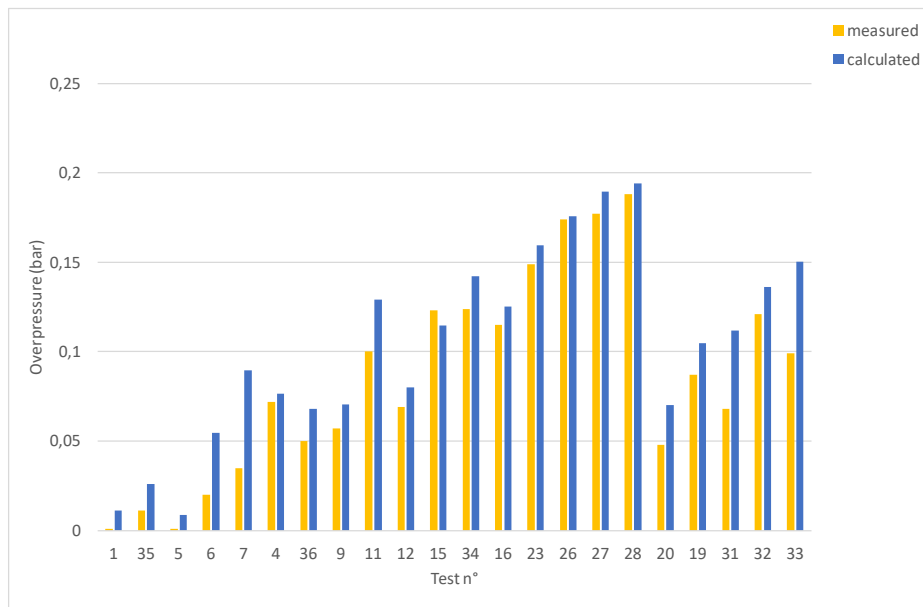


Figure 66. External overpressure prediction compared with tests conducted at INERIS (Duclos, 2019) at the L2 sensor located 5 m along the vent axis

In particular, the agreement is also satisfactory for sensors located perpendicular to the discharge axis of the burnt gases leaving the vent. This confirms the isotropic nature of the expansion in air. The predominant effect here is an isotropic external explosion that expands in all directions and not of a thrust of gases oriented in a preferential direction.

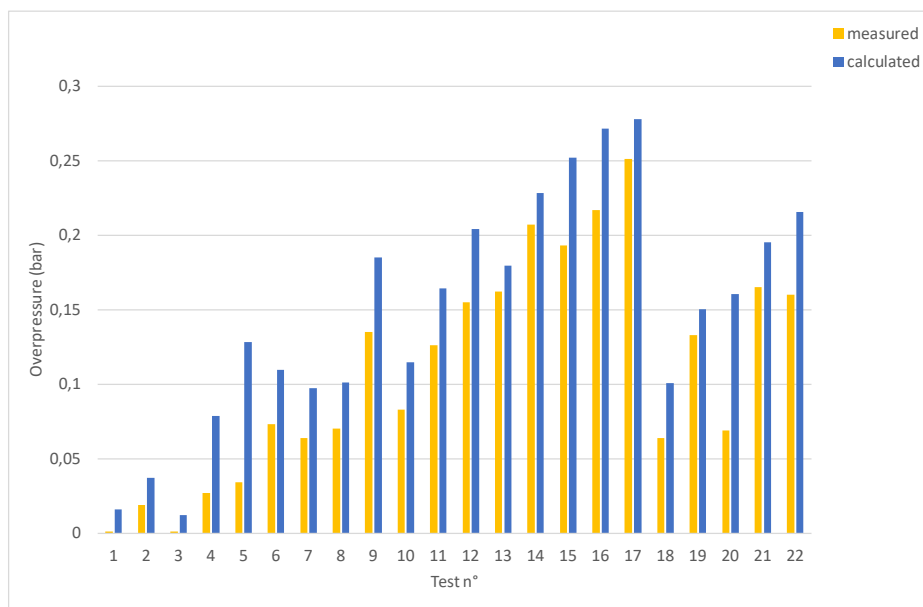


Figure 67. External overpressure prediction compared with tests carried out at INERIS (Duclos, 2019) at sensor L3 located 2 m from the axis of the gas outlet through the vent

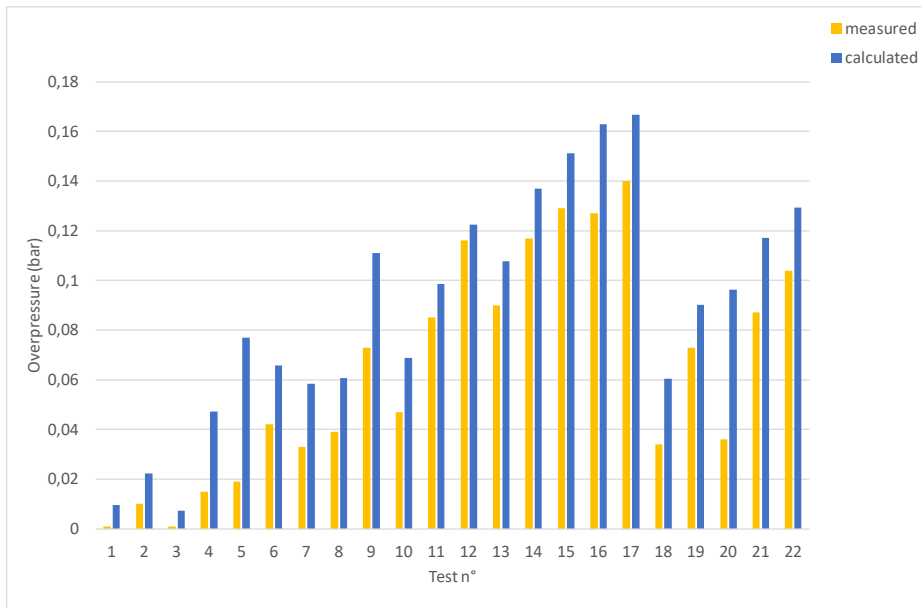


Figure 68. External overpressure prediction compared with tests carried out at INERIS (Duclos, 2019) at sensor L4 located 5 m from the axis of the gas outlet through the vent

The SECEX code also seems to give conservative results for external effects, making it a potentially well-suited tool for industrial safety studies.

5. Conclusions

This report focuses on confined gas explosions in the industrial environment.

This document presents the physical phenomena dominating confined gases in deflagration modes leading to explosions in cubic enclosures, as well as explosive effects on the environment. The report addresses marginally the problems of explosions in pipes, detonations and explosions of dust, and other hybrid particle-gas and multiple-gas mixtures.

A confined explosion is a flame that transforms cold reactants into hot burnt products. These hot gases expand, which in a confined environment results in an increase in pressure. Because of the brevity of the phenomenon, it is often assumed that the temperature exchange with the enclosure walls does not have time to take place and that adiabatic compression is involved. The major difficulty in this case is to estimate the rate of production of the gases burnt by the flame, which must then be compared with the possible rate of leakage of the fresh or burnt gases from the containment.

The main factors influencing the confined explosion are therefore:

- the nature of the combustible mixture, the type of gas and its concentration or distribution in the enclosure prior to the reaction;
- the geometry of the containment, any obstacles and openings;
- the nature of the flow and the intensity and scale of the turbulence before and during the explosion;
- the location and violence of the ignition source.

The violence of the explosion and the amplitude or extent of its effects on the associated environment result from a combination of these factors and physical phenomena, which are highly interconnected. A wide range of numerical models, both CFD and empirical, as proposed in European standards, are used to predict the effects of confined explosions in industry. Phenomenological modelling is less well represented in industry, but these codes can also be used for engineering and research purposes. All these models do not have the same field of application, but they do have one thing in common: in the absence of a generalised theory of turbulent combustion, they all depend, to a greater or lesser extent, on empirical building blocks.

Today, turbulent combustion is a research subject, the major evolutions of which can be grasped qualitatively. However, it remains unpredictable without recourse to empirical approximations. Nevertheless, it should be noted that most of the codes for confined explosions aim to determine an explosion pressure by solving a fluid flow problem. As the explosion is characterised by its effects, we are also particularly interested in the propagation of pressure waves outside the confinement. Several methods for estimating these effects are presented in the report. It should be noted, however, that the chemical aspects of the reaction, the propagation of pressure waves in the air and their interaction with structures are usually dealt with using simple rules based on tables or abacus. These estimates are only refined if a particular issue is at stake, as in the case of the resistance of a particular enclosure or an anthropogenic issue.

A modern approach based on artificial neural networks is also presented in this report. With these methods, which will probably become increasingly widespread in all scientific fields, the modelling paradigm has changed: the formalisation of the problem is no longer the focus. The excellent performance that can be achieved with this type of tool for a small investment should not, however, blind us to the fact that it remains empirical and defers the problem to the initial data and the interpretation that is made of it on the one hand, and to an interpolation that is invisible to the user, on the other. In this respect, although methods do exist, they are still relatively complex compared to the simplicity with which these calculations can be implemented, and the lack of formalism makes it more difficult to identify errors.

6. Bibliography

6.1 Publications

- 1) Abbasi, T., Abbasi, S.A., 2007. Dust explosions-Cases, causes, consequences, and control. *Journal of Hazardous Materials* 140, 7-44. <https://doi.org/10.1016/j.jhazmat.2006.11.007>
- 2) Abdel-Gayed R.G. & Bradley, D., Combustion regimes and the straining of turbulent premixed flames, *Combustion and Flame*, 76, 1989, pp. 213-218
- 3) Addai, Emmanuel Kwasi, Gabel, Dieter, Krause, Ulrich, 2016. Models to estimate the lower explosion limits of dusts, gases and hybrid mixtures. *Chemical Engineering Transactions* 48, 313-318. <https://doi.org/10.3303/CET1648053>
- 4) Albahri, T.A., 2003. Flammability characteristics of pure hydrocarbons. *Chemical Engineering Science* 58, 3629-3641. [https://doi.org/10.1016/S0009-2509\(03\)00251-3](https://doi.org/10.1016/S0009-2509(03)00251-3)
- 5) Andrews G.E., Bradley D., 1972, "The burning velocity of methane-air mixtures", *Comb. and Flame*, vol. 19, pp. 275-288
- 6) Andrews G. E., Phylaktou P. N., 2010, *Handbook on Combustion- Vol.1. Explosion Safety: Wiley-VCH Books*
- 7) Andrews, G.E., Phylaktou, H.N., 2010. *Explosion Safety*, in: Lackner, M., Winter, F., Agarwal, A.K. (Eds.), *Handbook of Combustion*. Wiley-VCH Verlag GmbH & Co. KGaA, Weinheim, Germany. <https://doi.org/10.1002/9783527628148.hoc016>
- 8) Andrews G.E., 2017, *Explosion Prediction and Mitigation CAPE5560M*, School of Chemical and Process Engineering, U. Leeds
- 9) Arntzen B.J., 1998, *Modelling of turbulence and combustion for simulation of gas explosion in complex geometries*. Doctoral thesis, Norges teknisk-naturvitenskapelige universitet, Series Dr. ingeniøravhandling, 0809-103X; 1998:120
- 10) Astbury, G.R., Hawksworth, S.J., Spontaneous ignition of hydrogen leaks: A review of postulated mechanisms. *Int. J. of Hydrogen Energy*, 32, 2007, pp. 2178-2185
- 11) Bartknecht, W. 1981. *Explosions, course, prevention, protection*. Heidelberg: Springer-Verlag. 251 p. ISBN 3-540-10216-7
- 12) Bartknecht, W. 1993. *Explosionsschutz: Grundlagen and Anwendung*. Berlin: Springer- Verlag. 891 p. ISBN 3-540-55464-5. (Referred to by Siwek (1996))
- 13) Bauwens, C.R., Chaffee, J., Dorofeev, S.B., 2011. Vented explosion overpressures from combustion of hydrogen and hydrocarbon mixtures. *International Journal of Hydrogen Energy* 36, 2329-2336. <https://doi.org/10.1016/j.ijhydene.2010.04.005>
- 14) Bauwens C.R., Chao J., Dorofeev S.B., 2012. Effect of hydrogen concentration on vented explosion overpressures from lean hydrogen-air deflagrations. *International Journal of Hydrogen Energy* 37, 17599-17605, <https://doi.org/10.1016/j.ijhydene.2012.04.053>
- 15) Bauwens, C.R., Chao J. and Dorofeev. S. B., (2012). Evaluation of a multi-peak explosion vent sizing methodology, IX ISHPMIE. *International Symposium on Hazard, Prevention and Mitigation of Industrial Explosions*
- 16) Bauwens, C.R., Dorofeev, S.B., 2014. Effect of initial turbulence on vented explosion overpressures from lean hydrogen-air deflagrations. *International Journal of Hydrogen Energy* 39, 20509-20515. <https://doi.org/10.1016/j.ijhydene.2014.04.118>
- 17) Bjerketvedt, D., Bakke, J. R. & van Wingerden, K. 1993. *Gas explosion handbook*. Version 1.2. Bergen: Christian Michelsen Research. 225 p. (Report CMR-93-A25034)
- 18) Blanchard R., Arndt D., Grätz R., Poli M., Scheider S. (2010), Explosions in closed pipes containing baffles and 90-degree bends, *Journal of Loss Prevention in the Process Industries*, 23: 253-259
- 19) Borghi R., 1988, Turbulent combustion modelling, *Progress in Energy Combustion Science*, vol. 14
- 20) Bradley B., Mitcheson A., 1978, "The venting of gaseous explosions: I- theory", *Combustion and Flame*, vol. 32
- 21) Bradley B., Cresswell T.M., Puttock J.S., 2001: Flame acceleration due to flame-induced instabilities in large scale explosions, *Comb and Flame*, vol. 124, pp 551-559
- 22) Bray K., 1990, "Studies of turbulent burning velocity", *Proceedings of the Royal Society of London*, Vol. A431, pp. 315-325

- 23) Breitung W., Chan C., Dorofeev S., Eder A., Gerland B., Heitsch M. Klein R., Malliakos A., Shepherd J., Studer E. and Thibault P., 2000, Flame acceleration and deflagration-to-detonation transition in nuclear safety. State-of-the-Art Report, OECD/NEA/CSNI/R7
- 24) Brode, H. L., 1955. "Numerical solutions of spherical blast waves." J. Appl. physics, Vol. 26, No. 6, pp. 766-775, DOI: 10.1063/1.1722085
- 25) Bychkov V.V., Liberman M.A., 2000, Dynamics and stability of premixed flames, Physics Reports, 325: 115-237
- 26) Chao, J., Bauwens, C.R., Dorofeev, S.B., 2011. An analysis of peak overpressures in vented gaseous explosions. Proceedings of the Combustion Institute 33, 2367-2374. <https://doi.org/10.1016/j.proci.2010.06.144>
- 27) Chapman D.L., 1899, On the rate of explosion in gases. Philosophical Magazine; 47, pp. 90-104
- 28) Ciccarelli G., Dorofeev S. 2008, Flame acceleration and transition to detonation in ducts, Progress in Energy Combustion Science, 34: 499-550
- 29) Clarke J.F. 1989, "Fast flames", Progress in Energy Combustion Science, vol. 15
- 30) Cooper M.G, 1986: On the mechanism of pressure generation in vented explosions, Combustion and flame n°65, pp 1-14
- 31) Cooper P.W., 1996, Explosives Engineering, Wiley-VCH, ISBN: 978-0-471-18636-6
- 32) Cybenko, G. 1989. Approximation by superpositions of a sigmoidal function Mathematics of Control, Signals, and Systems, 2(4), 303-314
- 33) Dahoe, A.E., Skjold, T., Roekaerts, D.J.E.M., Pasman, H.J., Eckhoff, R.K., Hanjalic, K., Donze, M., 2013. On the Application of the Levenberg-Marquardt Method in Conjunction with an Explicit Runge-Kutta and an Implicit Rosenbrock Method to Assess Burning Velocities from Confined Deflagrations. Flow Turbulence and Combustion 91, 281-317. <https://doi.org/10.1007/s10494-013-9462-z>
- 34) Darrieus G. 1946, "Propagation d'un front de flamme. Essais de théorie anormales de déflagration par développement spontané de la turbulence", 6th International Congress of applied mechanics, Paris
- 35) Daubech J., Proust Ch., Sochet I., 2006: Flame front perturbations induced by concentration gradients, 6th ISHPMIE, Halifax
- 36) Daubech J., 2008, Contribution à l'étude de l'effet de l'hétérogénéité d'un prémélange gazeux sur la propagation d'une flamme dans un tube clos, PhD thesis, Université d'Orléans
- 37) Daubech J., Proust C., Jamois D., Leprette E., 2011, Dynamics of vented hydrogen-air deflagrations, Proceedings of the 4th International Conference on Hydrogen Safety (ICHHS), Sep 2011, San Francisco, United States. ineris-00973626e, <https://hal-ineris.archives-ouvertes.fr/ineris-00973626/document>
- 38) Daubech J., Proust C. and Lecocq G., 2016, Propagation of a confined explosion to an external cloud, 11th International Symposium on Hazards, Prevention and Mitigation of Industrial Explosions, Dalian, China
- 39) Daubech J., Leprette E., Proust C., Lecocq G., 2018, Further insight into the gas flame acceleration mechanisms in pipes. Part I: experimental work, 12th International Symposium on Hazards, Prevention and Mitigation of Industrial Explosions, Kansas City, USA
- 40) Deshaies B., Joulin G. 1989, Flame-speed sensitivity to temperature changes and the deflagration to detonation transition, Combustion and Flame, 77: 201-212
- 41) Dold J.W., Joulin J., 1995. An evolution equation modeling inversion of tulip flames, Combustion and Flame 100, 450-456. [https://doi.org/10.1016/0010-2180\(94\)00156-M](https://doi.org/10.1016/0010-2180(94)00156-M)
- 42) Döring, W., Über den detonation vorgang in gasen. Ann. Phys, 1943. 43 (5): p. 421–436 (in German)
- 43) Dorofeev S., 2007, Hydrogen flames in tubes: critical run-up distances, Proceedings of the International Colloquium on Hydrogen Safety, San Sebastian, Spain, Sept. 2007
- 44) Duclos A., 2013, "Flame acceleration processes and associated pressure effects", Final year internship report, Compiègne University of Technology
- 45) Duclos A., 2019, Development of phenomenological and explosion risk control models for the emerging hydrogen energy sector. Thesis manuscript. Compiègne University of Technology
- 46) Ducros F., Nicoud F., Poinso T., 1998, Wall-adapting local eddy-viscosity models for simulations in complex geometries, M.J. Baines (Ed.), ICFD (1998), pp. 293-300

- 48) Escande J., Le Coze J.-C., Proust C., Marlair G., 2013 Signaux faibles: un concept pertinent? 14. Congrès de la Société Française de Génie des Procédés "Les sciences du génie des procédés pour une industrie durable" (SFGP 2013), Oct 2013, Lyon, France. pp.NC. ineris-00973715
- 49) Fairweather M., Ormsby M.P., Sheppard C.G.W., Woolley R., 2009, "Turbulent burning rates of methane and methane-hydrogen mixtures", *Combustion and Flame*, Volume 156, Issue 4, April 2009, Pages 780-790
- 50) Fakandu, B.M., Yan, Z.X., Phylaktou, H.N., Andrews, G.E., 2013. The Effect of Vent Area Distribution in Gas Explosion Venting and Turbulent Length Scale Influence on the External Explosion Overpressure, *Proceedings of the Seventh International Seminar Fire and Explosion Hazards*. Research Publishing Services, pp. 717-726. https://doi.org/10.3850/978-981-07-5936-0_11-05
- 51) Fakandu B. M., 2014, Vented gas explosions. PhD thesis, University of Leeds
- 52) Fakandu B., Khan I., Andrews G., Phylaktou H., 2018, Influence of a Wall Close to a Vent Outlet. In: *Proceedings of the 12th International Symposium on Hazards, Prevention and Mitigation of Industrial Explosions (ISHPMIE 2018)*. ISHPMIE 2018, 12-17 Aug. 2018, Kansas City, MO, USA. ISHPMI
- 53) Flauw Y., 2012, DRA-11-117406-03282A "Revue des valeurs génériques pour les probabilités d'inflammation présentes dans la littérature", INERIS
- 54) Filler WS, 1956, Post-detonation and thermal studies of solid high explosives in a closed chamber. *Combustion of explosives and solid propellants 1956*; 648-657
- 55) Gamezo, V.N., Ogawa, T., Oran, E.S., 2007. Numerical simulations of flame propagation and DDT in obstructed channels filled with hydrogen-air mixture. *Proceedings of the Combustion Institute* 31, 2463-2471. <https://doi.org/10.1016/j.proci.2006.07.220>
- 56) Gelfand, B. and Silnikov, M., 2004. Translation from Russian to English the Book "Blast Effects Caused by Explosions", DTIC Document, London, England
- 57) Germano M., Piomelli U., Moin P., Cabot W.H., 1991, A dynamic subgrid-scale eddy viscosity model. *Phys. Fluids A*, 3:1760-1765
- 58) Ginsburg I., Buckley W.L., 1963, Hydrocarbon-air detonations...industrial aspects, *Chemical Engineering Progress*, 59: 82-86
- 59) Glas A.G., Matkowsky B., Kliencko A.Y., 2001, "Stability of planar flames as gas-dynamic discontinuities", *Journal of Fluid Mechanics*, vol 491, pp 51-63
- 60) Gostintsev Y.A., Istratov A.G., Shulenin Y.V., 1989, Self-similar propagation of a free turbulent flame in mixed gas mixtures, *Combustion, Explosion, Shock Waves*, pp.563-569
- 61) Grégoire Y., Proust C., Leprette E., Dust explosion development in a vessel-duct arrangement, *Tenth International Symposium on Hazards, Prevention, and Mitigation of Industrial Explosions*, Bergen, Norway 2014
- 62) Grégoire Y., Leprette E. and Proust C., 2019, On the usefulness of phenomenological approach to model explosions in complex industrial systems, *Proceedings of the Ninth International Seminar on Fire and Explosion Hazards (ISFEH9)*, St Petersburg, Russia
- 63) Guenoche H. (1952) in Markstein G.H. (1964), "Non-steady flame propagation", Pergamon Press, Oxford, U.K
- 64) Gülder O.L. 1990: Turbulent Premixed Flame Propagation Models for Different Combustion Regimes, 23rd Symposium (Int.) on Combustion, The Combustion Institute, pp 743-750
- 65) Gülder O.L. and G. J. Smallwood 1995: Inner cut-off scale of flame surface wrinkling in turbulent premixed flames, *Combustion and Flame*, vol. 103, pp. 107-114
- 66) Harris, R. J. 1983. *The investigation and control of gas explosions in buildings and heating plant*. London: E & FN Spon. 194 p. ISBN 0-419-13220-1
- 67) Henrych, J. and Major, R. (1979). *The dynamics of explosion and its use*, Elsevier, Amsterdam.
- 68) Hinze J.O., 1975, "Turbulence", 2nd edition, Mc Graw-Hill company, New-York, ISBN 0-07-029037-7
- 69) Hjertager B.H., Fuhre K., Bjørkhaug M., 1988. Concentration Effects on Flame Acceleration by Obstacles in Large-Scale Methane-Air and Propane-Air Vented Explosions *Comb. Sci. Technical* 7
- 70) Hjertager B.H., Fuhre K., Bjørkhaug M., 1988. Spherical Gas Explosion Experiments in a High-Density Obstructed 27 m² Corner, presented at the 6th International Conference on Loss Prevention and Safety Promotions in the Process Industries, Oslo, Norway, June 1989
- 71) Hopkins-Brown, M. A. and Bailey, A. (1998). Chapter 2 (Explosion Effects) Part 1, AASTP-4 Royal Military College of Science, Cranfield University

- 72) Jallais S., Kudriakov S. An inter-comparison exercise on engineering models capabilities to simulate hydrogen vented explosions, ICHS5; Brussels September 2013 Paper 176
- 73) Jones W. P. and Launder B. E., 1972, "The prediction of laminarization with a two-equation model of turbulence", *International Journal of Heat and Mass Transfer*, vol. 15, no. 2, pp. 301-314
- 74) Jones S.A.S, Thomas G.O., 1991, "Pressure hot-wire and laser doppler anemometer studies of flame acceleration in long tubes", *Comb. and Flame*, vol. 87
- 75) Jouguet J.C. On the propagation of chemical reactions in gases, *J. des Mathématiques Pures et Appliquées*; vol. 1, 1905, pp.347-425, continued in vol. 2, 1906, pp. 5 - 85
- 76) Joulin G. and Sivashinsky G. 1991, Pockets in Premixed Flames and Combustion Rate. *Combustion Science and Technology*. 77. 329-335. 10.1080/00102209108951735.
- 77) Karpathy A., 2015, The Unreasonable Effectiveness of Recurrent Neural Networks, Hacker's guide to Neural Networks, Andrej Karpathy blog, <https://karpathy.github.io/2015/05/21/rnn-effectiveness/>
- 78) Kasmani, R. M., Willacy, S. K., Phylaktou, H. N. & Andrews, G. E. Year, 2006, Self-accelerating gas flames in large vented explosions that are not accounted for in current vent design. In: *Proceedings of the 2nd International Conference on Safety and Environment in Process Industry*, Naples, Italy
- 79) Kasmani, R.M., Andrews, G.E. and Phylaktou, H.N., 2010, The influence of vessel volume and equivalence ratio in vented gas explosions". *Fourth International Conference on Safety and Environment in Process Industry. Chemical Engineering Transactions*, Vol. 19, p.463-468, 2010. DOI:10.3303/CET1019076
- 80) Kerampran S., 2000, Etude des mécanismes d'accélération des flammes se propageant depuis l'extrémité fermée vers l'extrémité ouverte de tubes horizontaux de longueur variable, PhD thesis, Univ. Of Poitiers, France
- 81) Kessler, D.A., Gamezo, V.N., Oran, E.S., 2012. Gas-phase detonation propagation in mixture composition gradients. *Philosophical Transactions of the Royal Society A*. 370, 567-596. <https://doi.org/10.1098/rsta.2011.0342>
- 82) Kinney, G. F. and Graham, K. J., 1985. Explosive shocks in air, Springer-Verlag, Berlin and New York
- 83) Kordylewski, W. and Wach, J., 1986, Influence of ducting on explosion pressure, *Combustion and Flame*, 66: 77-79
- 84) Kordylewski, W. and Wach, J., 1988, Influence of ducting on explosion pressure: small scale experiments, *Combustion and Flame*, 71: 51-61
- 85) Kumar, R.K., Dewit, W.A., Greig, D.R., 1989. Vented Explosion of Hydrogen-Air Mixtures in a Large Volume. *Combustion Science and Technology* 66, 251-266. <https://doi.org/10.1080/00102208908947153>
- 86) Kumar, R.K., 2006. Vented Combustion of Hydrogen-Air Mixtures in A Large Rectangular Volume, in: 44th AIAA Aerospace Sciences Meeting and Exhibit. Presented at the 44th AIAA Aerospace Sciences Meeting and Exhibit, American Institute of Aeronautics and Astronautics, Reno, Nevada. <https://doi.org/10.2514/6.2006>
- 87) Kumar, R.K., 2009, Vented Turbulent Combustion of Hydrogen-Air Mixtures in A Large Rectangular Volume. In 47th AIAA aerospace sciences meeting including the new horizons forum and aerospace exposition. Paper AIAA 2009-1380
- 88) Kuznetsov M., Alekseev V., Matsukov I., Dorofeev S. (2005), DDT in a smooth tube filled with a hydrogen-oxygen mixture, *Shock Waves*, 14: 205-215
- 89) Landau L., 1944, "Theory of slow combustion", *Acta Physicochim*, vol. 19, p. 77
- 90) Lannoy A., 1984, Analyse des explosions air-hydrocarbure en milieu libre : Etudes déterministe et probabiliste du scénario d'accident. Prediction of suppression effects. *Bulletin Direct. Etudes et Recherches EDF*. A4
- 91) Lannoy A., Leyer J.C., Desbordes D., St Cloud J.P. (1989), "Déflagrations sans turbulence en espace libre : expérimentation et modélisation", *Bulletin de la DER, série A, Electricité de France*
- 92) Launder B.E., Spalding D.B., 1974, "The numerical computation of turbulent flows". *Computer Methods in Applied Mechanics and Engineering*. 3 (2): 269-289. doi:10.1016/0045-7825(74)90029
- 93) Lautkaski R., 1997, Understanding vented gas explosions. Espoo 1997. Technical Research Centre of Finland, VTT Tiedotteita - Meddelanden - Research Notes 1812. 129
- 94) Lecocq G, Richard S., Colin O., Vervisch L., 2011, Hybrid presumed pdf and flame surface density approaches for Large-Eddy Simulation of premixed turbulent combustion Part 1: Formalism and simulation of a quasi-steady burner, *Combustion and Flame* 158: 1201- 1214

- 95) Lecocq G., Leprette E., Daubech J., Proust C., 2018, Further insight into the gas flame acceleration mechanisms in pipes. Part II: numerical work, 12th International Symposium on Hazards, Prevention and Mitigation of Industrial Explosions, Kansas City, USA
- 96) Lee J.H.S, Knystautas R., Chan C.K. (1984), "Turbulent flame propagation in obstacle-filled tubes", 20th International Symposium on Combustion, pp. 1663-1672
- 97) Lewis B., Von Elbe G., 1987, "Combustion, flames and explosions of gases: 3rd edition", Academic Press, London, ISBN 0-12-446751-2
- 98) Leyer J.C, 1969, Interaction between combustion and gas motion in the case of flames propagating in tubes, *Astronautica Acta*, Volume 14, Issue 5, June 1969, Pages 445-451
- 99) Li, J. and Ma, S., 1992, *Explosion mechanics*, Science Press, Beijing
- 100) Liang, Z., 2017. Scaling effects of vented deflagrations for near lean flammability limit hydrogen-air mixtures in large-scale rectangular volumes. *International Journal of Hydrogen Energy* 42, 7089-7103. <https://doi.org/10.1016/j.ijhydene.2016.12.086>
- 101) Liberman, M.A., Ivanov, M.F., Kiverin, A.D., Kuznetsov, M.S., Rakhimova, T.V., Chukalovskii, A.A., 2010. On the mechanism of the deflagration-to-detonation transition in a hydrogen-oxygen mixture. *J. Exp. Theor. Phys.* 111, 684-698. <https://doi.org/10.1134/S1063776110100201>
- 102) Lilly D.K., 1992, A proposed modification of the Germano subgrid-scale closure method. *Phys. Fluids A*, 4:633-635
- 103) Lunn, G.A. & Pritchard, D.K., 2003, A modification to the KG method for estimating gas and vapour explosion venting requirements. *Institution of Chemical Engineers Symposium Series*. 227-245
- 104) Markstein G.H., 1964, "Non-steady flame propagation", Pergamon Press, Oxford, U.K.
- 105) Marshall, M. R. 1983. The effect of ventilation on the accumulation and dispersal of hazardous gases. 4th International Symposium on Loss Prevention and Safety Promotion in the Process Industries. Harrogate, 12 - 16 Sept. 1983. Rugby: The Institution of Chemical Engineers. Vol. 3. P. E11 - E22
- 106) Matalon M., Matkowsky B.J., 1982, "Flames as gas dynamic discontinuities", *Journal of Fluid Mech*, vol 124, pp 239-259
- 107) Matignon C., 2000, Etude de la détonation de deux mélanges stœchiométriques (CH₄/H₂/O₂/N₂ et CH₄/C₂H₆/O₂/N₂) Influence de la proportion relative des deux combustibles et de la température initiale élevée. *Electrical energy*. University of Poitiers, 2000. French, tel-00010305
- 108) McCann, D.P.J., Thomas, G.O. and Edwards, D.M., 1985, Gas dynamics of vented explosion. Part I: experimental studies, *Combustion and Flame*, 59: 233-250
- 109) Mecklenburgh, J. C. 1986. Hazard zone sizes within buildings. In: 5th International Symposium "Loss Prevention and Safety Promotion in the Process Industries". Cannes, 12 - 16 Sept. 1986. Paris: Société de Chimie Industrielle. Vol. 2. P. 52-1 - 52-15
- 110) Merilo, E.G., M.A. Groethe, R.C. Adamo, R.W. Schefer, W.G. Houf, D.E. Dedrick, 2012, Self-ignition of hydrogen releases through electrostatic discharge induced by entrained particulates, *Int. J. Hydrogen Energy*, 37 (2012) 17561-17570
- 111) Mills, C. A., 1987. "The design of concrete structure to resist explosions and weapon effects." *Proceedings of the 1st Int. Conference on Concrete for Hazard Protections*, pp. 61-73
- 112) Moen I.O., Bjerketvedt D., Engenbretsen T., Jenssen A., 1989, "Transition to detonation in a flame jet", *Combustion and Flame* 78: 297-308
- 113) Mogi T., Kim W., Terasawa K., Dobashi R., 2010, Fundamental study for consequence analysis of gas explosions in an open space. *The Proceedings of the Thermal Engineering Conference*. 2010. 307-308. [10.1299/jsmeted.2010.307](https://doi.org/10.1299/jsmeted.2010.307)
- 114) Molkov V., Dobashi R., Suzuki M., and Hirano T. Modeling of vented hydrogen-air deflagrations and correlations for vent sizing, *J. of Loss Prevention in the Process Industries*, Volume 12, 1999, pp. 147-156
- 115) Molkov, V., Bragin, M., Hydrogen-air deflagrations: vent sizing correlation for low-strength equipment and buildings, *Fifth International Conference on Hydrogen Safety (ICHHS)*, 9-11 September 2013, Brussels, Belgium, 13 pp
- 116) Molkov, V., Shentsov, V. and Quintiere, J, 2014, Passive ventilation of a sustained gaseous release in an enclosure with one vent, *Int. J. of Hydrogen Energy*, Volume 39, Issue 15, 2014, pp. 8158-8168
- 117) Molkov, V.V., 1994, Venting of deflagrations: dynamic of the process in systems with a duct and receiver, *Proceedings of the Fourth International Symposium on Fire Safety Science*, 1245-1254

- 118) Molkov V.V., Baratov A.N. and Korolchenko A.Ya., 1993, Dynamics of gas explosions in vented vessels: a critical review and progress, *Progress in Astronautics and Aeronautics*, 154: 117-131
- 119) Mullins and Penner, *Explosions, Detonations, Flammability, and Ignition*; AGARD, Pergamon, 1959
- 120) Naumyenko, I. and Petroskyi, I., *The shock wave of a nuclear explosion*. BOEH, CCCP, 1956
- 121) Oran E.S. and Boris J.P., 2001, *Numerical Simulation of Reactive Flow*. 2nd edition, Cambridge University Press
- 122) Oran, E.S., Gamezo, V.N., 2007. Origins of the deflagration-to-detonation transition in gas-phase combustion. *Combustion and Flame* 148, 4-47. <https://doi.org/10.1016/j.combustflame.2006.07.010>
- 123) Oran E.S., Kessler D.A., 2011, Deflagrations, Detonations, and the Deflagration-to-Detonation Transition in Methane-Air Mixtures, Naval Research Laboratory, report NRL/MR/6400--11-9332
- 124) Pasman, H.J., Groothuisen, Th.M. and Gooijer, P.H., 1974, Design of Pressure Relief Vents, In *Loss Prevention and Safety Promotion in the Process Industries*, Ed. Buschman C.H., New-York, 185-189
- 125) Pekalski, A. A., Zevenbergen, J. F., Lemkowitz, S. M., & Pasman, H. J. (2005). A review of explosion prevention and protection systems suitable as ultimate layer of protection in chemical process installations. *Process Safety and Environmental Protection*, 83(1), 1-17. Copyright 2005 by Elsevier B.V.
- 126) Phylaktou H. and Andrews G.E., 1991, The acceleration of flame propagation in a tube by an obstacle, *Combustion and Flame* 85:363-379 363
- 127) Phylaktou H. and Andrews G.E., 1991, "Gas explosions in long closed vessels", *Combustion Science and Technology*, vol. 77
- 128) Phylaktou H. and Andrews G.E., 1994, Prediction of the maximum turbulence intensities generated by grid-plate obstacles in explosion-induced flows, twenty-fifth (international) symposium on combustion/the combustion institute, pp. 103-110
- 129) Phylaktou .N; Andrews G.E., 1999, Explosion development in pipeline systems and linked vessels UKELG 25th meeting, Industrial Combustion Hazards Joint meeting with the Combustion Institute (British Section)
- 130) Pope S., 2004, Ten questions concerning the large-eddy simulation of turbulent flows. *New Journal of Physics* 6 35
- 131) Ponizy, B. and Leyer, J.C., 1999, Flame dynamics in a vented vessel connected to a duct: 1. Mechanism of vessel-duct interaction, *Combustion and Flame*, 116: 259-271
- 132) Ponizy, B. and Leyer, J.C., 1999, Flame dynamics in a vented vessel connected to a duct: 2. Influence of ignition site, membrane rupture, and turbulence, *Combustion and Flame*, 116: 272-281
- 133) Ponizy, B. and Veyssiere, B., 2000, Mitigation of explosions in a vented vessel connected to a duct, *Combustion, Science and Technology*, 158: 167-182
- 134) Proust, C, Veyssiere, B. Fundamental Properties of Flame Propagating in Starch Dust-air Mixtures. *Combustion Science and Technology*, 1988, 62(4): 149-172
- 135) Proust, C., 1993. Experimental Determination of the Maximum Flame Temperature and of the Laminar Burning Velocities for some Combustible Dust/Air Mixtures. *Proc. of the Fifth Int. Colloq. on Dust Explosions*, Bergen
- 136) Proust C., 1996, Dust explosions in pipes: a review, *Journal of Loss Prevention in the process industries*, vol. 9, (4), pp. 267-278
- 137) Proust C., 2000, EFFEX, a simulation tool. Ministère de l'Aménagement du Territoire et de l'Environnement. Report, www.ineris.fr
- 138) Proust C., 2004, Habilitation à diriger des recherches : mémoires de travaux ; Formation-Inflammation-Combustion des atmosphères explosives (ATEX) et effets associés, Institut National Polytechnique de Lorraine
- 139) Proust C., 2005, The usefulness of phenomenological tools to simulate the consequences of dust explosions: the experience of EFFEX. International ESMG symposium, Nürnberg, Germany
- 140) Proust C., Daubech, J., Leprette, E., 2009. Differentiated routes for the simulation of the consequences of explosions. *Journal of Loss Prevention in the Process Industries* 22, 288-294. <https://doi.org/10.1016/j.jlp.2008.09.006>
- 141) Proust, C. and Leprette, E., 2010, The dynamics of vented gas explosions, *Process Safety Progress*, vol. 29, 3, 2010, pp. 231-235
- 142) Proust C., 2015, Gas flame acceleration in long ducts. *Journal of Loss Prevention in the Process Industries*, Volume 36, Pages 387-393

- 143) Proust C., 2019, Fire and Explosion Safety in Hydrogen Containing Processes: State of the Art and Outstanding Questions, Proceedings of the Ninth International Seminar on Fire and Explosion Hazards (ISFEH9), pp.28-40, ISBN: 978-5-7422-6496-5, DOI: 10.18720/spbpu/2/k19-134
- 144) Quillatre P., 2014, Simulation at large scales in a confined environment. Thesis manuscript. University of Toulouse.
- 145) Rayleigh J.W.S., 1883, "Investigation of the character of the equilibrium of an incompressible heavy fluid of variable density", Proceedings of the London Mathematical Society, vol. 14, 1883, pp. 170-177 (DOI 10.1112/plms/s1-14.1.170)
- 146) Rian K.E., Evanger T., Vembe B.E., Lilleheie N.I., 2016, Coherent Computational Analysis of Large-Scale Explosions and Fires in Complex Geometries - From Combustion Science to a Safer Oil and Gas Industry. Chemical Engineering Transactions
- 147) Rocourt X., Awamat S., Sochet I., Jallais S. Vented hydrogen-air deflagrations in a small enclosed volume, ICHS5; Brussels September 2013 Paper 135
- 148) Rodgers and Zalosh, 2013, NFPA 68 new gas venting equations, Proceedings of the 9th Global Congress on Process Safety, 28 April - 2 May 2013, San Antonio, Texas, USA
- 149) Russo, P., Di Benedetto, A., 2007. Effects of a Duct on the Venting of Explosions-Critical Review. Process Safety and Environmental Protection 85, 9-22. <https://doi.org/10.1205/psep.04268>
- 150) Rzal F., 1992, "Etude expérimentale de l'interaction d'un anneau tourbillonnaire avec une flamme laminaire dans un mélange gaz-particules solides", PhD thesis from the University of Poitiers, no. 509
- 151) Sadovskiy, M. A., 2004, Mechanical effects of air shock waves from explosions according to experiments, Selected works: Geophysics and physics of explosion, Nauka Press, Moscow
- 152) Schmidt E., Steinicke H., Neubert U., 1951, Flame and Schlieren Photographs of Combustion of Gas-Air Mixtures in Tubes. VDI-Forschungsheft 431, Ausgabe Band 17, Deutscher Ingenieur-Verlag, Dusseldorf, 31 pp
- 153) Silvestrini M. Genova B., Parisi G., Leon Trujillo F. (2008), "Flame acceleration and DDT run-up distance for smooth and obstacles filled tubes, Journal of Loss Prevention in the Process Industries, 21: 555-562
- 154) Sivashinsky G.I., 1977, Diffusional-thermal theory of cellular flames. Combustion Science and Technology, 15 (3/4) (1977), pp. 137-145
- 155) Skjold, T., Hisken, H., Lakshminpathy, S., Atanga, G., Bernard, L., van Wingerden, M., Olsen, K.L., Holme, M.N., Turøy, N.M., Mykleby, M., van Wingerden, K., 2019. Vented hydrogen deflagrations in containers: Effect of congestion for homogeneous and inhomogeneous mixtures. International Journal of Hydrogen Energy 44, 8819-8832. <https://doi.org/10.1016/j.ijhydene.2018.10.010>
- 156) Smagorinsky J.S., 1963, "General Circulation Experiments with the Primitive Equations: I. The basic Experiment", Monthly Weather Review, vol. 91, no 3, pp. 99-164
- 157) Spalart P. R. and Allmaras S. R., 1994, A One-Equation Turbulence Model for Aerodynamic Flows, Aérospatiale Research, No. 1, pp. 5-21
- 158) Sochet I., 2010, Blast effects of external explosions. Eighth International Symposium on Hazards, Prevention, and Mitigation of Industrial Explosions, Yokohama, Japan. HAL-00629253e
- 159) Solberg, D. M., Pappas, J. A. & Skramstad, E. 1981. Observations of flame instabilities in large-scale vented explosions. In: 18th Symposium (International) on Combustion. Pittsburg: The Combustion Institute. P. 1607 - 1614
- 160) Sun, S., Wang, M., Gao, K., Zhao, T., Guo, Q., 2018. Effect of vent conditions on internal overpressure time-history during a vented explosion. Journal of Loss Prevention in the Process Industries 54, 85-92. <https://doi.org/10.1016/j.jlp.2018.03.002>
- 161) Taylor G.I., 1950, "The instability of liquid surfaces when accelerated in a direction perpendicular to their planes", Proceedings of the Royal Society of London. Series A, Mathematical and Physical Sciences, vol. 201, no. 1065, 1950, pp. 192-196 (DOI 10.1098/rspa.1950.0052)
- 162) Toliás I., Venetsanos A., 2018, An improved CFD model for vented deflagration simulations - Analysis of a medium-scale hydrogen experiment. International Journal of Hydrogen Energy 43.
- 163) Thomas G., Oakley G., Bambrey R., 2010, An experimental study of flame acceleration and deflagration to detonation transition in representative process piping, Process Safety and Environmental Protection, 88: 75-90

- 164) Thomas, G., 2012. Some observations on the initiation and onset of detonation. *Phil. Trans. R. Soc. A.* 370, 715-739. <https://doi.org/10.1098/rsta.2011.0368>
- 165) Ullah, A., Ahmad, F., Jang, H.-W., Kim, S.-W., Hong, J.-W., 2017. Review of analytical and empirical estimations for incident blast pressure. *KSCE J Civ Eng* 21, 2211-2225. <https://doi.org/10.1007/s12205-016-1386-4>
- 166) Ural, E.A., 1993, A simplified method for predicting the effect of ducts connected to explosion vents, *Journal of Loss Prevention in the Process Industries*, 6: 3-10
- 167) Van den Berg A.C., 1984, The Multi-Energy Method - a framework for vapour cloud explosion blast prediction. Report TNO-PML 1984-C72
- 168) Van den Berg A.C, Lannoy A., 1993, Methods for vapour cloud explosion blast modelling, *Journal of Hazardous Materials*, 34 (1993) 151-171
- 169) Vesper A., Breitung W., Dorofeev S., 2002, Run-up distances to supersonic flames in obstacle-laden tubes, IV ISHPMIE, *Journal of Physics IV*, 12: 333-340
- 170) Veynante D., and Vervisch L., 2002, Turbulent Combustion Modelling, *Prog. Energy Combust. Sci.*28(3), pp. 193-266
- 171) Vieille P., 1900, Rôle des discontinuités dans la propagation des phénomènes explosifs. *C. R. Acad. Sci.* 131, Paris: 413-416
- 172) Von Neumann, J., Theory of detonation waves in *Off. Sci Res. Develop* 1942
- 173) Wang, J., Guo, J., Yang, F., Zhang, J., Lu, S., 2018. Effects of hydrogen concentration on the vented deflagration of hydrogen-air mixtures in a 1-m³ vessel. *International Journal of Hydrogen Energy* 43, 21161-21168. <https://doi.org/10.1016/j.ijhydene.2018.09.108>
- 174) Wilcox D.C., 2008, Formulation of the k- ω Turbulence Model Revisited, 46, *AIAA Journal*, pp. 2823-2838, Bibcode:2008, AIAAJ..46.2823W, doi:10.2514/1.36541
- 175) Wilén, C., A., 1999, "Safe handling of renewable fuels and fuel mixtures." VTT Publications Finland, 394: 1-117
- 176) Williams F.A., 1985, "Combustion theory: 2nd edition", Benjamin/Cummings Publishing Company Inc, Amsterdam, ISBN 0-8053-9801-5
- 177) Xiao H., 2012, Experimental and numerical investigation of premixed flame propagation with distorted tulip shape in a closed duct. *Combust. Flame* 159(4)
- 178) Yao C., 1974, Explosion venting of low strength equipment and structures. *AIChE Loss Prevention Symposium*, Vol. 8
- 179) Zalosh R. G., 2008, "Explosion Venting Data and Modeling Literature Review," Fire Protection Research Foundation Report
- 180) Zeeuwen J.P., van Wingerden C.J.M., Dauwe R.M, 1983: Experimental investigation into the blast effect produced by unconfined vapour cloud explosions, 4th. Int. Symp. Loss Prevention and Safety Promotion in the Process Industries Harrogate, U.K., pp D20-D29
- 181) Zeldovich Y., The theory of the propagation of detonation in gaseous systems. *Journal of Experimental and Theoretical Physics*, 1942. 10 p. 542
- 182) Zeldovich Y., Librovich V.B., Makhviladze G.M., Sivashinsky G.I., 1970, On the development of detonation in a nonuniformly heated gas, *Astronautica Acta* 15 313-321
- 183) Zeldovitch Y., Istratov, A., Kidin, N. and Librovitch, V., Flame propagation in tubes: hydrodynamics and instabilities, *Combustion Science and Technology*, vol. 24, pp. 1-13, 1980

6.2 Other works

- 1) Daubech J., 2016, OMEGA UVCE: Unconfined gas and vapour explosions, N° DRA-16-133610-06190A
- 2) Heudier L., Proust C., 2017, OMEGA 5 - Le BLEVE : phénoménologie et modélisation des effets thermiques, N° DRA-17-164793-09921A
- 3) Reimeringer M., Mercier F., Richomme S., 2007, Projet OMEGA - La résistance des structures aux actions accidentelles, INERIS-DRA-2007-N° 46055/77288
- 4) NF EN 14491:2012 : dust explosion venting system
- 5) NF EN 14994:2007 : gas explosion venting system
- 6) NFPA68:2017: Standard on Explosion Protection by Deflagration Venting
- 7) Thomsen K., 2004-04-26. <http://www.home.att.net/~numericana/answer/ellipsoid.htm>
- 8) Unified Facilities Criteria 3-340-02: Structures to resist the effects of accidental explosions, Dept. of the Army, the NAVY and the Air Force, Washington DC, USA.

